FACULTY OF BIOSCIENCE ENGINEERING

Poly(2-isopropenyl-2-oxazoline) based nanofiber networks

a versatile platform for sensor applications

Daniël Peeters
Student number: 01600039

Promotors: Prof. dr. Richard Hoogenboom, Prof. dr. Peter Ragaert
Tutor: Ronald Merckx

Master's Dissertation submitted to Ghent University in partial fulfilment of the requirements for the degree of Master of Science in Bioscience Engineering: Cell and Gene Biotechnology

Academic year: 2020 – 2021

UNIVERSITEIT GENT

Preface

Throughout my entire school career, I have been intrigued by the intricacies of both biology and chemistry. The choice of pursuing the study of bio-engineering permitted me to learn about both of these worlds. To finalise my time at Ghent University with a master thesis consisting of a joint project between the bio-engineering and chemistry departments felt like a dream come true. This dream was made possible by several people who more than deserve to be thanked for their help.

Firstly, professor dr. Richard Hoogenboom and Professor dr. ir. Peter Ragaert, who both made it possible for me to start this project. Furthermore, their expertise in both the fields of polymer chemistry and food safety was of great importance in guiding me throughout the entire project, for which I would like to explicitly show my gratitude.

I would also like to thank the Supramolecular Chemistry Group for making the entirety of my thesis project a fun and joyful experience. Within this research group, I specifically am grateful for my supervisor Ronald Merckx. Due to his expertise and cheerful way of working, I was able to achieve goals within this thesis project I had never envisioned beforehand, all the while fully enjoying the work, to the point where a personal interest was spiked to potentially pursue a career in research.

My family deserves their due credit as well. I would like to thank my parents for their everlasting support, not only during my master thesis but during my entire life. Due to them, I am where I am today, which is reason enough to highlight my appreciation. Furthermore, my brother, Joachim, has always been an example for me. I could and still can always count on him for advice and help, for which I will forever be grateful. Lastly, my sister, Astrid, never fails to brighten me up when needed, a characteristic often called upon in difficult, stressful times. Without the support of my family, I can hardly imagine myself in my current position.

To finalise, I would like to express my gratitude towards friends. The Corona pandemic has made the last few years a troubling time and the amounts of joy I drew from this group is proof of how important they are to me. Some among them also found themselves in the same position of working on their thesis scripture, which has led to some interesting and fun occasional writing sessions.

Daniël Peeters, 27th of May 2021

Abstract

The rising amount of food waste demands for creative solutions to minimise unnecessarily wasted food products. To potentially reduce this issue in the household and retail sectors, this work presents a colour-based sensor system focused on detecting premature spoilage in food packaging. In order to achieve this goal, four chemical dyes have been tested for their applicability as food spoilage detectors, including two thiol responsive dye compounds as well as two halochromic dyes. The selected dyes were immobilized onto a homemade reactive nanofibrous network, based on poly(2-isopropenyl oxazoline) (PiPOx), and studied to evaluate their colour response during the decay of different food products, including chicken, beef, and cod. Furthermore, water-stability tests and infrared spectroscopy revealed the expected stable and efficient linkage of the dye compounds onto the polymeric chains, as the PiPOx network is shown to be a readily available platform for further functionalisation. Real-life sample testing showed that the sensor array, placed over a container containing a sample of meat or fish, underwent a progressive colour change as spoilage proceeded. This colorimetric response was followed as a function of time by smartphone pictures. The respectively obtained RGB indices per picture were further used to calculate a Euclidean Colour Distance (ECD) in between the functionalised membranes in different timeframe pictures, providing an objective indication of the effectiveness of spoilage metabolite detection. Through the obtained results, we demonstrate that the array allows for the monitoring of the overall spoilage process of chicken, beef, and cod, matching the depicted expiry dates on the food product. Finally, the sensor array was demonstrated to be efficient under different atmospheres as results were achieved in both ambient air and nitrogen environment for different food products. The results thus indicate the future possibilities for the application of these materials within food packaging as well as the potential of automated result analysis through colour change tracking.

Contents

List of Figures

Abbreviations

ABN	4-Aminobenzoic acid
AIBN	Azobisisobutyronitrile
ANB	4-Amino-3-nitrobenzaldehyde
BT	Butanethiol
CFU	Colony Forming Units
DEA	Diethylamine
DMA	Dimethylacetamide
DMAP	4-Dimethylaminopyridine
DMF	*N*,*N*-Dimethylformamide
DMSO	Dimethylsulfoxide
DP	Degree of Polymerization
ECD	Euclidean Colour Distance
EtOH	Ethanol
FLW	Food Losses and Waste
FRP	Free Radical Polymerization
GC	Gas Chromatography
HCl	Hydrochloric acid
iPOx	2-Isopropenyl-2-oxazoline
IR	Infrared
MAP	Modified Atmospheric Packaging
MS	Mass Spectrometry
MeOH	Methanol
NMR	Nuclear Magnetic Resonance
N-PDE	*N*-phenyldiethanolamine
PA	Propylamine
PiPOx	Poly(2-isopropenyl-2-oxazoline)

RAFT	Reversible Addition-Fragmentation chain Transfer
SEC	Size Exclusion Chromatography
SET-LRP	Single Electron Transfer Living Radical Polymerization
SPME	Solid-Phase Microextraction
TCD	Tip to Collector Distance
TEA	Triethylamine
TMA	Trimethylamine
TNB^-	2-Nitro-5-thiobenzoate
VOC	Volatile Organic Compound
VSC	Volatile Sulfuric Compound

1. Introduction

Food losses and food waste (FLW) have attracted much attention in the world recently and have become a priority in the global and national political agenda (e.g., United Nations Sustainable Development Goals Target 12.3). A better understanding of the availability and quality of global FLW data is crucial for benchmarking reduction goals, environmental impact analysis, and informing mitigation measures. With the ever-growing world population and the need to store and transport the food from the place of production to another for consumption, food preservation becomes necessary to increase its shelf life and maintain its nutritional value, texture, and flavour. Therefore, good food preservation techniques must prevent microbial spoilage of food without affecting its quality and nutritional value. In literature, the problem of daily food waste has received increasing attention over the past decades. Although major progress has been made on food safety, preservation technologies, understanding of the nutritional aspects of different foods, and general health issues regarding food and diet, there is still a lack of innovative ways to reduce food waste.[1] In Europe alone, about 88 million tonnes of food is wasted annually of which an estimated 46.5 million tonnes are generated in households. This averages out to 173 kilograms of food wasted per person per year. Not only does this contribute to environmental problems but it also counts up to an annual loss of 143 billion euros on food waste alone.[2,3]

1.1 Food waste management

Several solutions have been put into practice to recover some of the value inside of the food waste. Through composting or total combustion, the internal energy and components of the food are at least to some extent used, albeit not in the field of human nutrition. A 2017 study in the United States showed that of the 40.7 million tonnes of household food waste, 2.6 million tonnes were composted (6.3%) and 7.5 million tonnes were combusted for energy (18.4%), stating that the major part of 30.6 million tonnes (75.2%), however, ended up in landfills. This led to food waste representing 22% of all municipal solid waste in landfills. In 2018, this study was repeated, but this time different techniques and categories were included in both sources of food waste, such as food donations and animal fodder, and food waste management techniques. These numbers, therefore, show a large increase in total food waste generation and should as such not directly be compared to those stated in Europe. Figure 1 shows the evolution of this food waste management throughout the years. It shows a positive increase in the amount of revalued food waste, but also a large increase in the total amount of food waste generated. There is still a need for innovative approaches to decrease the total amount of food that ends up as food waste altogether.[4]

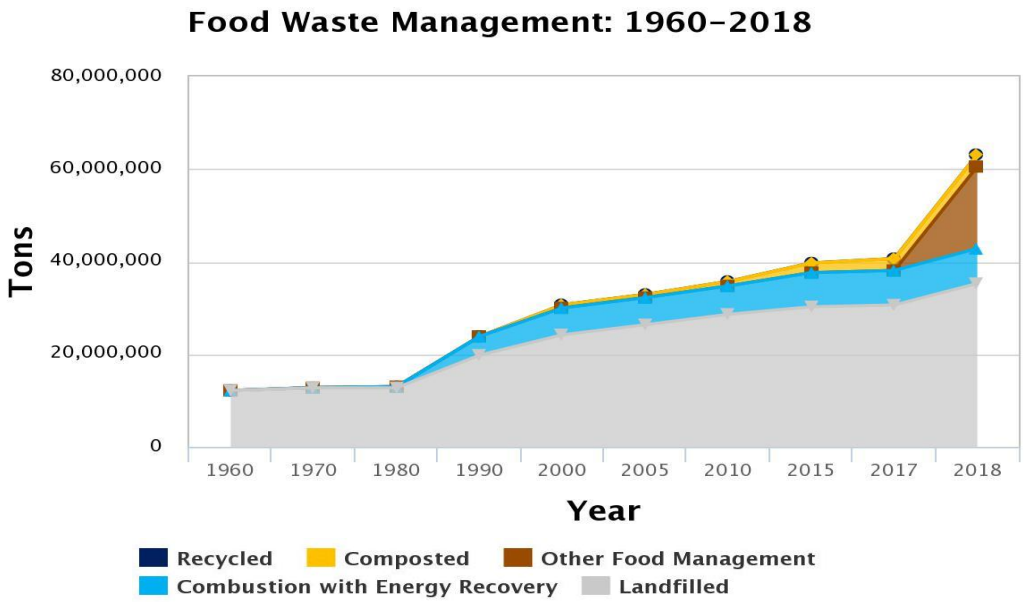

Figure 1 *Yearly food waste management US 1960-2018.*[4]

1.2 Origins of food waste

When considering food waste, it is important to note that waste is generated in all the different steps of the food production process and not only at the consumer level. Theoretically, the production process can be divided into five major sectors: production, processing, retail, communication, and consumers, as depicted in Figure 2. Each of these sectors contributes to the total food waste in a completely different manner and to effectively reduce food waste, specific solutions have to be developed for each of them separately.

Production, processing, and communication are sectors that can be considered industrial and large-scale sectors that often require solutions in the form of process optimization. These, however, are outside of the scope of this master thesis. The retail and consumer sectors on the other hand can be considered part of everyday life and will be the focus of this study. From the previously mentioned 88 million tonnes of annual food waste in Europe, around 4.6 tonnes are produced in retail. The consumer sector on the other hand nets up to 47 million tonnes per year. In comparison to all the other sectors, it is the household sector that contributes the major part to food waste.[3,5]

Figure 2 *Five sectors of the food production process.*

In these last two sectors, food waste is generated in many ways, including simply throwing away spoiled food. This could, to some extent, be considered as an unavoidable loss due to the health risks regarding the consumption of spoiled products. It does however raise

questions on how it can be minimized. On a consumer level, a solution would be to reinforce awareness and purchasing behaviour to consume or use all products before they spoil. To do so, it is of major importance to decide in real-time when food products are considered spoiled or unsafe. For certain foods, people can rely on their sensory capabilities to analyse the state of decay. Certain odours and tastes such as fishy smells and unexpected sourness or bitterness often indicate the decaying state of the products. Some visual signs also clearly show that the food is no longer meant for consumption. The presence of mouldy 'hairy' structures and coloured marks on the product indicates the growing colonies of contaminating micro-organisms such as bacteria and moulds.[6–8] These sensory signs of spoilage can however be misinterpreted, missed or even disregarded as normal in certain scenarios. They form a strong basis but are still subjective and rather uncertain tests to rely on for food safety. Other products, such as meat and fish, can even decay in such ways that the risk of consumption due to spoilage occurs earlier than human senses can detect.[9] As such, some form of verification had to be included which provides this crucial information to the consumer. This verification mechanism is the expiration date.

Expiration dates were first introduced on a consumer level in the 1970s. Nowadays, it is a standard addition to almost every packaging. Its function in households is mostly providing a control mechanism indicating whether food is still safe and edible. In supermarkets, the expiration dates serve this same purpose, yet also play an important role in influencing consumer behaviour.[10] Expiration dates are so popular because they remove the abovementioned problem of doubt about freshness. Because many forms of decay are not noticeable or easily mistaken, these expiration dates have provided a major improvement for both food quality and safety.

Regarding food safety and food quality, expiration dates are a nearly optimal solution. However, if the expiration date is considered from a food waste perspective, there is still room for improvement. The main issue is the premature disposal of food. The expiration dates originated as a tool for food safety which has led to extra measures being taken to ensure this safety, such as including additional safety and uncertainty margins in the expiry dates. These measures might however often increase unnecessary food waste. Expiration dates are often based on bacterial challenge studies. Zielińska and co-workers report that the studies consist of inoculating a product with a certain strain of bacteria that is expected to grow on this

product.[11] Next, it is kept in the required environment, in which it should also be stored in stores or at home, to reliably reproduce the real scenario. The growth of the bacteria is then monitored until they reach the maximal amount allowed for safe consumption. The results of several of these studies are then combined to form a critical date that represents the outer limit for safe consumption. Because of how biological processes work, however, there is a lot of uncertainty and variation that needs to be accounted for which results in a safety buffer of time being deducted from this critical date to fully ensure safe consumption.[12]

Other than these safety measures, there is also the impact of food quality on expiration dates. Companies often conduct many quality tests to analyse how long their products retain their optimal state. These quality aspects include criteria like colour, firmness, the production of certain off-odour smells, and many others that do not have a real impact on the food safety aspect of the product. To differentiate between the expiration dates based on this quality aspect and those indicating the moment pathogens might have grown to dangerous proportions, two types of expiration dates are employed, the ‘best before’ and ‘use by’ respectively. The crucial difference in the meaning of both the types of expiration dates, however, is little known to a large part of the population. This results in the common misinterpretation of ‘best before’ dates as the earlier mentioned critical dates for safe consumption, which further leads to unnecessarily thrown away food.[12]

As both the implemented safety buffer and the misinterpretation of ‘best before’ dates result in a significant part of the unnecessary food waste, there is a need for an alternative test that fits the normal household situation to further improve the food waste problem on the consumer and retail level. To fit these requirements, this thesis will focus on the production of a sensor focused on the real-time monitoring of the quality deterioration of food products. To create such a sensor, two main questions arise: What is to be detected and how to detect it?

1.3 Biomolecules

To answer the question of what the sensing mechanism must detect, a closer look has to be taken at the exact structures that will be degraded through spoilage. Any organic lifeform is built up out of the four main groups of biomolecules as displayed in Figure 3 being lipids, carbohydrates, proteins, and nucleic acids. As illustrated below, each of these biomolecules is composed of smaller components. Carbohydrate structures and proteins are respectively made up of from series of monosaccharides and disaccharides, and multiple amino acids. As metabolic pathways often revolve around smaller molecules in biology, the larger biomolecules will first be broken down into their smaller components. With this in mind, the metabolism of each of these smaller components is what will lead to the potential target of the sensor. Before a choice is made on which group of compounds will be most interesting for spoilage detection, the mechanics behind spoilage and the breaking down of the biomolecules have to be investigated further.

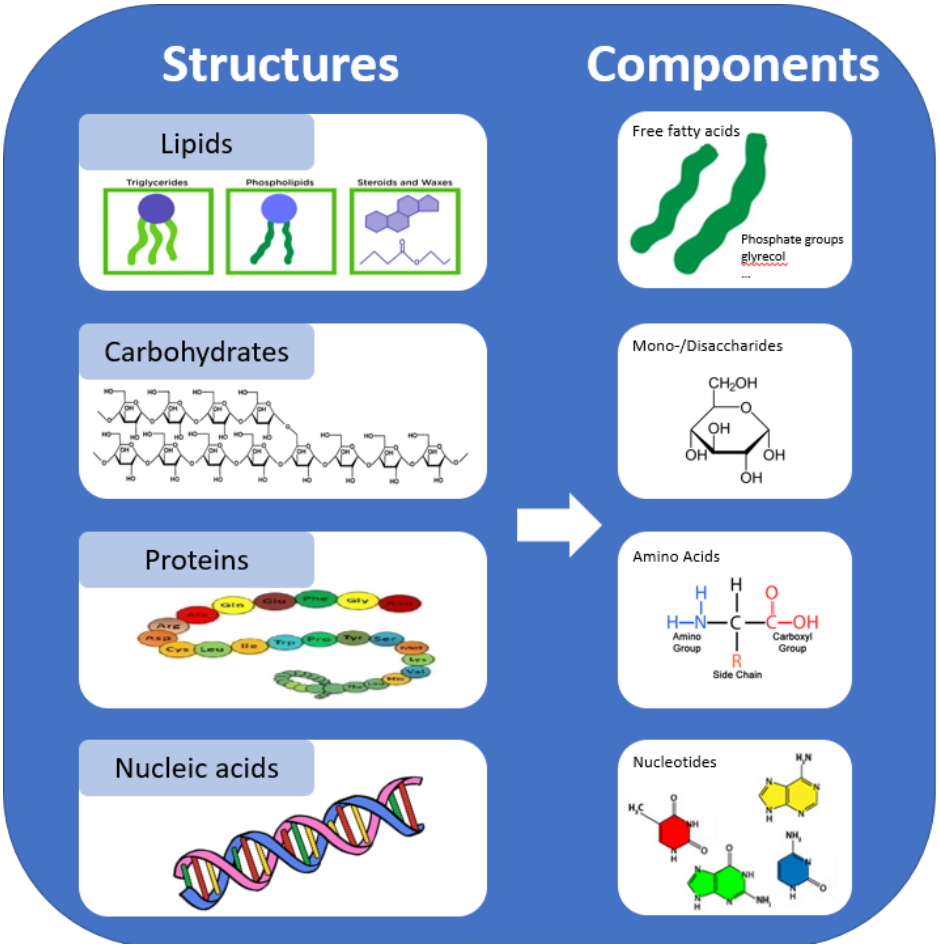

Figure 3 *Four types of biomolecules and their molecular components.*

1.4 Spoilage mechanisms

As a start, food spoilage is considered to be the process where a food product becomes sensorial unacceptable for ingestion by the consumer. This is caused by processes that convert the molecular structures present in food products to other, often smaller, molecules. Further literature review will focus on the different aspects of this food spoilage, rather than the presence and growth of possible pathogenic species on food products as this is beyond the scope of producing a quality assessment tool for food products.

1.4.1 Passive degradation, autolytical, and metabolic reactions

The degradation of the food structures is caused by three different mechanisms, being *passive degradation*, *autolytical reactions*, and *metabolic reactions*. These three mechanisms often occur all in parallel and greatly increase each other's effectiveness. Passive degradation envelops both the physical destruction of the food product and spontaneous chemical reactions. Physical destruction is self-explanatory as pressure, heat, and other physical factors can negatively alter food. Chemical reactions on the other hand are less self-explaining but still form an important food degradation mechanism that needs to be taken into account. Depending on which environment the product is kept in, certain chemical reactions will take place. Examples of such chemical interactions are the oxidation and hydrolysis of lipids, causing off-flavours and rancidity. Next to these spontaneous reactions, there are two types of enzymatic processes that affect the food product, autolytical and metabolic reactions.[13]

Autolysis is the process of enzymatic degradation of compounds of food caused by enzymes present in the organism itself. Enzymes cover an enormous array of possible functions through the catalysis of chemical reactions. Since food degradation is caused by chemical reactions, it is also governed by an array of enzymes such as proteases, carbohydrases, and many others. The process of an organism degrading its own structures works similarly through enzymes and is, in fact, a completely normal mechanism. Processes such as autophagy and programmed cell degradation occur constantly in living organisms and form an important basis for wound healing and the recycling and renewing of various types of structures in the body.[14,15] They are, however, strictly regulated processes under these circumstances. Upon death, these processes are suddenly left without control mechanisms and will eventually start to degrade all types of macromolecules in the product.[16] These biological processes and enzymatic

reactions work optimally at normal body temperatures and as such can largely be inhibited by keeping food products at low temperatures.[17,18]

The final form of degradation is caused by metabolic reactions. Although metabolic reactions are also governed by enzymes and are, as such, very alike to the previously mentioned category, the implied metabolic reactions are those of other organisms than the host. As the invading species require sustenance to survive and multiply, they will make use of the opportunity of the plentiful resources present in food products and start to grow on them. These organisms include bacteria and fungi, among others, and are often called microorganisms. Since these microorganisms will grow exponentially better in nutrient-rich environments, autolysis greatly increases their growth speed since it provides them with readily available smaller molecules through the degradation of the larger macromolecules. These microorganisms will degrade several of the components in the food product through their metabolic reactions and by doing so they generate structures of their own to grow and produce the energy they require to survive. Both these microorganisms themselves as the side products formed in the metabolic pathways are often not beneficial for consumption and are an important cause of food spoilage.[17–20]

1.4.2 Spoilage prevention

Since food spoilage is an irreversible loss, it has been a challenge since the dawn of time to preserve food for as long and as good as possible. Many sources confirm that food preservation methods have been in use since prehistoric times through the smoking of food for example. This smoking will simply seal off the outer layer of the food making it more difficult for contaminating organisms to enter the food. Other methods such as salting make the food environment very hypertonic. This means that the increased concentration of dissolved ions in the food draws out the water from possible contaminating microorganism cells through a process called osmosis. This makes it very hard for the microorganisms to survive which results in a longer lifetime of the food product.[21]

Throughout time, more sophisticated methods of food preservation have been developed like the addition of antimicrobial agents.[22–25] Also, several techniques have been developed which reduce the initial load of bacteria present on the food. Sterilisation, pasteurization, and freeze-drying are often used in industrial food production processes.[26–28] Other than these methods there are several techniques on how to store food products to further decrease the rate of

spoilage. The most common is storage in refrigerated temperatures which slows down nearly all biological processes including bacterial growth and metabolic/autolytic reactions. Vacuum packaging and modified atmosphere packaging (MAP) are two other methods that remove or reduce the presence of oxygen.[29] This slows down the speed at which bacterial populations will develop on the product because oxygen is often required for the bacteria to grow and multiply. Furthermore, MAP packaging includes the addition of CO_2 to the packaging atmosphere, which further reduces bacterial growth rates.[17,28,30] Although all these techniques are shown to vastly improve the shelf life of most products, they are finite. Eventually, the degradation and decay of the product will inevitably take place.

1.5 Fish food products

As all food products will show variation in spoilage mechanisms and involved microorganisms, it is important to differentiate the chosen technique for spoilage detection for each type of product separately. Within this work, the main objective is to reduce food waste by applying sensor technology for fish products.

Fish is an important dietary product consumed around the globe. Although the production process differs from standard plant foods or meat-based products, the same five general sectors as discussed in 1.1 can be found here as well. Figure 4 illustrates the total percentage of fish and seafood products that are wasted and the division over the different sectors throughout the world. The graph shows the same distribution on how fish food is wasted in the different sectors with the households, here denoted as 'consumption', accounting for a significantly large portion in the first world countries.[3]

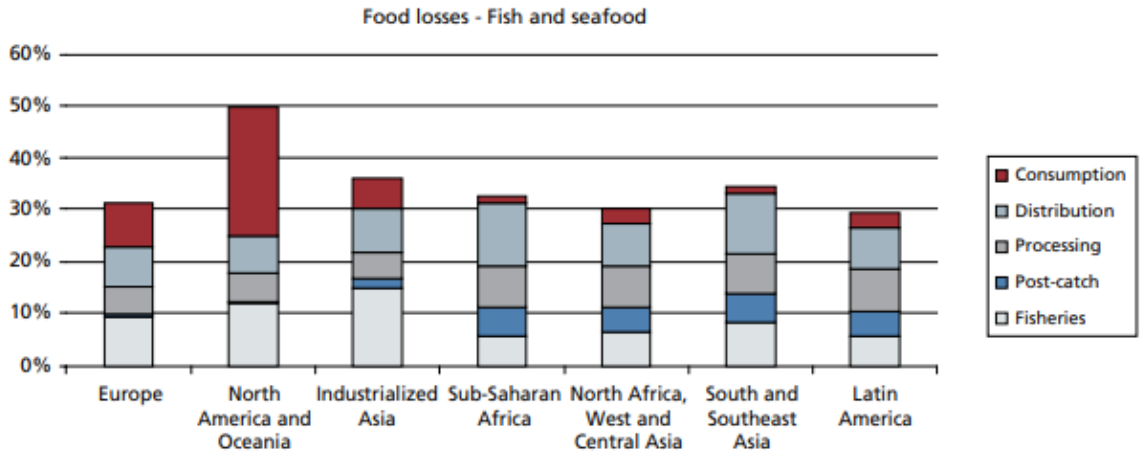

Figure 4 *Global fish and seafood waste of initial caught amount.*[3]

1.5.1 Spoilage of fish products

In the field of fish food products, all three of the earlier mentioned deterioration processes are of great importance when considering the whole of fish spoilage. Both Ghaly and Hansen et al. reported the autolytic enzymatic, oxidative, and microbial spoilage specifically for fish substrates.[17,18] Research stated that in frozen samples during the early stages of deterioration textural quality was reduced, but no off-odours or off-flavours were produced. The most important impact of this first spoiling process is the alterations of the textural aspect of the product caused by the release of hypoxanthine and formaldehyde.[18] During oxidative spoilage, lipid oxidation is a major cause of deterioration for the pelagic fish species such as mackerel

and herring with high oil/fat.[31] Oxidation typically occurs via radical driven reactions with oxygen and the double bonds of fatty acids present in the sample.[32] In fish, lipid oxidation can occur both enzymatically or non-enzymatically. During this process, lipases split the glycerides into free fatty acids which are responsible for the common off-flavour.[33] In the third process, microbial spoilage, the composition of the microflora is dependent on the microbial contents of the water in which the fish live. Microbial growth and metabolism is a major cause of fish spoilage which produces amines, biogenic amines (e.g., putrescine, histamine, and cadaverine), organic acids, sulfides, alcohols, and aldehydes with unpleasant and unacceptable off-flavours.[34–36] Important to note is that not all bacteria equally contribute to spoilage. Huss and co-workers reported that for fish kept in an aerobic atmosphere at a room temperature of 25 °C, the spoilage is a result of Gram-negative, fermentative bacteria (e.g., *Vibrionaceae*), whereas Gram-negative, non-fermentative bacteria (e.g., *Pseudomonas spp.* and *Shewanella spp*.) tend to spoil chilled fish under aerobic atmosphere. Further differences were observed between different atmospheric preservation techniques, as both in a vacuum and MAP packaging the Gram-negative, fermentative genus *Photobacterium* was present as one of the main contributors to spoilage. While trimethylamine (TMA) is mainly used to determine microbial deterioration leading to fish spoilage, Huss and co-workers found that among TMA other compounds were produced such as methanethiol, dimethyl sulfide, ammonia, and hydrogen sulfide.[37] This research shows that the mechanisms behind fish spoilage are well studied and documented, yet a choice still needs to be made on which of the degradation processes will be the focus for developing a sensing unit.

1.5.2 Detection of fish spoilage

Since the aim is to develop a sensing unit for early spoilage detection, certain criteria need to be fulfilled for such alternative real-time food spoilage sensors to be of use. First of all, it has to guarantee at least the same assurance as is given by the expiration dates. This means that the chosen analyte must be detected as soon as its concentration exceeds a predetermined threshold. To do so, the developed detection mechanism needs to show high specificity and sensitivity towards that certain analyte. Secondly, if the aim is to reduce food waste caused by misinterpretation of food spoilage, then the response must only be given when the measured concentration exceeds the olfactory threshold and not earlier. For both these requirements, the degradations products of proteins will greatly fit the picture.

A protein is composed of separate amino acids of which 20 different types occur in naturally built proteins. They are present in high concentrations in muscle structures and since standard products of meat and fish mostly consist of muscle, they make up a major part of what is present in the product. This makes them an important group when looking at spoiling mechanisms. Out of all the amino acids present in these proteins, two are important to take into consideration: cysteine and methionine. The structure of these sulfur-containing amino acids is depicted in Figure 5.

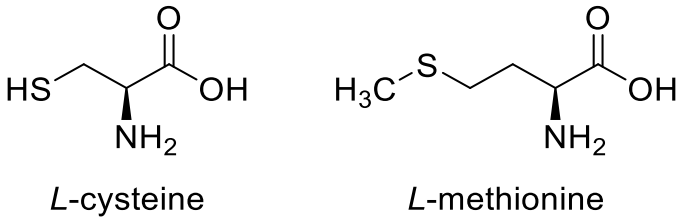

Figure 5 *Chemical structures of L-cysteine and L-methionine.*

Two reasons make them suitable candidates for this application. First of all, the bacterial metabolic pathways of cysteine and methionine end with the production of several small sulfur compounds (e.g., dihydrogen sulfide from cysteine, methanethiol, and dimethyl disulfide from methionine).[38,39] These compounds possess low vapour pressures hence the name: volatile sulfur compounds (VSC). These VSCs have a very low olfactory threshold concentration, indicating facile perception in low concentrations by humans as a bad odour and/or bad taste. Since bad odours and tastes are two main factors in deciding whether or not a product is spoiled, these VSCs are one of the first compounds to make a product perceived as such.[40] Secondly, Miller and co-workers have shown that none of these VSCs are formed in sterile fish muscle. This implies that the autolytical processes will not degrade these two amino acids meaning that all the VSCs present in fish food are produced through bacterial metabolism making them a certain indicator of active bacterial mediated food decay.[41]

1.5.3 Bacterial metabolism

During the lifetime of a fish, plenty of bacteria are present which rapidly start metabolizing it after it dies. This is why many procedures of cleaning, gutting, and electrolyzed water washing are performed to decrease the initial bacterial load of the fish product.[42,43] Through cold storage and vacuum or MAP-packaging, the growth of the remaining bacterial population is inhibited as much as possible. But even in cold storage, the bacteria will grow and multiply and slowly but steadily start to metabolize the fish. Several species have been identified as

contributors to the spoilage of fish products. Which of them finally are present on the fish is mostly based on what type of fish is studied, what type of environment it originates from, and what treatment the fish undergoes before storage. Most of them do show active metabolism of the sulfur-containing amino acids and production of the VSC side products. Species identified as fish spoilage bacteria are *Pseudomonas*, *Schwenella*, *Acinetobacter*, and *Lactobacillus* genus among others.[34,44–46] In fish, it is important to note that spoilage occurs at a high pace since the initial bacterial load on freshly caught fish is quite high. Mikš-Kranjik and co-workers report initial bacterial loads of 10^6 colony forming units per gram (cfu/g) on freshly caught fish. Knowing that rejection starts around values of 10^7-10^8 cfu/g and the fact that fish itself is a wealthy growth environment due to high water content and suitable pH, immediate preservation techniques must be employed to preserve the fish as well as possible.[46]

1.5.4 Methionine and cysteine metabolism

Methionine metabolism consists of two main steps as can be seen in Figure 6. In the first step, the amine group is removed by oxidative deamination. This results in loss of ammonia and the formation of an alfa-keto-butyric acid. From this second compound, methanethiol is removed by a process called demethiolation, leaving a carbohydrate chain available for the bacteria. This methanethiol is often considered as the final side product, yet a portion of it is further oxidized to dimethyl disulfide. Both these compounds are volatile to some extent. Studies show that almost the entire amount of methionine present in fish samples will eventually be degraded into these two volatile compounds when left decomposing.[44]

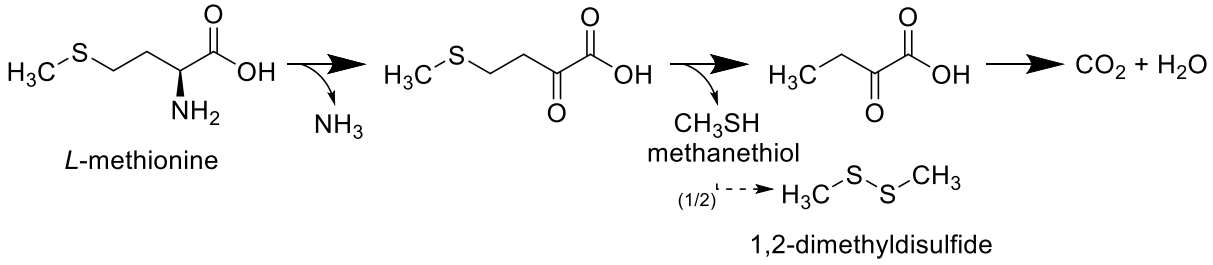

Figure 6 *Bacterial metabolism of methionine with the formation of sulfur-containing end products.*

Cysteine, on the other hand, is metabolized to form pyruvate which is used as a central carbon molecule in various biological processes. Multiple pathways are known which result in the degradation of cysteine but all of them finally result in dihydrogen sulfide being formed next to pyruvate.[47] The amine group is released as free ammonia or incorporated in bacterial structures. A commonly occurring pathway is shown in Figure 7 in which the sulfur group of

cysteine is first removed by an enzyme called L-Cysteine desulfhydrase. Further on, the amine group is removed from the structure to form free ammonia and pyruvate.[48]

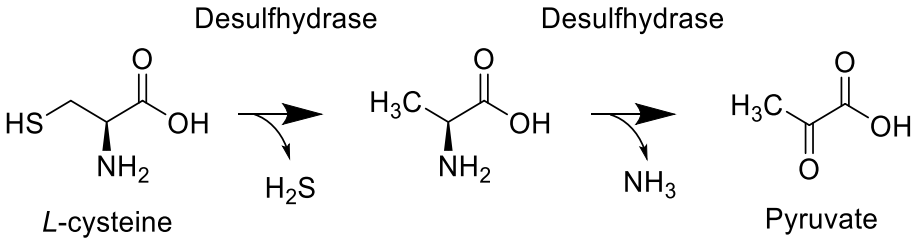

Figure 7 *Cysteine metabolism pathway with the formation of pyruvate, ammonia, and hydrogen sulfide.*

The preservation of food has created the need to develop methods that can easily track the food freshness and safety throughout the shelf life of the product (production, storage, shipment, and consumption). To detect the abovementioned degradation products, a "technological nose" can be designed to measure markers of freshness and provide an "index of quality" of the product in real-time or identify the presence of any spoilage indicating components.

1.6 Sensors

Although the word sensor might not be used as frequently in daily life, it is one of the most common objects that surrounds us. Sensors tell us the temperature, the weather, how many steps we take, and many other things. The use of sensors has been made customary to our lives and a life without them is something most of us cannot imagine. Since the subject of spoilage detection can be translated to an analyte detection problem, it is the category of analyte sensors that is of interest in this study. Traditionally, analyte sensors are composed of chemical or biological receptors. These receptors are specifically targeted against a certain analyte and use a physical transducer that converts the detected change in the environment into a measurable signal, generating a quantitative and/or qualitative output.[49] The basic working pattern of a sensor is illustrated in Figure 8.

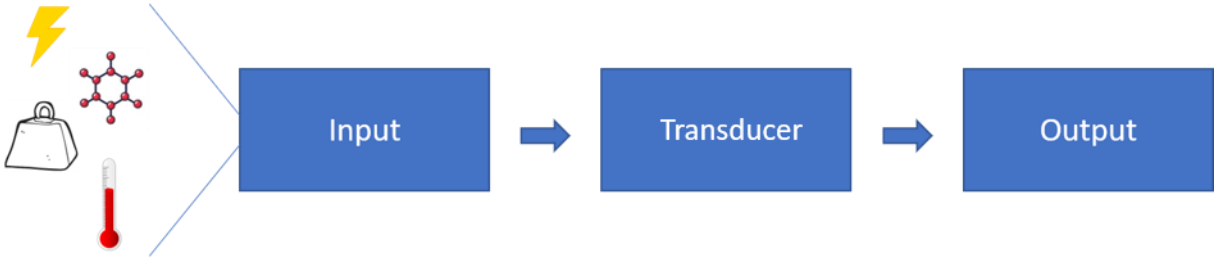

Figure 8 *Basic working mechanism of a sensor.*

Since sensors come in a variety of forms and different mechanisms behind their functioning, they are subdivided into different categories. Firstly, non-optical sensors are distinguished from optical sensors. Secondly, optical sensors will be discussed based on their sensing type (e.g., acidity and redox). Lastly, different fabrication methods will be considered.

1.6.1 Non-Optical sensors

Non-optical sensors are nothing new in the detection of analytes and have also been introduced in the detection of food spoilage. Currently, the majority of these sensors consist of resistors as electronic units that keep track of changes in conductivity during interactions between analyte molecules and an active surface. This process of transferring an electrical signal upon analyte detection is also seen in the human body in the process of tasting and smelling. The mammalian olfactory system is, in a way, a large array of bioelectrical receptors, which has evolved over thousands of years to specialize itself in the matter of food spoilage detection.[50,51] To mimic these olfactory receptors, a broad range of electrochemical sensors has been explored. The most widely used electrochemical sensors include metal oxide

semiconductors (e.g., SnO_2) for triethylamine (TEA) detection.[52,53] Zou and co-workers prepared a hollow SnO_2 microfiber which showed a quick response towards TEA with a limit of detection as low as 2 ppm. Although non-optical sensors showed sensitive and efficient analyte detection, they still require aspects that make them impractical for everyday real-time food spoilage monitoring in a normal household situation. The need for electricity as well as specialised equipment is not conveniently available at all times, and, as such, render non-optical sensors not an option for the envisioned application in food packaging.

1.6.2 Optical sensors

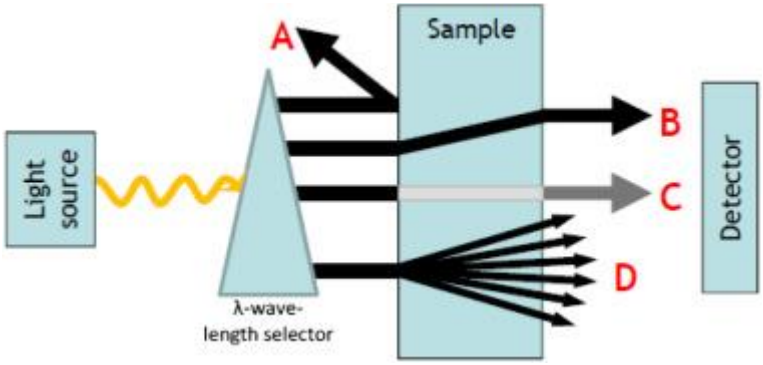

Figure 9 *General arrangement of spectroscopic measurements: (A) light reflection, (B) light refraction, (C) light absorption, (D) fluorescent emission.*[54]

Where non-optical sensors use changes in conductivity, optical sensors use visible or ultraviolet light as the input source for analysis. Optical sensors can be represented in general terms as a wavelength-selectable light source, the sensor material itself, and a light detector. What the detector monitors varies by technique (e.g., scattering, absorbance, reflectance, photoluminescence, chemiluminescence). The most common optical sensors are based on colorimetric or fluorescent changes originating from intermolecular interactions between the chromophore or fluorophore with the analyte molecules.[55] Colorimetry (i.e., quantitative measurement of absorbance or reflectance spectra) is, of course, one of the oldest analytical techniques with “naked-eye” visual quantification.[56]

As an example, one of the most straightforward optical sensors utilizes the well-known dye phenolphthalein. This sensor will display a colour shift upon detecting a change in acidity. Ranging from a colourless solution to a pink-purple solution upon reaching a basic pH due to the change in the molecule from a protonated to a deprotonated ionic state. If the dye sensor is meant for analyte detection, it is required that the optical output signal changes upon interaction with the analyte. To do so, the dye often has to react with its analyte leading to

changes in its structure or electron configuration. Alberti and co-workers illustrated this principle using Ellman's reagent combined with cysteine. Upon contact with the analyte, the designed sensor showed a redshift towards 420 nm displaying a bright yellow colour.[57,58] To obtain more analyte selectivity, often colorimetric sensor arrays are used. This technology relies on an array of dyes immobilized on a solid support where upon exposure to the analytes the dye array changes colour. Colorimetric sensor arrays have proven to be useful in the detection, identification, and quantification of volatile organic compounds (VOC) in the gas phase.[59–61] Furthermore, they have been used to detect and differentiate the mixtures of compounds dissolved in aqueous solutions.[62,63] Each dye is chosen to react chemoselectively with certain analytes of interest. Magnaghi et al. selected a panel of pH indicators and a colorimetric dye, selective for thiols. Using the selected chromophores in a colorimetric sensor array, meat spoilage could be followed and differentiated based on the response.[64] The abovementioned work, however, still contains some important limitations. The usage of ionic interactions to immobilize the dye compounds to a carrier material allows for potential dye-leaching, the leaking of the dye compounds from the carrier matrix, which is a frequently reported issue in other works.[65,66]

1.6.3 Sensor materials

For the chemical dyes to change colour, they have to be able to effectively sense their surroundings. The proof of concept for chemical sensors is often demonstrated in solution providing close proximity and good interaction between dye and analyte. However, to detect food spoilage within the packaging, the environment of the sensor will be the headspace of the product and, therefore, the sensor dye has to be incorporated into a solid-state functional unit and be able to detect the analyte in the gas phase. To do so, an appropriate material is required to support the dye and enable gas sensing while no dye-leaching on and into the food product may occur. To obtain an effective sensor material, the support material must meet two different criteria. Firstly, the need for optimal analyte contact, the carrier material should allow effective contact between the sensing molecules and their respective analytes. Secondly, the material should have a large surface to volume ratio, which increases the potential for dye immobilisation as well as for dye-analyte interactions. Three candidate carrier material types that suffice for these requirements will be discussed, namely nanoparticles, thin films, and nanofibers.

1.6.3.1 Nanoparticles

The first widely used carrier materials for sensors are nanoparticles. Many different support materials are used such as graphene, carbon nanotubes, metallic carriers, and they are used for various types of sensors.[67] These nanoparticles add several functionalities to the sensing unit as it not only adds robustness to the system but also serves as a functional unit itself, often increasing the effectiveness of the linked sensing unit.[68] Another advantage of nanoparticles is that multiple sensing units can be connected to one particle. By combining several of the sensors, the combined output signal is larger than that of separate sensing units leading to a lower limit of detection thus providing opportunities for analytes that require more sensitive detection.[69–71] Nanoparticles are however still separate particles which makes them not much better in terms of a solid sensor support unit to be included in food packaging.[72]

1.6.3.2 Thin films

Thin films are layers of material deposited on a bulk substrate to give properties that cannot be easily attained (or not attained at all) by the base material. Thin-film deposition refers to the action of applying a thin film of any substance, for example a functional metallic or polymeric coating, on a surface. Through precise construction of the film structure, a large concentration of sensing units can be combined on a defined surface both leading to increased sensitivity and ease of detection. Figure 10 shows SEM images of a thin film structure created by Fong et al, clearly displaying the film as a flat surface-functionalized sensor area.[73] The film structure allows for the production of a solid-state sensor that can function in a gas headspace as is required for a sensor in food packaging. An example of a metallic thin-film sensor for thiol detection is that of the study of S. Briglin and co-workers.[74] The thin film is created by coating a surface with Au nanocrystals fully capped with amine chains. Upon detection of thiols in the surrounding gas, these amine chains will be swapped out for the thiols finally resulting in measurable changes in the conductivity of the film structure. Although a film structure fulfils the requirements needed for this application, it is still not the best option.

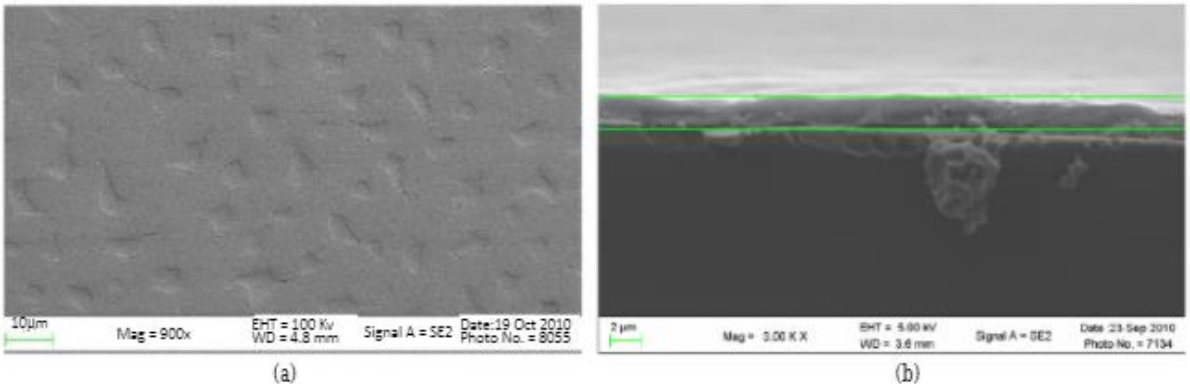

Figure 10 *Film sensor SEM images a) surface b) cross-section.*[73]

1.6.3.3 Nanofibers

The third type of used sensor support materials are nanofiber membranes, typically these consisting of very thin fibres with a diameter below 500 nm. Nanofibrous membranes have already proven to be useful as supports for ultra-sensitive sensor materials thanks to the large specific surface area created by the many pores between the fibres of sub-micron thickness.[75–78] Due to this specific structure, nanofibers combine the most important properties of nanoparticles and films, which are a large surface to volume ratio and the capability of functioning as a solid-state sensor. To produce these thin fibres, which is commonly done by electrospinning, high molar mass polymers are typically required to form the necessary chain entanglements that keep the fibrous structure together. The type of polymer determines the properties of the membrane where the spinning parameters influence the fibre diameter.[79] Since the scope of this work is the development of nanofibrous nanofiber networks, this option will be discussed in more detail in the following sections.

1.7 Electrospinning

Electrospinning is a widely used production technique for the development of polymeric fibres with diameters ranging from several micrometres down to several nanometres by using high voltage electric fields.[80–83] In Figure 11, a typical electrospinning set-up is depicted consisting of a high voltage power supply, spinneret, and a collector. The needle of a syringe, which contains a polymer solution, is placed under high voltage (kV).

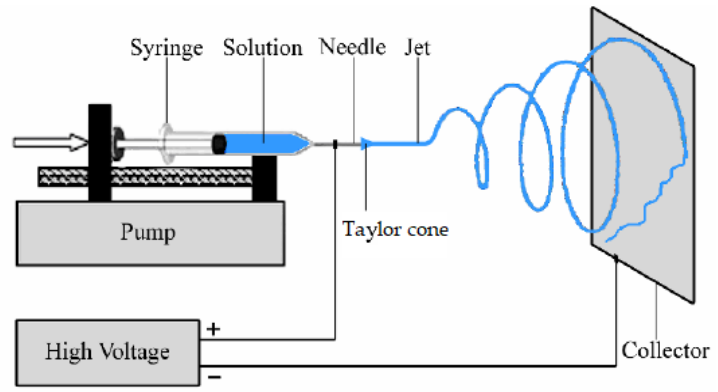

Figure 11 *Solvent electrospinning setup.*[84]

The erupting jet forms a Taylor cone, travelling towards a grounded collector plate. When the polymer reaches the collector plate, all solvent of the polymer solution should be evaporated. The electrospinning process provides high flexibility and versatility over the fabrication of these fibres, offering unique advantages to produce uniform nanofibers and fabrics with controllable pore structure.

1.7.1 Production process

In literature, researchers were able to develop a wide variety of synthetic and natural polymer nanofibrous membranes by electrospinning, with each material having unique, polymer-based properties.[85–89] According to the desired application, parameters can be modified to obtain the desired nanofibrous membranes with certain properties. These parameters can be split up into three categories: the polymer solution, the processing parameters, and environmental conditions.

1.7.1.1 Polymer solution

The polymer solution plays a crucial role in the electrospinning process. This starts with finding the optimal solvent. Even though some exceptions have been reported on electrospinning of polymer latices[90,91], the polymer should preferably be perfectly soluble in the solvent, while during the electrospinning of the polymer, the solvent should be able to rapidly evaporate.

Too high solvent volatility will lead to unwanted blockage of the needle, but too low volatility will lead to bead formation due to solvent presence inside the membrane.[92] Besides the solvent choice, the amount of polymer dissolved in the solution, often expressed as weight percentage, will also greatly affect the production process. Increasing the polymer concentration will lead to a higher viscosity, which affects the stability of the abovementioned Taylor cone and therefore the quality of the fibre membrane.[93] Again a certain viscosity window should be defined for each polymer-solvent system. Too low polymer concentrations will result in insufficient entangled polymer chains leading to spraying of beads rather than fibre formation. However, too high viscosity will cause a blockage of the needle tip.[94] The last important solution parameter is conductivity. For each polymer solution, a threshold value is required to charge the polymer in order to form the Taylor cone. However, the formation of the Taylor cone is impaired when conductivity exceeds certain limits. The stable Taylor cone observed during the electrospinning process is depicted in Figure 12.

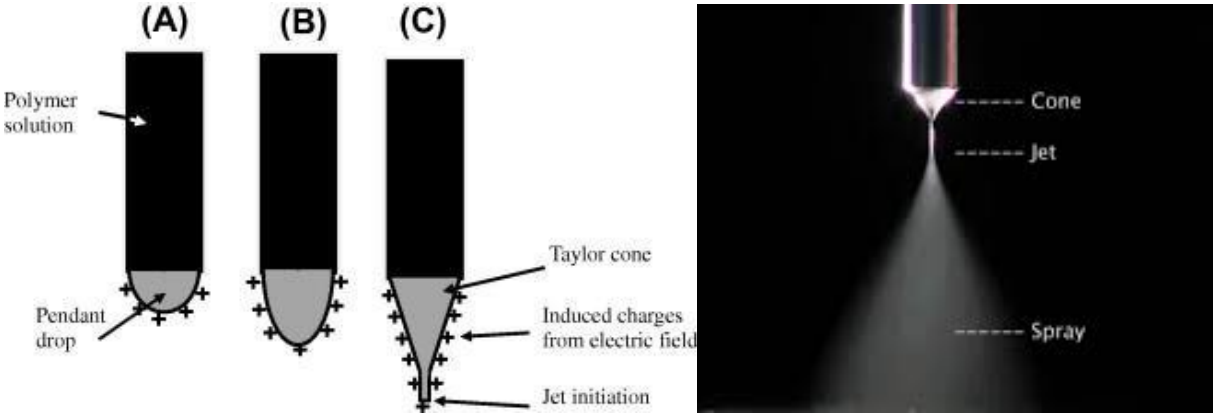

Figure 12 *Formation of a Taylor cone and jet.*[95]

1.7.1.2 Processing parameters

Processing parameters during electrospinning include the flow rate of solution, the needle tip-to-collector distance (TCD), and the applied voltage. The optimal processing parameters are influenced by the solution parameters due to the nature of the polymer and the solvent. Firstly, the required flow rate is dependent on the applied polymer-solvent system. Again, too high flow rates will lead to bead formation due to insufficient solvent evaporation while too low flow rates will result in a repeated interruption of the production process. The TCD or the distance between the needle and collector is critical as it influences the evaporation time for the solvent. Lastly, the polymer type and solvent will also determine the critical voltage of an

electrospinning process. Often the applied voltage is adjusted by trial and error until a stable electrospinning process is obtained.[96,97]

1.7.1.3 Environmental conditions

Finally, environmental parameters should be taken into account as with every process. Two notably important factors are temperature and humidity as they both greatly influence the evaporation step of the electrospinning procedure. Changing the temperature will affect the evaporation rate as well as the viscosity of the mixture. Increasing humidity will increase the evaporation time required for beadless nanofiber formation. Both aspects should be taken into consideration when optimizing the electrospinning of a polymer solution to obtain nanofibers, as illustrated by Figure 13.[83]

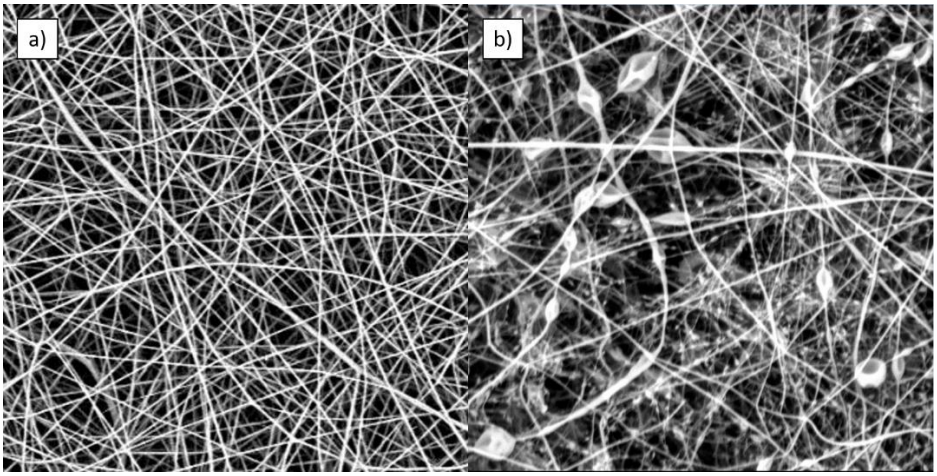

Figure 13 *SEM images of a) clear nanofibers and b) beaded nanofibers.*

1.8 Development of “smart” nanofiber materials

Intelligent materials, better known as smart or responsive materials, are materials that have one or more properties that change in response to external stimuli, such as a variation in pH, temperature, light, or concentration of chemical compounds. Within this work, this smart behaviour will be added to the nanofiber membranes by the attachment of a sensing dye molecule.

For sensor applications, two methods exist to incorporate the dye inside the nanofiber network. On the one hand, the dye can be blended inside the nanofiber membrane and on the other hand, the dye can be covalently attached to the polymer fibres. The difference is depicted in Figure 14.

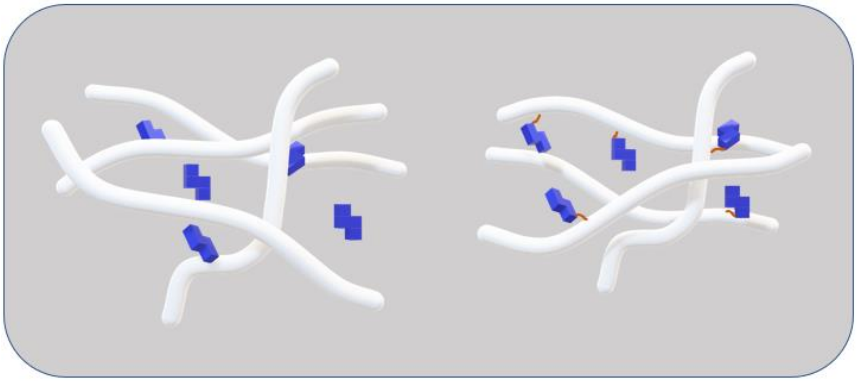

Figure 14 *Blend nanofiber system (left), covalent nanofiber system (right).*

1.8.1 Smart blend nanofiber materials

The blending technique introduces the sensing molecules into the nanofiber network by blending them into the electrospinning polymer solution. This process is also called ‘dye-doping’. The technique is easy and fast which results in fluent and cost-efficient production processes.[78,98] Dyes that do not possess the required chemical functionality for covalent binding are often incorporated using this method to produce a solid-state sensor. As mentioned before, due to the absence of covalent linkage of the dye to the network, it can be extracted from the network in a process called ‘leaching’.[85] In many applications, this would not only be a major issue for partially losing its sensing capabilities but also for contaminating the product. In food-related applications, for example, this poses a major issue.[78,99] In addition, dyes that are fully entrapped into the nanofiber structures may not be exposed to the analyte, imparting their sensing ability.

1.8.2 Smart covalent nanofiber materials

Covalent nanofibers will make use of the covalent attachment of the dye onto the nanofibrous material. By attaching the desired functionality onto the material the possibility of leakage is significantly decreased.[100] To do so, both the used material and the dye are required to have available reactive groups. By performing chemical alterations to the dye molecules, a wide variety of dyes can be incorporated onto diverse materials as illustrated by the example below.

De Smet and co-workers introduced the concept of fabricating coloured materials with low dye leaching through covalent immobilization of the desired dye using plasma-generated surface radicals, as depicted in Figure 15. They reported the functionalization of dye molecules with a polymerizable group. Through a short period of plasma treatment radicals were formed leading to the addition of the dye functionality onto the sensor material. Thanks to the non-specific nature of the generated radicals, they were able to include azobenzenes and sulfonphthalein's onto various materials including polypropylene, polyethylene and Teflon sheets, as well as polyamide, cellulose and polyethylene (nano)fibers.[65]

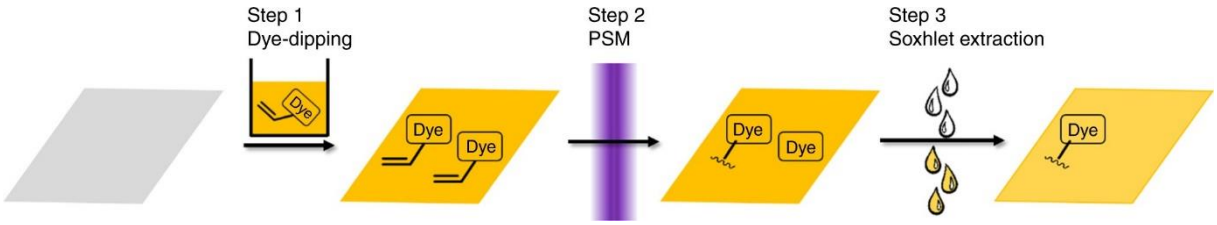

Figure 15 *Schematic representation of the plasma dye coating procedure.*[65]

1.9 Goal of the thesis

The ultimate goal of this project is to provide a reliable sensor system for the early detection of food spoilage within food packaging. The proposed system consists of a colorimetric nanofibrous sensor network focussed on food spoilage analytes, which provides an easy-to-interpret colour response that allows customers to perform a facile analysis of the product's edibility. To achieve this challenging yet realistic goal, analyte responsive dyes will be immobilized on a suitable support material, capable of detecting specific spoilage metabolites.

The first part of the project is focused on finding, selecting and synthesising promising dye candidates to detect food spoilage metabolites. Within the application, the first subclass of dyes is those able to detect thiols, a group of metabolites directly linked to several spoilage processes. However, next to thiols, other chemical groups that are directly correlated to spoilage will be considered, i.e., amines and alcohols. Both are observed as metabolites in different food decomposition pathways and influence environmental parameters such as pH, humidity, and oxygen content of the headspace in food packaging. Therefore, halochromic dyes responsive to the pH environment will be included as a second subclass of dye compounds. In total, four different dyes will be investigated, two thiol-responsive colourants and two halochromic dyes. The colorimetric response of each dye will be evaluated towards its analyte.

The second part of the thesis is focused on the carrier material for the sensor application. To produce an effective solid-state sensor that can function within food packaging, several requirements must be met. The sensor should be non-toxic and must guarantee that no chemicals can be introduced into the food product. To this end, the colorimetric dye molecules will be covalently attached to the carrier material. Throughout the literature review, several types of carrier materials were discussed, with an emphasis on the need for dye immobilisation. Therefore, the base material should have prerequisite compatibility with the selected colourants. In this study, poly(2-isopropenyl-2-oxazoline) (PiPOx) was selected as versatile base material. This hydrophilic polymer possesses several promising characteristics, including non-cytotoxicity and being easily modifiable without the need for catalysts or the formation of by-products. This polymer will be synthesised within this project through free radical polymerization with optimisation of the molar mass characteristics towards

electrospinning processing. The latter will be used to design well-defined PiPOx nanofiber membranes, with an excellent surface-to-volume ratio for sensor applications.

The third part of the thesis will focus on the functionalisation of the abovementioned nanofiber membranes to obtain the proposed nanofiber sensor network. Firstly, the nanofiber membranes will be crosslinked to ensure the water stability of the envisioned hydrophilic material. Secondly, all the selected dye candidates will be immobilised on the nanofibrous membranes, making use of the remaining pendant oxazoline rings on the PiPOx material. According to their sensitivity and colour response towards their respective analyte, the conditions will be optimized to obtain the desired sensor material.

Finally, response rate analysis will be investigated towards real-life samples, mimicking food packaging conditions. Following the metabolite evolution in food packaging, using this colorimetric sensor array is expected to provide a categorical classification based on pattern recognition. Via the implementation of Euclidean Colour Distance calculations, an attempt will be made to lay the foundation of a potential automated objective detection of colour change through image analysis.

2. Materials and methods

2.1 Materials

All the commonly used solvents were HPLC grade and include: acetic acid (> 99%, Sigma Aldrich), acetone (> 99.8%, Sigma Aldrich), chloroform (CHCl3, > 99%, Fisher Chemical), dichloromethane (DCM, > 99.8%, Sigma Aldrich), diethyl ether (> 99.9%, Chem-Lab), 1,4-dioxane (> 99.8%, Sigma Aldrich), ethanol (EtOH, > 99.9%, VWR Chemicals), ethyl acetate (> 99.5%, Sigma Aldrich), hydrochloric acid (HCl, 37 V%, Fisher Chemical), hexane (> 95%, Sigma Aldrich), methanol (MeOH, > 99.8%, Sigma Aldrich), *N*,*N*-dimethylformamide (DMF, > 99%, Biosolve), petroleum ether (Chem-Lab).

The following chemicals were used as received: 4-Fluoro-3-nitrobenzaldehyde (> 95%, Tokyo Chemical Industry), *N*-phenyldiethanolamine (N-PDE, 97%, Sigma Aldrich), 4-aminobenzoic acid (ABN, > 99%, Sigma Aldrich), L-cysteine ethyl ester (98%, Acros Organics), 1-butanethiol (BT, > 98%, Sigma Aldrich), propylamine (PA, > 98%, Tokyo Chemical Industry), diethylamine (DEA, > 99.5% Sigma Aldrich), triethylamine (TEA, > 99%, Sigma Aldrich), Disperse Red 1 (95%, Sigma Aldrich), Ellman's reagent (99%, Sigma Aldrich), NaOH (micro-pearls, Acros Organics), Na_2CO_3 (> 99.5%, Sigma Aldrich), phenol (> 99%, Sigma Aldrich), 4-(dimethylamino)pyridine (DMAP, 99%, Sigma Aldrich), V-70 (> 95%, Fujifilm Wako Chemicals), VA-044 (> 97%, Sigma Aldrich).

Azobisisobutyronitrile (AIBN) was bought from Sigma Aldrich and was recrystallised from MeOH before use and was kept in the freezer at – 30 °C. The iPOx monomer was bought from Sigma Aldrich and before usage, it was vacuum distilled over CaH_2 to remove the inhibitor. After the distillation, it was kept under an argon atmosphere in the freezer at – 30 °C.

2.2 Equipment

Centrifuge Centrifugation was performed on an ALC multispeed refrigerated centrifuge PK 121R from Thermo Scientific using 50 ml centrifuging tubes with screw caps from VWR or 15 ml high clarity polypropylene conical tubes from Falcon.

Deionised water Deionised water was prepared with a resistivity of less than 18.2 MΩ x cm using an Arium 611.

DMA-SEC Size-exclusion chromatography (SEC) was performed on an Agilent 1260-series HPLC system equipped with a 1260 online degasser, a 1260 ISO-pump, a 1260 automatic liquid sampler (ALS), a thermostatted column compartment (TCC) at 50 °C equipped with two PLgel 5 µm mixed-D columns and a precolumn in series, a 1260 diode array detector (DAD) and a 1260 refractive index detector (RID). The used eluent was DMA containing 50 mM of LiCl at a flow rate of 0.500 ml/min. The spectra were analysed using the Agilent Chemstation software with the GPC add on. Molar mass values and Đ values were calculated against PMMA standards from PSS.

UV-VIS spectrometer UV-VIS spectra were recorded on a Varian Cary 100 Bio UV-VIS spectrophotometer equipped with a Cary temperature and stir control. Samples were measured in either quartz or disposable cuvettes with a path length of 1.0 cm in the wavelength range of 200 to 700 nm.

Reflective UV-Vis Reflective UV-VIS measurements were performed using a Perkin-Elmer Lambda 900 spectrophotometer, which is a double-beam UV-Vis spectrophotometer. The spectra were recorded from 280 nm to 780 nm with a data interval of 4 nm. Reflection values are converted into k/s through the Kubelka-Munk formula, as these values provide a comparable result to transmission UV-Vis absorption spectra.

Infrared spectroscopy Infrared spectra were measured on a PERKIN-ELMER 1600 series FTIR spectrometer and were reported in wavenumber (cm^{-1}).

Size-exclusion chromatography with light scattering (LS) Light scattering (LS) measurements are performed on a 3-angle static light scattering (MALS) detector, i.e., miniDAWN TREOS, from Wyatt Technology. The detector is coupled on-line to an Agilent 1260 Infinity HPLC system (vide DMA-SEC) and used to determine the absolute molar mass of the analysed polymer samples. The measurements are performed at ambient temperature, i.e., no

temperature control unit is supplied/installed with the above-mentioned LS detector. The refractive index (RI) increment (dn/dc) values are either used as reported for the certain polymer in *N*,*N*-dimethyl acetamide (DMA) or determined via online size-exclusion chromatography (SEC) equipped with an RI detector, which measures the RI increase for a 1-10 mg/mL concentration series of the mentioned polymers. The LS results are further analysed with the provided Astra 7 software, also designed by Wyatt Technology.

NMR Proton magnetic resonance spectra were recorded on a Bruker Avance 300 MHz at room temperature. NMR spectra were measured in chloroform-d ($CDCl_3$) from Euriso-top. The chemical shifts are given in parts per million (δ), relative to $CDCl_3$ at 77.36 ppm.

Chromatographic columns Chromatography on aluminium oxide and silica were performed on Merck Alox 90 standard aluminium oxide and Davisil chromatographic silica mecia LC60A 70-200 micron respectively.

TLC Silica TLC was performed on pre-coated Macherey-Nagel ALUGRAM SIL G/UV254 plates. Aluminium oxide TLC was performed on Merck TLC aluminium oxide 60 F254 neutral.

Flash chromatography with UV and ELSD detectors Column chromatography was performed on a Grace Reveleris® flash chromatography system using silica Reveleris flash cartridges.

Rotating drum electrospinning Solvent electrospinning experiments were carried out using a mono-nozzle set-up with an 18 gauge Terumo mixing needle without bevel. A ring-electrode was mounted around the needle to efficiently guide the jet towards the collector, which enhanced process stability and reduced the deposition area giving thicker membranes. A rotating drum was used as the receiving plane in the setup to ensure homogenous fibre deposition.

SEM imaging Fiber morphology was examined using a scanning electron microscope (FEI Quanta 200 F or FEI Phenom desktop SEM) at an accelerating voltage of 20 kV. Sample preparation was carried out using a gold sputter coater (Balzers Union SKD 030 or Emitech K550X). The nanofiber diameters were measured using UTHSCSA ImageTool version 3.0, developed by the University of Texas Health Science Center. The average fibre diameters and their standard deviations are based on at least 15 measurements per sample.

2.3 Compound synthesis

2.3.1 Dye synthesis

Synthesis of (E)-4-((4-(bis(2-hydroxyethyl)amino)phenyl)diazenyl)-3-nitrobenzaldehyde (C_0)

Synthesis of 4-amino-3-nitrobenzaldehyde (ANB)

5 g (29.6 mmol) of 4-fluoro-3-benzaldehyde was dissolved in 50 ml of 1,4-dioxane. The solution was added dropwise to 63.4 ml (15 equivalents) concentrated MeOH solution (7M) and left to stir at 100 °C for 2h. After cooling the mixture to room temperature, the formed ammonia was removed by piercing the septum of the microwave cap and subsequent argon bubbling for 30 minutes. Afterwards, the solvent was removed under reduced pressure until a yellow-orange solid was obtained. The product was taken up in ethyl acetate and extraction with saturated $NaHCO_3$ solution was performed. The water fraction was extracted three times with ethyl acetate. The solvent of the resulting organic phase was removed under reduced pressure, after which the orange solid was dissolved in a small amount of ethyl acetate. The remaining impurities were removed from the concentrated solution by column chromatography (Al_2O_3) using an acetone/hexane (50/50) eluent. Finally, the solid of pure 4-amino-3-nitrobenzaldehyde (ANB) was dried in a vacuum oven overnight at 50 °C and evaluated using ^{1}H-NMR spectroscopy.

Yield: 74.5%

^{1}H NMR: (300 MHz, DMSO) δ 9.82 (s, J = 0.5 Hz, 1H, O=C-*H*), 8.64 (s, J = 1.9 Hz, 1H, NO_2-C-*CH*), 8.24 (d, 2H, *NH_2*), 7.87 (d, J = 8.9, 1.9 Hz, 1H, CO-C-*CH*-CH), 7.17 (d, J = 8.7 Hz, 1H, NH_2-C-*CH*).

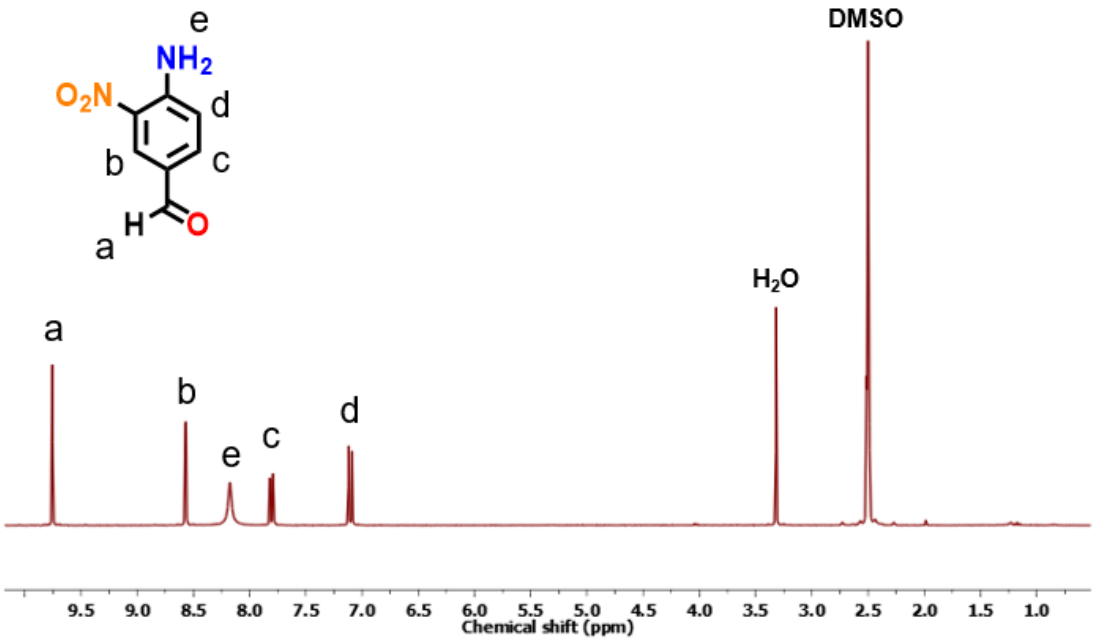

Figure 16 *^{1}H-NMR of 4-amino-3-nitrobenzaldehyde.*

Synthesis of (E)-4-((4-(bis(2-hydroxyethyl)amino)phenyl)diazenyl)-3-nitrobenzaldehyde (C_0)

0.6 g (3.6 mmol) of 4-amino-3-nitrobenzaldehyde (ANB) was weighed in a 250 ml beaker and charged with 60 ml HCl (6M). In the meanwhile, 0.3 g (3.6 mmol) of $NaNO_2$ was dissolved in 12 ml deionized water and stirred at 0 °C. The $NaNO_2$-solution was added dropwise to the 4-amino-3-nitrobenzaldehyde solution under stirring. The resulting solution was left stirring under continuous cooling for 30 minutes. Two spatula tips of crushed Urea were added to remove any formed Nitric Acid.

During the cooling reaction, 0.7 g (3.6 mmol) of *N*-phenyldiethanolamine was dissolved in a mixture of 17.7 ml Acetic Acid and 59 ml Ethanol. The resulted solution was cooled to 4 °C and added dropwise to the formed diazonium salt, resulting in a bright red solution. The resulting mixture was left to react overnight under continuous stirring. The solution was neutralized using a saturated NaOAc solution with a subsequent extraction using DCM to separate the azo dye from the aqueous solution. The organic fraction was dried over $MgSO_4$ and the solvent was removed under reduced pressure, resulting in a dark red-brown solid.

The solid was taken up in Acetone and passed over a silica column using an Acetone/Hexane (40/60) eluent. The final product was dried overnight in a vacuum oven at 50 °C and evaluated using ^{1}H-NMR spectroscopy.

Yield: 14.3%

UV-vis: λ_{max} DMSO: 519 nm

^{1}H NMR: (300 MHz, CDCl3) δ 9.99 (s, 1H, O=C-*H*), 8.25 (d, J = 1.6 Hz, 1H, NO_2-C-*CH*), 8.02 (m, J = 19.9, 10.0 Hz, 1H, CNO_2-CN_2-*CH*), 7.80 (m, J = 9.2 Hz, 3H, CO-C-*CH*-CH + N_2-C-*(CH)$_2$*), 6.68 (d, J = 10.4 Hz, 2H, $(CH_2)_2$-N-C-*(CH)$_2$*), 3.90 (t, J = 4.9 Hz, 4H, N-*(CH$_2$)$_2$*), 3.69 (t, J = 4.9 Hz, 4H, CH_2-*CH_2*), 2.92 (s, 2H, CH_2-*OH*).

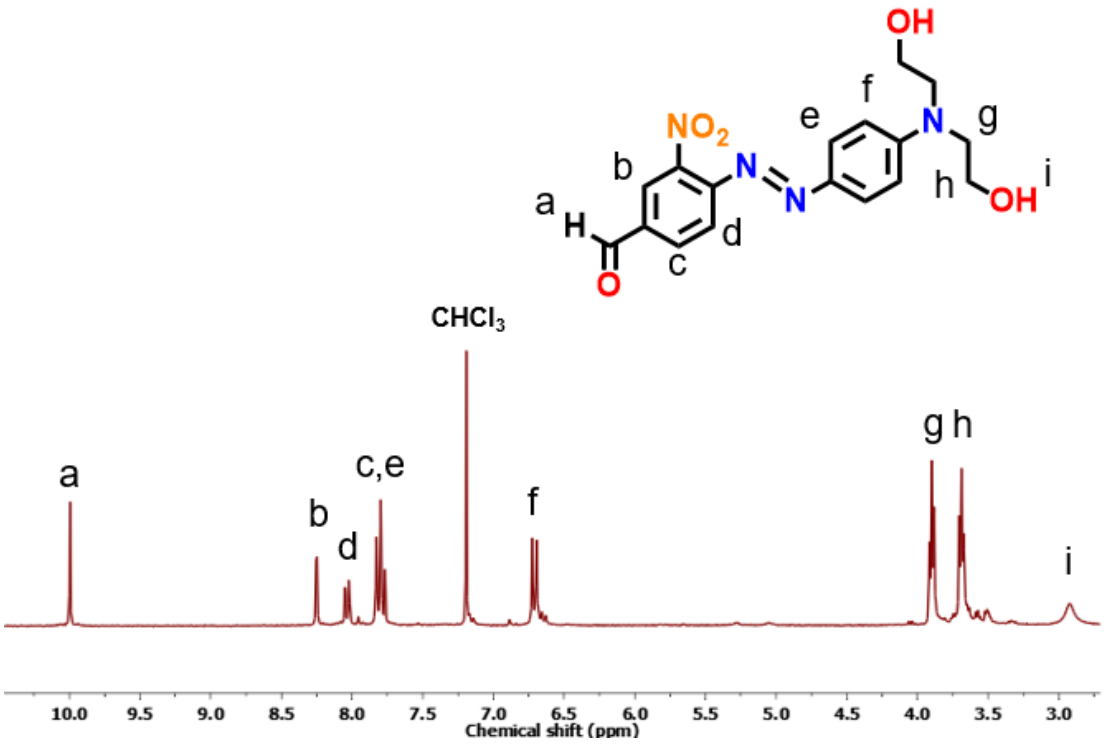

Figure 17 *^{1}H-NMR of (E)-4-((4-(bis(2-hydroxyethyl)amino)phenyl)diazenyl)-3-nitrobenzaldehyde (C_0).*

Synthesis of (E)-4-((4-hydroxyphenyl)diazenyl)benzoic acid (C_1)

4.5 g (32.8 mmol) of dry 4-aminobenzoic acid (ABN) was mixed in a mortar with 2.4 g (34.0 mmol) of $NaNO_2$ with the addition of 6 ml of water until a dark yellow paste was obtained. The paste was poured into a mixture of 200 ml of ice water and 10 ml of HCl (37 V%). The solution was left to stir at room temperature for 1h.

Meanwhile, a solution of 1.4 g (3.5 mmol) NaOH, 3.7 g (3.5 mmol) Na_2CO_3, and 3.2 g (3.4 mmol) phenol was prepared in 200 ml of ice water. The first solution was added dropwise to this second solution resulting in a dark red mixture. The mixture was left to stir overnight at room temperature during which dye particles started to precipitate out of the solution.

The mixture was then brought to neutral pH to ensure dye precipitation after which it was filtered off on a Buchner filter. After filtration, the dye was washed with water and dried in the vacuum oven for three days. The final product was evaluated using ^{1}H-NMR spectroscopy.

Yield: 47.78%

UV-vis: λ_{max} EtOH/H_2O (75/25): 454 nm

^{1}H NMR: (400 MHz, DMSO) δ 8.08 – 8.00 (m, 2H, HOOC-C-*(CH)$_2$*), 7.85 – 7.72 (m, 4H, *(CH)$_2$*-C-N_2-C-*(CH)$_2$*), 6.97 – 6.85 (m, 2H, HO-C-*(CH)$_2$*).

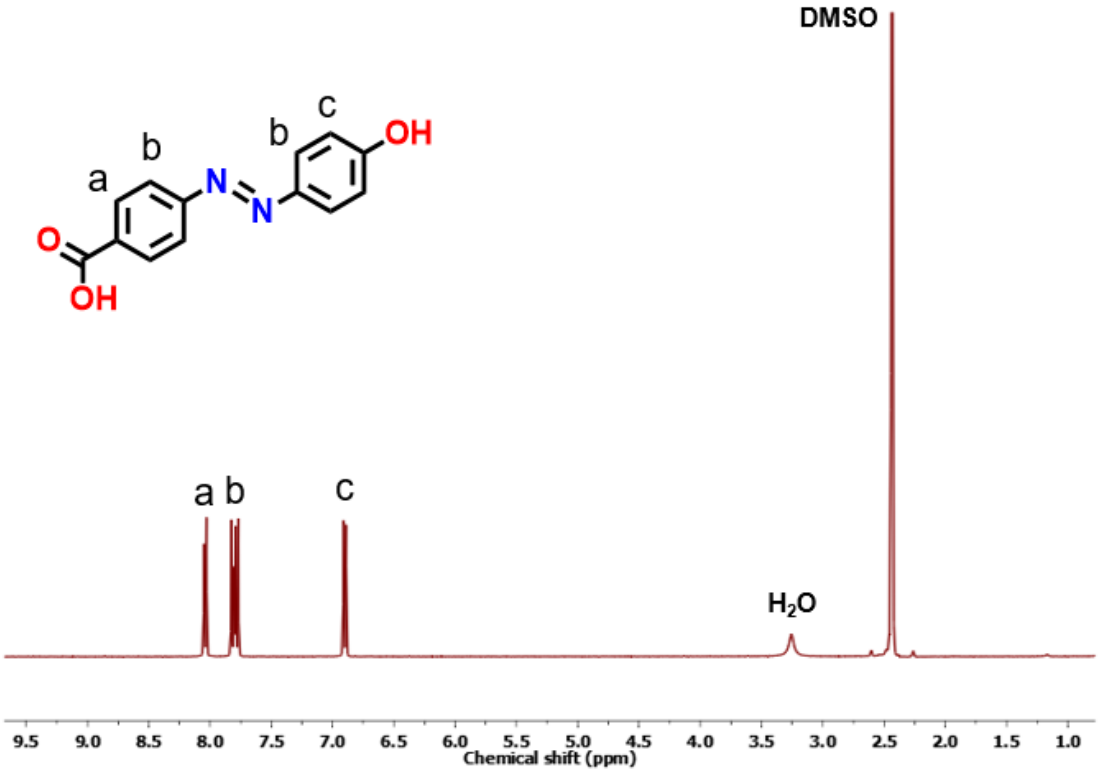

Figure 18 ^{1}H-NMR of (E)-4-((4-hydroxyphenyl)diazenyl)benzoic acid (C_1).

Synthesis of

(E)-4-(2-(ethyl(4-((4-nitrophenyl)diazenyl)phenyl)amino)ethoxy)-4-oxobutanoic acid (C_4)

3 g (9.54 mmol) of Disperse Red 1 was weighed in a 500 ml round-bottom flask and charged with 350 mL of DMF. To this mixture, 1.146 g (11.5 mmol) of succinic anhydride and 0.058 g (0.477 mmo) 4-(dimethylamino)pyridine (DMAP) catalyst were added under continuous stirring. The round-bottom flask was provided with a reflux condenser and an argon balloon, and the mixture was heated to 70 °C for 24h. Afterwards, the DMF was removed under reduced pressure until a dark red solid was obtained. The solid was taken up in DCM and

washed with deionized water and brine respectively. The organic layer was dried over $MgSO_4$ and the solvent was removed under reduced pressure. Finally, the remaining DMAP was removed from the solution by column chromatography (SiO_2) using an acetone/petroleum ether (80/20) eluent. The final product was dried overnight in a vacuum oven at 50 °C and evaluated using ^{1}H-NMR spectroscopy.

Yield: 51%

UV-vis: λ_{max} EtOH/H_2O (75/25): 513 nm

^{1}H NMR: (300 MHz, $CDCl_3$) δ 8.34 (d, *J* = 11.0 Hz, 2H, NO_2-C-*CH_2*), 7.98 (m, *J* = 8.9, 3.9 Hz, 4H, *$(CH)_2$*-C-N_2-C-*$(CH)_2$*), 6.83 (d, *J* = 13.2 Hz, 2H, $(CH_2)_2$-C-N-$(CH_2)_2$), 4.35 (t, 2H, N-CH_2-*CH_2*-O), 3.72 (t, 2H, N-*CH_2*-CH_2-O), 3.55 (q, 2H, *CH_2*-CH_3), 2.78 – 2.51 (m, 4H, CO-*CH_2*-*CH_2*-COOH), 1.27 (t, *J* = 7.0 Hz, 3H, CH_2-*CH_3*).

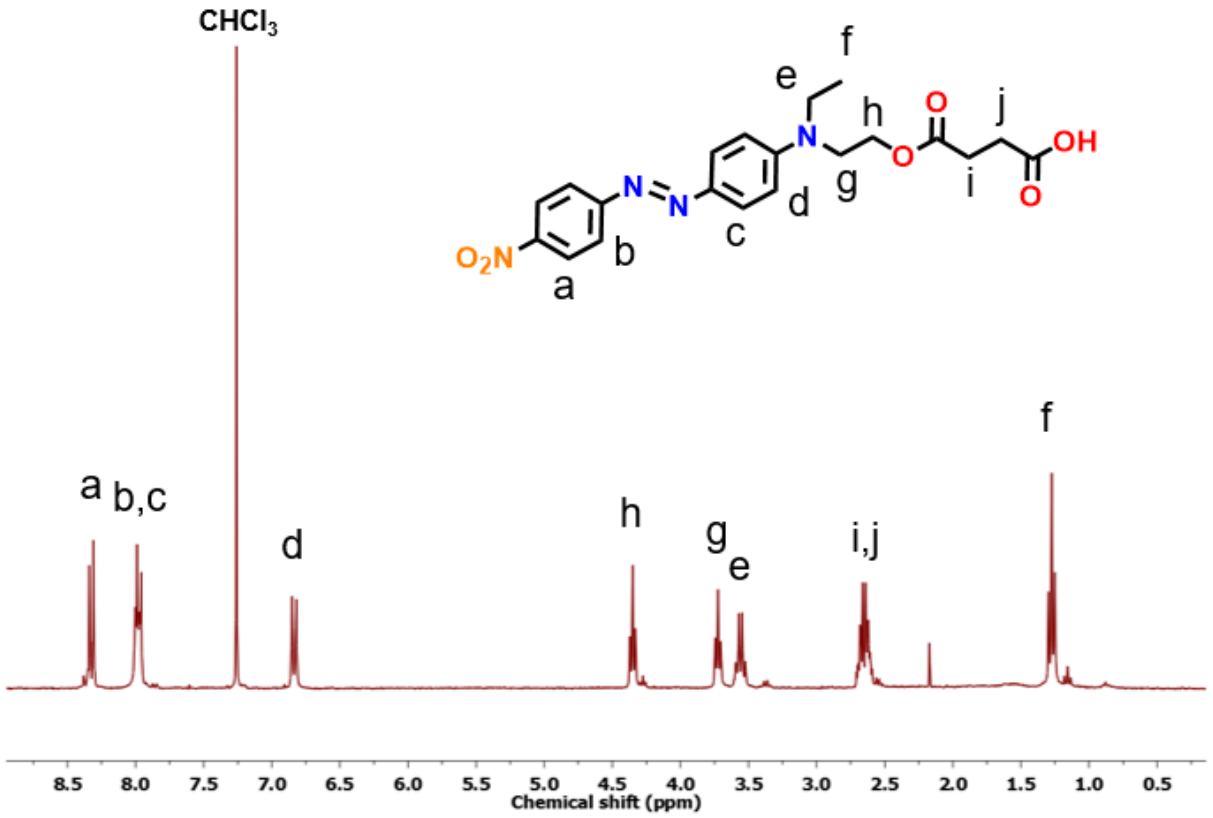

Figure 19 ^{1}H-NMR of (E)-4-(2-(ethyl(4-((4-nitrophenyl)diazenyl)phenyl)amino)ethoxy)-4-oxobutanoic acid (C_4)

2.3.2 Polymer synthesis

Synthesis of Poly(2-isopropenyl-2-oxazoline) (PiPOx) through free radical polymerization

The polymer was synthesised using free radical polymerization initiated by azobisisobutyronitrile (AIBN). 123 mg (0.75 mmol) of AIBN was dissolved in 29 ml of DMSO inside of a 200 ml round bottom flask. A spinning bar was placed inside the round bottom flask for future stirring. To this solution, 21 ml of iPOx (0.20 mol) was added resulting in a final 4 M monomer concentration. The solution was then argon bubbled for 30 minutes to ensure the complete removal of any residual oxygen. After Argon bubbling, the mixture was heated for 24h at 65 °C under continuous stirring.

The obtained polymer solution was cooled down to room temperature with subsequent precipitation in an excess of ice-cold diethyl ether. The obtained white polymer powder was dried in the vacuum oven overnight at 60 °C. After drying the polymer was dissolved in deionized water and remaining DMSO traces and residual monomer units were removed by membrane dialysis. Water baths were replaced every 24h. After 3 days, the dry, pure polymer was obtained through freeze-drying and characterised using ^{1}H-NMR spectroscopy, size exclusion chromatography and infrared spectroscopy.

Yield: 53.7%

^{1}H NMR: (300 MHz, CDCl3) δ 4.09 (t, J = 8.9 Hz, 2H), 3.70 (t, J = 8.8 Hz, 2H), 2.06 – 1.59 (m, 2H), 1.12 (m, 3H).

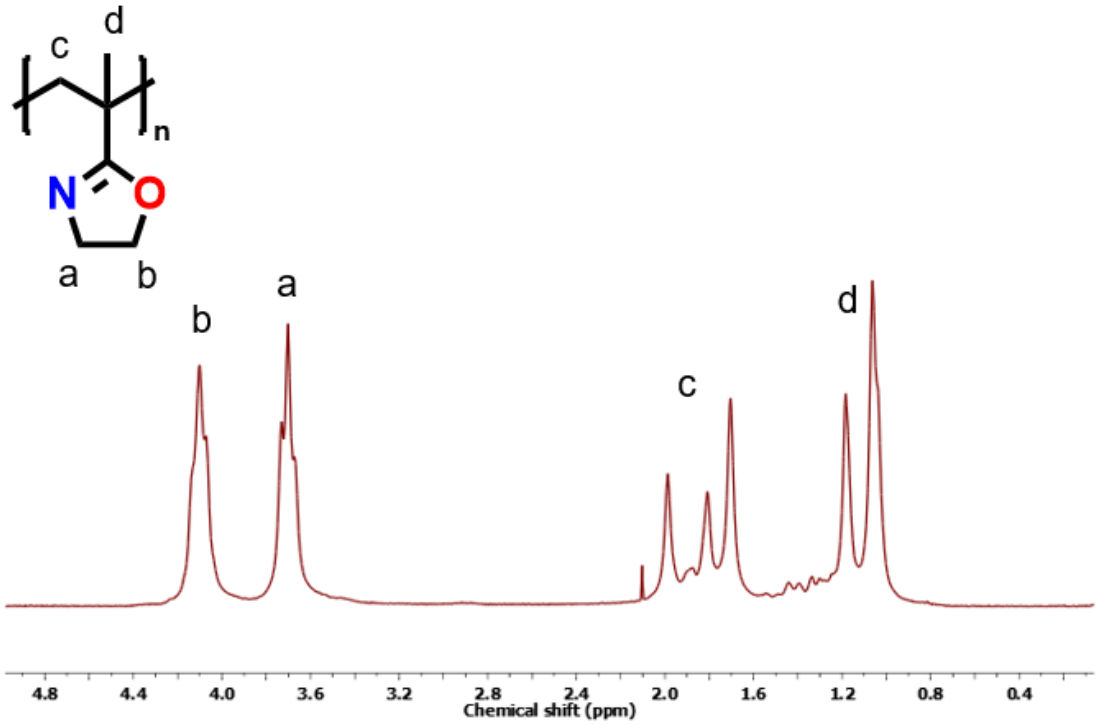

Figure 20 [1]*H-NMR of FRP synthesised Poly(2-isopropenyl-2-oxazoline).*

Synthesis of Poly(2-isopropenyl-2-oxazoline) (PiPOx) through bulk free radical polymerization

The bulk polymer was synthesised using free radical polymerization with AIBN as an initiator. 7.4 mg of AIBN (0.045 mmol) was weighed inside a 5 ml microwave vial together with a stirring bar. Subsequently, the microwave vial was charged with 3 ml of iPOx (28.6 mmol) and capped. Afterwards, the solution was argon bubbled for 30 minutes to remove any residual oxygen. After argon bubbling, the mixture was heated at 65 °C for 24h under continuous stirring. The obtained solution was precipitated in an abundance of ice-cold diethyl ether and dried overnight in a vacuum oven at 60 °C. The dried polymer was then evaluated and characterised using [1]H-NMR spectroscopy and size exclusion chromatography.

Yield: 85.5%

[1]H NMR: (300 MHz, CDCl3) δ 4.22 (m, 2H), 3.72 (m, 2H), 1.92 – 1.55 (m, 2H), 1.26 – 0.92 (m, 3H).

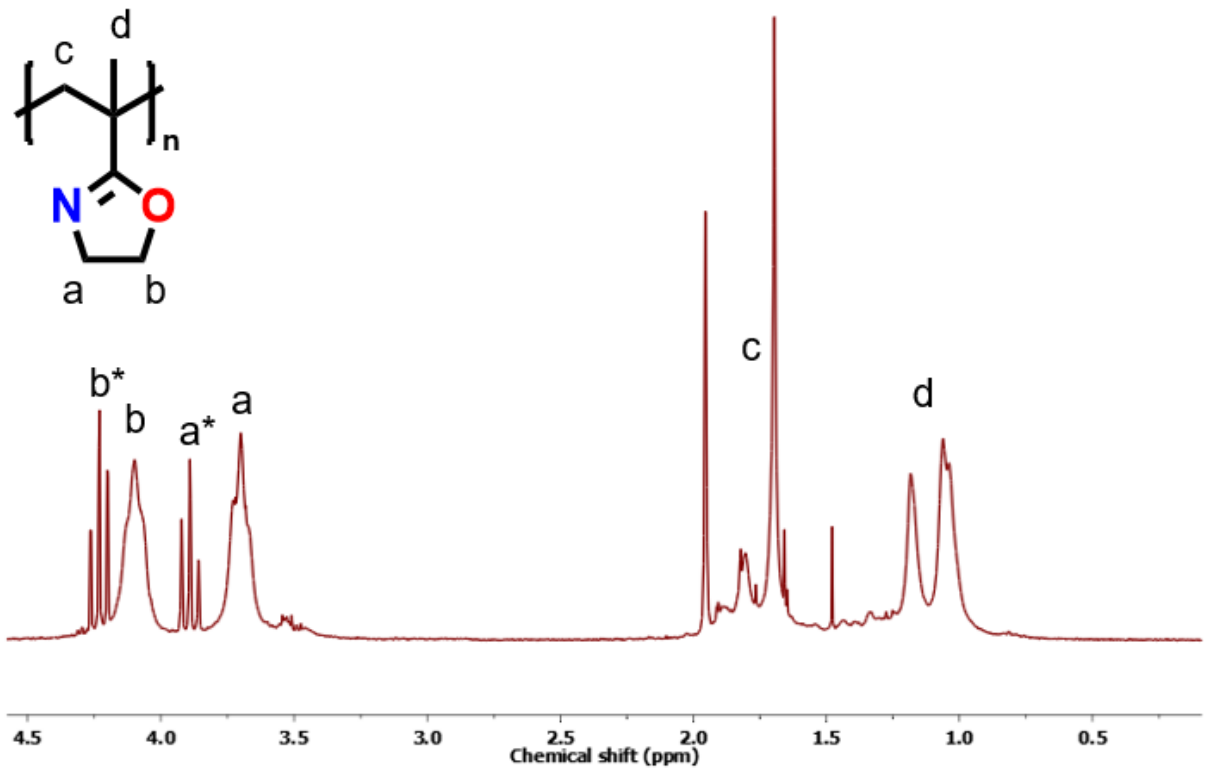

Figure 21 *^{1}H-NMR of bulk synthesised Poly(2-isopropenyl-2-oxazoline) where star-assignments indicate residual monomer units.*

2.4 Solvent electrospinning and membrane crosslinking

Preparation of the crosslinked membranes from the polymer obtained by solution free radical polymerization

Typically, the electrospinning experiments were performed by dissolving the polymer in a mixture of water/ethanol (50/50 vol/vol) to obtain a solution with 20 w% polymer. To this mixture, 10 mol% of succinic acid was added after which the solution was stirred at room temperature until completely dissolved. During the electrospinning procedure, a voltage of 15 keV, a constant flowrate of 0.8 ml/h, and a tip to collector distance of 10 cm were used to enable a stable Taylor-cone and electrospinning process. All processes were performed in a climate chamber (Weisstechnik WEKK 10.50.1500) to maintain a relative humidity of 30% and a constant temperature of 25 °C. After electrospinning, the membranes were heat-treated at 140 °C for 5h to enable an effective reaction between the succinic acid and the pendant 2-oxazoline rings to finally obtain crosslinked nanofiber networks.

Preparation of the crosslinked membranes from the commercial WS-300 polymer

Typically, the electrospinning experiments were performed by dissolving the polymer in a mixture of water/ethanol (10/90 vol/vol) to obtain a solution with 22 w% polymer. To this mixture, 10 mol% of succinic acid was added after which the solution was stirred at room temperature until completely dissolved. During the electrospinning procedure, a voltage of 13 keV, a constant flowrate of 0.5 ml/h, and a tip to collector distance of 10 cm were used to enable a stable Taylor-cone and electrospinning process. All processes were performed in a climate chamber (Weisstechnik WEKK 10.50.1500) to maintain a relative humidity of 30% and a constant temperature of 25 °C. After electrospinning, the membranes were heat-treated at 140 °C for 5h to enable an effective reaction between the succinic acid and the pendant 2-oxazoline rings to finally obtain crosslinked nanofiber networks.2.5 Network functionalisation with colorimetric dyes

Two-step functionalisation procedure

For all samples prepared using the two-step procedure, small samples of 2 cm x 1 cm crosslinked electrospun fibre were prepared and weighed before functionalisation. DMF was added based on their weight to prepare a solution with a concentration of 0.03 M of free oxazoline rings, taking into account the crosslinking degree, i.e., 10 mol%. Based on the

volume of DMF required, the amounts of the three dyes were weighed to finally obtain solution concentrations of 0.1 M (**C_1** and **C_3**) and 0.01 M (**C_4**). The dyes were dissolved in their respective amounts of DMF after which the respective fibrous mat was submerged in the solution. The mixtures with the fibres were capped and heated for 24h at 140 °C. After the reaction, the vials were cooled down to room temperature and the fibres were then removed from the solution. The fibres were washed multiple times using an excess of methanol to remove any residual solvent and free dye. This was repeated until the washing solution appeared colourless. The functionalised networks were then dried for 1h at 100 °C.

One-step functionalisation procedure

For all samples prepared using the one-step procedure, based on the applied weight percentage of the polymer solution in the electrospinning procedure, 5 mol% of the **C_1** compound is dissolved together with 10 mol% of succinic acid in the polymer solution. Due to changes in hydrophilicity and viscosity, membranes were spun with optimised conditions for every different solution. After electrospinning, the membranes were thermally treated for 5h at 140 °C. To remove residual solvent and remaining free dye, the membranes were washed multiple times using an excess of methanol until the washing solution appeared colourless. The resulting networks were then dried for 1h at 100 °C.

2.5 Real-life sample testing

Real-life sample testing setup

To mimic the conditions in food packaging, samples with comparable weight, ranging from 10.5 to 11 grams, were prepared for different food products (cod, beef, and chicken). All food samples used within the same series of tests were obtained the same day from the cooled storage of the local supermarket (Delhaize Ghent Ster, Kortrijksesteenweg 906, 9000 Ghent). Each food sample was placed within a sealable container provided with each of the produced sensor networks (**C_1**, **C_3**, and **C_4**), ensuring no direct contact between the sample and the sensor membranes would be possible. Ambient air tests were sealed with parafilm under normal conditions where nitrogen atmosphere containers were firstly flushed under a strong nitrogen flow for thirty seconds and immediately sealed with additional parafilm afterwards. The sealed container setup is depicted in Figure 22.

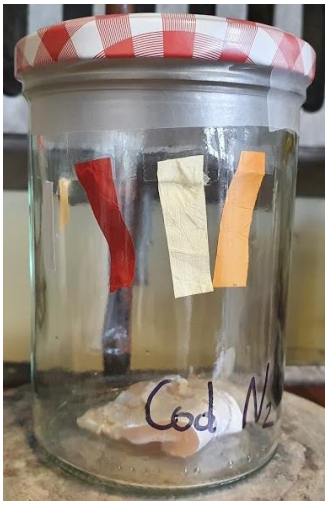

Figure 22 *Real-life sample test setup for a cod sample with all three sensor membranes C_4 (left), C_3 (middle), and C_1 (right).*

The sealed containers are kept at room temperature (average of 21 °C) outside of direct sunlight for a total of 4 to 6 days, depending on the test. Timeframe picture were obtained through the usage of the built-in camera of the smartphone Samsung Galaxy S10e.

Euclidian Colour Distance analysis

The colour change throughout the real-life sample experiments was quantified using the Euclidian Colour Distance. This method utilizes the red (R), green (G) and blue (B) values observed through imaging, which will be used to obtain a three-dimensional vector indicating

the colour change in between different pictures. The first obtained picture of each experiment is used as the reference timepoint for each ECD calculation.

$$ECD = \sqrt{(R_2 - R_1)^2 + (G_2 - G_1)^2 + (B_2 - B_1)^2}$$

3. Results and discussion

3.1 Analyte-responsive dyes

3.1.1 Thiol selective azo dye

To start the construction of a colour-based sensor material, a thiol-sensitive dye molecule must be selected first. This dye is required to be both sensitive for thiol compounds and subsequently capable of transforming the detection into a visible and measurable colour change. Through literature research, a potential candidate was selected, further referenced as compound **C_0** as depicted in Figure 23.

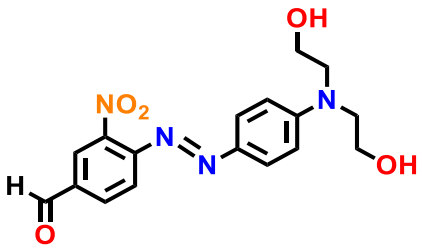

Figure 23 *Molecular structure of compound C_0 reported by Zhang et al.*

Zhang et al. reported the selective responsiveness of **C_0** towards cysteine in solution. This detection resulted in a noticeable hypsochromic shift from 515 nm (pink) to 475 nm (yellow), visible to the naked eye. The capability of detecting cysteine due to reaction with the thiol functionality provided the basis for selection of this day within this study, although it is not certain that the dye will detect VSCs nor that cysteine will be volatile enough to be detected in the gas phase. The mechanism of detection relies on the aldehyde functional group on the central structure of the azo dye. This aldehyde provides a point of attack for nucleophilic addition of thiols as is shown in Figure 24.[101,102] Upon interacting with the thiol, the conjugated push-pull-system of the dye compound is altered, resulting in the colour change.

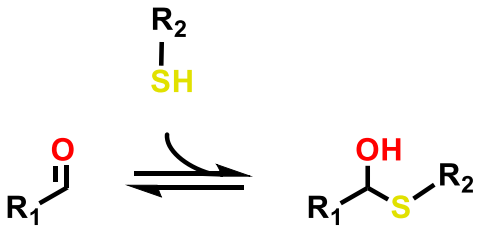

Figure 24 *Reaction mechanism of the nucleophilic addition of thiols to aldehydes.*

The synthesis of Compound **C_0**, as shown below in Figure 25, was performed, and optimised, to obtain the dye. The step-by-step acquired compounds and their purity were evaluated using ^{1}H-NMR spectroscopy in DMSO-*d6*. Preparation of compound **C_0** started from 4-Fluoro-3-nitrobenzaldehyde **1**, as depicted in Figure 26. First, the fluor group was replaced via nucleophilic substitution by an amino group resulting in the aniline **2**, with the corresponding shift of the neighbouring, aromatic -*CH* proton from 7.7 to 7.2 ppm. Then the aniline was converted into the diazonium salt and reacted with *N*-phenyldiethanolamine (N-PDE) **3** to obtain the resulting azo dye **4** after column chromatography. The final product displayed the characteristic doublet peaks of the coupled N-Phenyldiethanolamine at 7.7 and 7.75 ppm. In the final product **4** traces of N-PDE and DCM could still be observed at 7.2 ppm and 5.3 respectively. These minor impurities did not interfere with the response rate analysis and therefore did not influence the modest response signal of the obtained molecule. Furthermore, the synthesis of **C_0** reported a low overall yield of 14 % due to excessive purification by column chromatography over SiO_2.

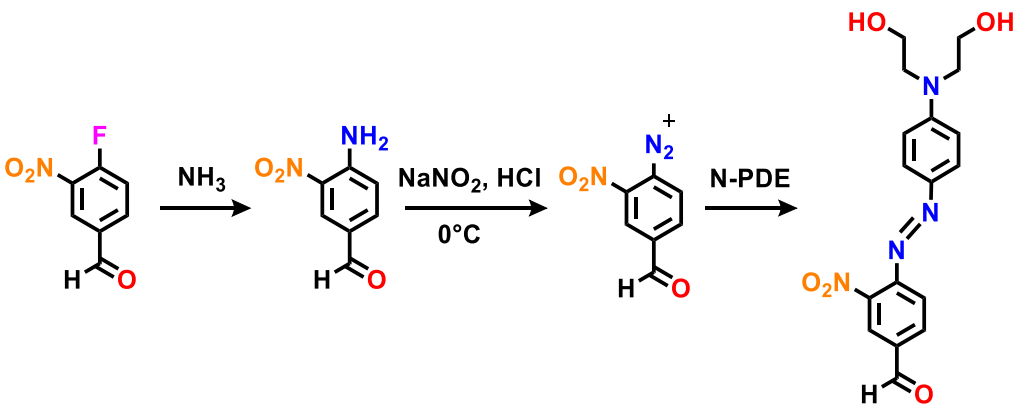

Figure 25 *Synthesis route of compound C_0.*

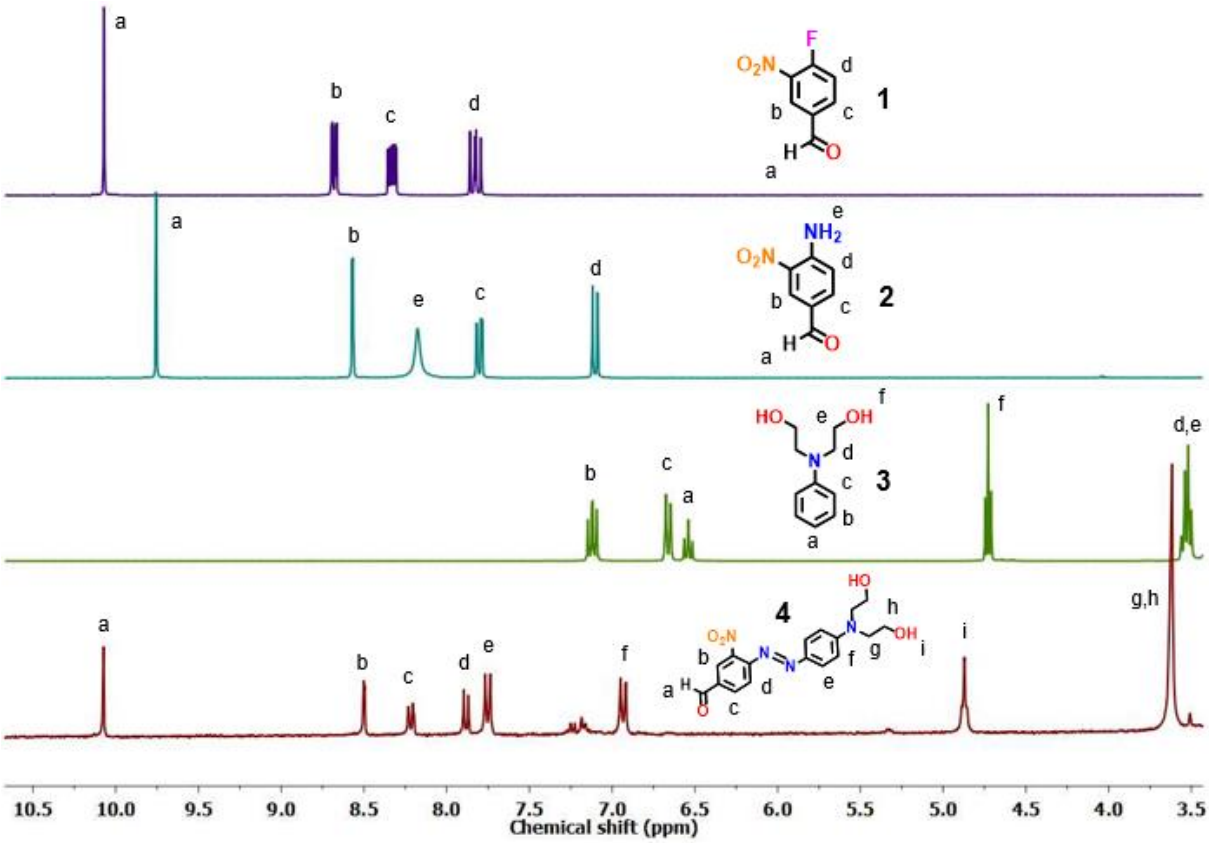

Figure 26 ^{1}H-NMR spectra of compound C_0 synthesis.

3.1.2 Response rate analysis

Colour characterisation of the abovementioned azo dye was performed by transmission UV-Vis spectroscopy. This technique allows the analysis of the compound-specific absorption pattern within the visible and ultraviolet wavelength spectrum. To be applicable within this work on sensors, the dye molecule is required to show a distinctive change in absorption upon detection of its analyte. For the envisioned application, the change in absorption must be detectable to the naked eye.

To analyse the responsiveness of compound **C_0**, a titration of the analyte to a dye solution (2 x 10^{-5} M) was performed together with an evaluation of the absorption spectrum after each step. As the compound detects its analyte, the absorption maximum is expected to shift resulting in a colour change. During the titration, a slight hypsochromic shift of the absorption maximum is observed upon the addition of 6000 ppm of cysteine-ethyl ester, as depicted in Figure 27a. The visual response of this test illustrated that compound **C_0** is not providing the colour change to the extent that was expected based on literature.

Detection is only observed upon the addition of high quantities of cysteine-ethyl ester. Only after the addition of 3000 - 4000 ppm cysteine-ethyl ester, the hypsochromic shift can be observed. Safety regulations of food products however limit the permitted concentration of spoilage analytes in packaging headspace to much lower amounts, typically in the range of 500 ppm, thus the detection of the depicted high concentrations is outside the scope of this study. Furthermore, the shift of absorption maximum itself is smaller than anticipated, as can be seen in Figure 27b. Plotting the UV absorption maxima in function of the added concentration confirms the abovementioned shift. However, the shift is less than 10 nm and is unfit for naked-eye detection. Based on these results, it was concluded to exclude the **C_0** compound from further study and to evaluate alternative dyes.

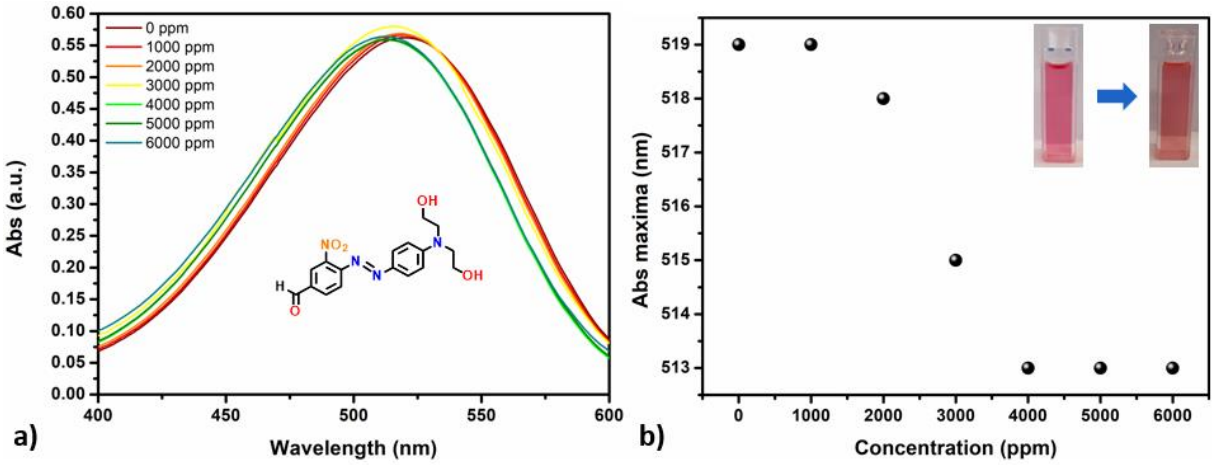

Figure 27 *a) Absorption spectrum of C_0 (2 x 10^{-5} M) upon stepwise addition of cysteine ethyl ester. b) Absorption maximum plot and pictures of corresponding solutions of C_0 in DMSO with 0 ppm (left) and 6000 ppm cysteine ethyl ester (right).*

3.2 Sensor array

To find new potential compounds, the specific application of the dyes was put into a broader context. Within the spoiling scenario, not only thiols are formed due to microbiological activity. Other analytes such as amines and environmental characteristics are also indicators of spoilage. As such, multiple dyes will be combined into a sensor array, with their sensing application targeted to different aspects within spoilage. Combining them into a sensor array will provide a larger and more significant amount of information (pattern recognition) on the freshness state of the food product.[103,104] Furthermore, in the prospect of the eventual need of immobilization of the dyes to a carrier material, they will also be selected based on having a chemical handle for linkage or being easily modifiable to obtain such a linking unit. Based on these criteria, three dyes were selected for further investigation: (E)-4-((4-hydroxyphenyl)diazenyl)benzoic acid (**C_1**), Disperse Red 1 (**C_2**), and Ellman's reagent (**C_3**).

3.2.1 Halochromic dyes

The pH is an important indicator of food spoilage as acidification can occur during the early stages of degradation due to the bacterial metabolism of the readily available sugars present in food products. These acids could be released into the headspace of the packaging and act as an early indicator of spoilage by protonating indicator dyes. During later phases of the spoiling process, amines are formed as the final decomposition products of proteins in food. The presence of these free amines, which function as proton acceptors, can deprotonate indicator dyes.[105,106] Therefore, acid and base monitoring will play an essential role within the sensor array. Both **C_1** and **C_2** are promising candidates to detect the abovementioned release of acids and bases, where **C_1** will be implemented to be deprotonated by the amines, and **C_2** can be protonated by acids.

3.2.1.1 (E)-4-((4-hydroxyphenyl)diazenyl)benzoic acid

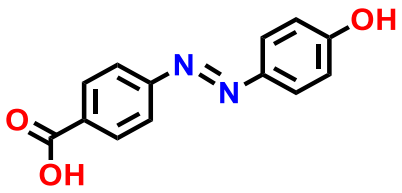

Figure 28 *Chemical structure of (E)-4-((4-hydroxyphenyl)diazenyl)benzoic acid (C_1).*

The first pH-sensitive dye, (E)-4-((4-hydroxyphenyl)diazenyl)benzoic acid (**C_1**), was selected on the presence of a phenolic alcohol group and its pKa value. Due to the electron pull from this

azo structure, the alcohol its pKa value is shifted to a lower value of 8.7, making it more available for deprotonation. As such, the alcohol can function as a pH detector through the capability of losing its proton. The potential acid-base interaction makes the compound sensitive for amines within the food spoiling sector, as they will function as recipients for the protons. The deprotonation will result in an electron shift within the conjugated pi-system of the chromophore, which influences the absorption spectrum and the observed colour of the compound. Furthermore, the compound contains an available carboxylic functional group that can act as a chemical handle for immobilization to a carrier platform.

Due to commercial unavailability, **C_1** was synthesized in-house during this project following the synthesis method depicted in Figure 29. The 4-aminobenzoic acid was first mixed with the $NaNO_2$ in an acidic aqueous solution to obtain the diazonium salt as a yellow paste. During the subsequent diazotization reaction, the obtained diazonium compound was coupled to phenol under basic conditions, resulting in the product as a bright orange powder. The coupling reaction was confirmed by the complete disappearance of the amine peak from structure **1** at 5.85 ppm and the shift of the phenolic protons present in the azo dye **2** to 7 - 8 ppm, as displayed in Figure 30. The ^{1}H-NMR spectroscopy confirms the purity and structure of the azo dye, and it was used without further purification. Due to the activating nature of the hydroxyl group in the phenol molecule, the *para*- position is readily available for electrophilic substitution leading to a high purity product, without the need for column chromatography, and a yield of 47 %.

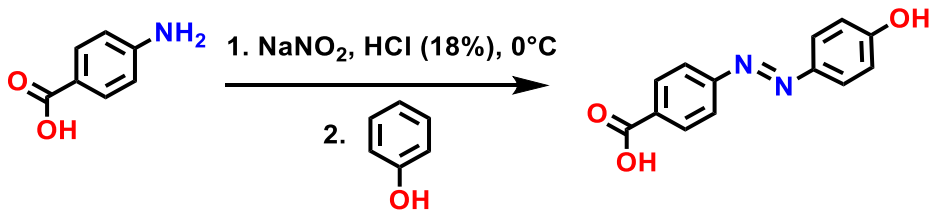

Figure 29 *Synthesis route of (E)-4-((4-hydroxyphenyl)diazenyl)benzoic acid (C_1).*

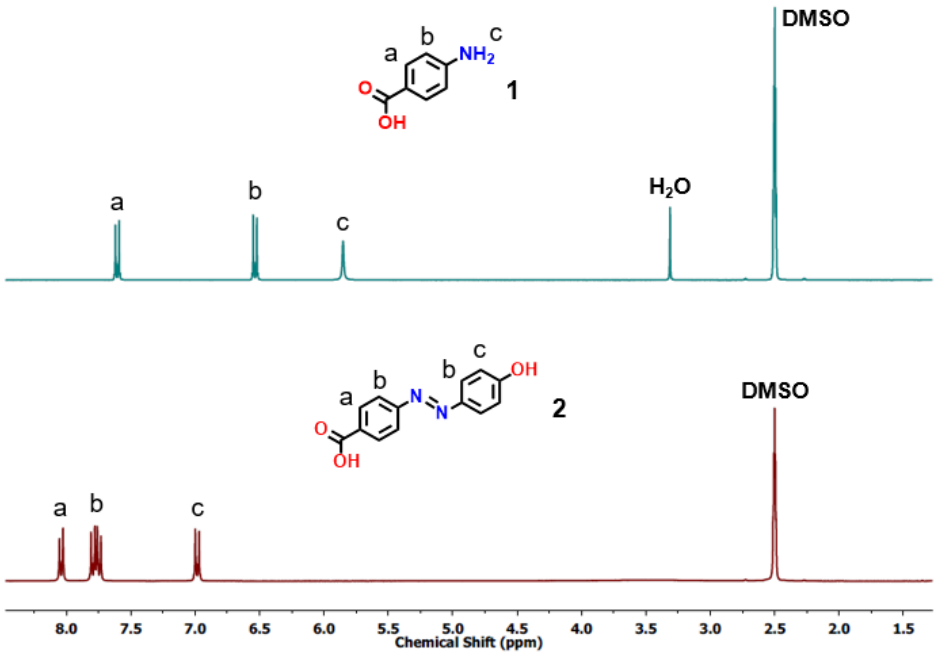

Figure 30 ^{1}H-NMR spectra of compound C_1 synthesis.

After synthesis, the response rate of **C_1** was evaluated by a pH titration followed by UV-Vis spectroscopy, illustrated in Figure 31a. A dye solution of 2 x 10^{-5} M was prepared in a 50/50 methanol-water mixture and a NaOH solution (0.1 M) was added stepwise to gradually change the pH of the solution. The titration illustrated a halochromic shift of the absorption maximum with a new absorption maximum at 454 nm. Figure 31b displays a plot of the absorption measured at 454 nm throughout the pH titration ranging from 4 to 12, indicating a pKa of 8.7. As TMA, one of the main spoilage related amines, has a pKa of 9.81, it is capable of deprotonating the **C_1** dye, thus allowing for effective amine detection using this dye compound. This switching from the protonated to the deprotonated form of **C_1** can be observed through the appearance of the peak maximum at 454 nm. This protonation change resulted in a colour shift ranging from orange in the protonated state to a dark-yellow deprotonated state.

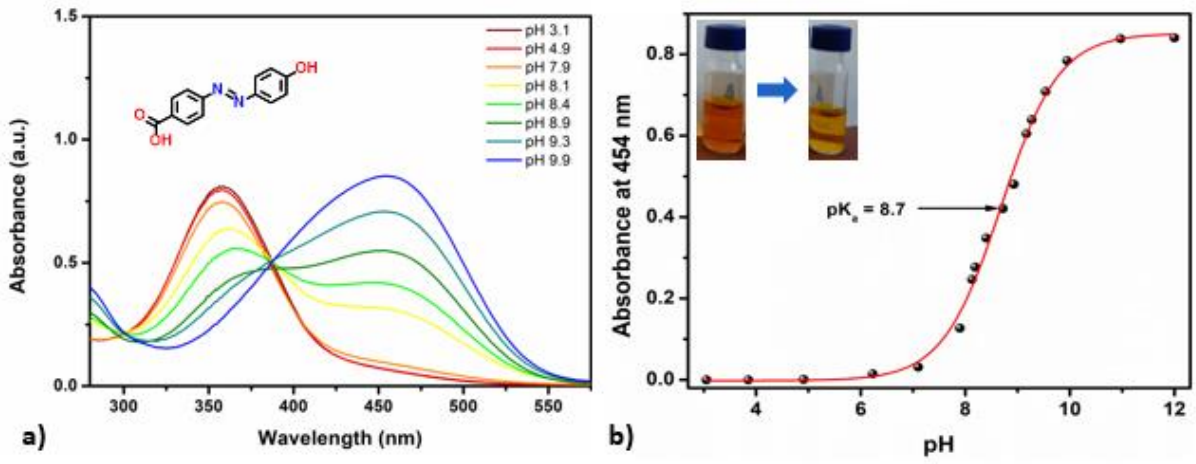

Figure 31 *a) Absorption spectrum of C_1 (2 x 10^{-5} M) through pH titration. b) Absorption at 454 nm of C_1 through pH titration and pictures of corresponding solutions of C_1 in methanol-water solutions at pH 3 (left) and pH 12 (right).*

3.2.1.2 Disperse red 1

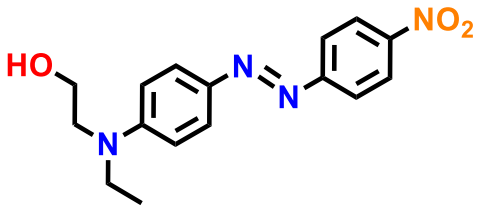

Figure 32 *Chemical structure of Disperse Red 1 (C_2).*

The second pH sensing dye, Disperse Red 1 (**C_2**), is a commercially available dye mainly used for dyeing of textile fabric. As mentioned earlier, the determination and monitoring of pH change in food packaging are quite important. In literature, it was described that Disperse Red 1 could perform as a pH indicator for the acidic compounds, forming the monoprotonated ammonium form. However, depending on the pH, a double protonated species could also be produced, forming the azonium ammonium, which might be responsible for high red shifts. This mechanism, however, is still under discussion and further spectroscopic studies are required.[107] Therefore, the halochromic effect of **C_2** was also investigated with the addition of HCl (1 M in water) to the dye solution (2 x 10-5 M) in a methanol-water mixture. The change in the UV-vis absorption spectra of the dye upon addition of acid is illustrated in Figure 33. Upon addition of HCl to a dye solution, a major colour change was observed from orange to red-pink with the appearance of a new absorption band at 525 nm and a well-defined isosbestic point at ca. 474 nm. During food spoilage, acidic compounds are formed, such as lactic acid, butyric acid with a pKa value of 3.8 and 4.8, respectively. Although its response

might be limited due to the low pKa value of 2.1, **C_2** will be included in the sensor array for potential monitoring of acidic compounds.

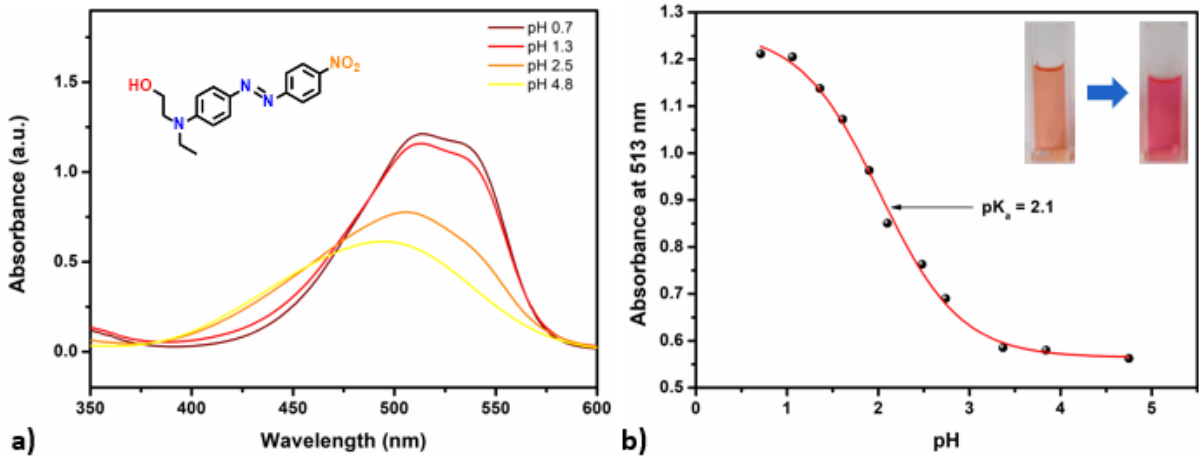

Figure 33 *a) Absorption spectrum of C_2 through pH titration. b) Absorption at 513 nm of C_2 through pH titration and pictures of corresponding solutions of C_2 in methanol-water at pH 7.8 (left) and pH 0.7 (right).*

To enable the immobilization of the dyes, a chemical handle is required. As discussed in the previous section, the primary alcohol group present in **C_2** allows for further modification to a useable chemical handle for coupling the PiPOx nanofibers. In line with the other dye compounds, the introduction of a carboxylic acid was chosen. As displayed below in Figure 34, the alcohol was modified to a carboxylic acid in a simple one-step synthesis using succinic anhydride, resulting in the production of (E)-4-(2-(ethyl(4-((4-nitrophenyl)diazenyl)phenyl)amino)ethoxy)-4-oxobutanoic acid (**C_4**). The reaction of Disperse red 1 with succinic anhydride resulted in a nearly quantitative reaction yield for the final product. Purification by column chromatography over silica, however, limited the overall yield to 51 %. The reaction was confirmed by ^{1}H-NMR spectroscopy, as displayed in Figure 35, showing the appearance of the ester from the modified structure **2** at 4.35 ppm in comparison to the initial -*CH_2*-OH peak residing at ca. 3.55 for Disperse Red 1 **1**. Furthermore, the additional peak for both the central -*CH_2*- groups from the added succinic anhydride can be observed at 2.64 ppm.

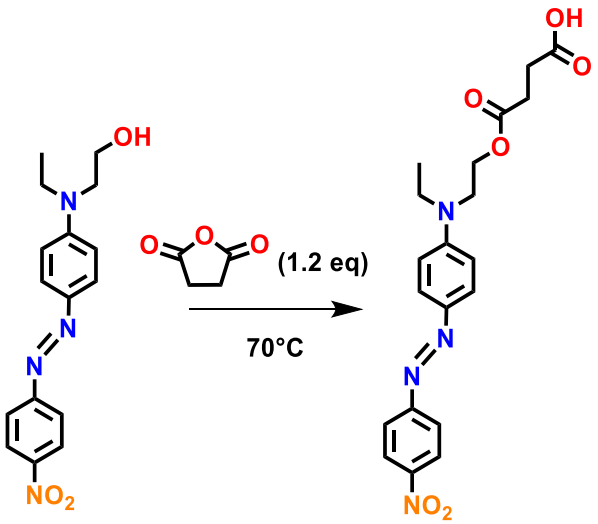

Figure 34 Synthesis route of (E)-4-(2-(ethyl(4-((4-nitrophenyl)diazenyl)phenyl)amino)ethoxy)-4-oxobutanoic acid (C_4).

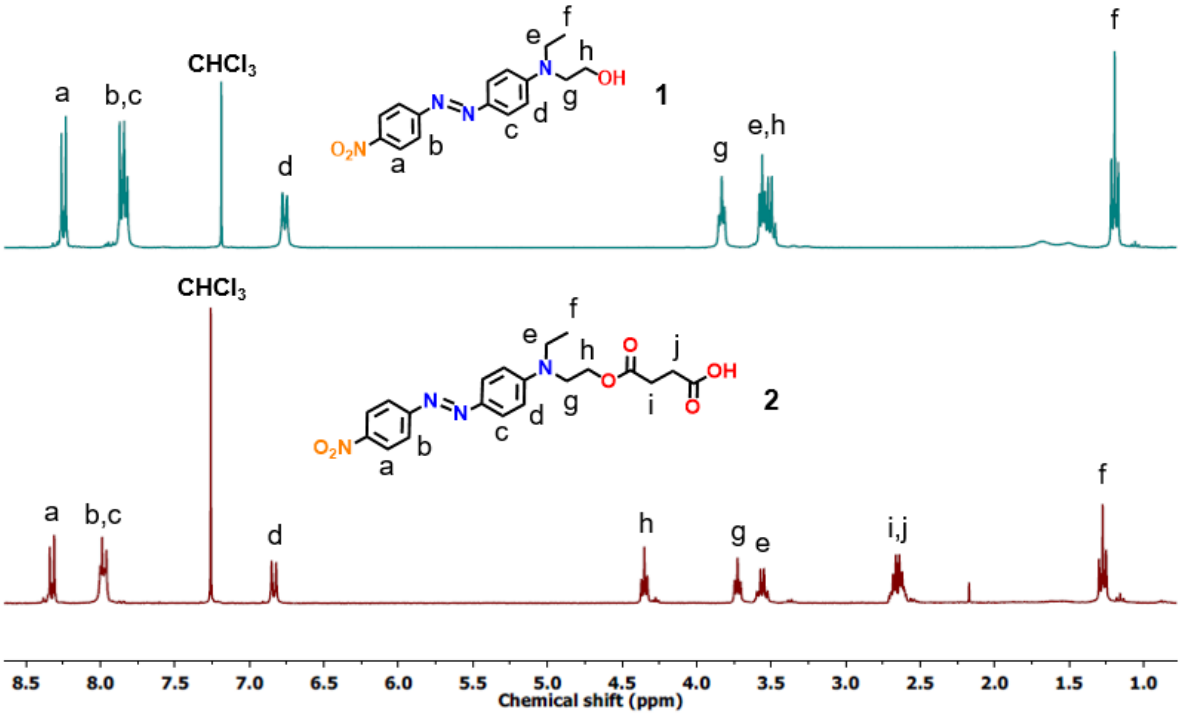

Figure 35 1H-NMR spectra of compound C4 synthesis.

3.2.2 Thiol-sensitive dyes

3.2.2.1 Ellman's reagent

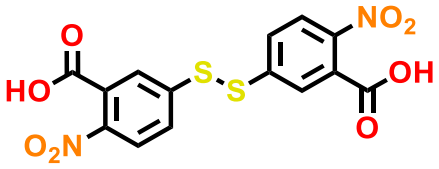

Figure 36 Chemical structure of Ellman's reagent (C_3).

The third and final candidate for the sensor array is Ellman's reagent (**C_3**). This dye is proposed to target the same analyte as the previously described compound **C_0**, namely thiols. The molecule is commercially available and is a routinely used dye for detecting thiols in solution.[108–111] Various Researchers report the use of **C_3** in quantitative thiol detection in solution with a characteristic colour change upon thiol detection from colourless solutions to a distinctive yellow colour. Thiols react with this compound, cleaving the disulfide bond to give 2-nitro-5-thiobenzoate (TNB^-), as depicted in Figure 37, which gives rise to the characteristic yellow colour.[108–111]

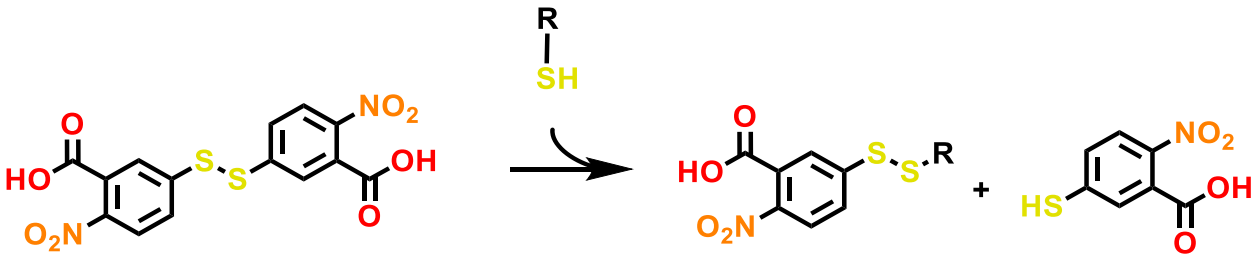

Figure 37 *Ellman's reagent mechanism of thiol detection.*

To evaluate the response rate, a dye solution of 2 x 10^{-5} M was prepared in a DMSO and stepwise amounts of 5 ppm cysteine-ethyl ester in water were added. The titration, as shown in Figure 38, illustrated a clear colour shift upon addition at low concentrations, indicating the formation of TNB^-. Switching from the disulfide product **C_3** to the cleaved product can be observed through the appearance of the peak at ca. 500 nm. Structurally, Ellman's reagent provides two carboxylic acids available for immobilization on a carrier material, further increasing the potential of Ellman's reagent as a candidate within this project.

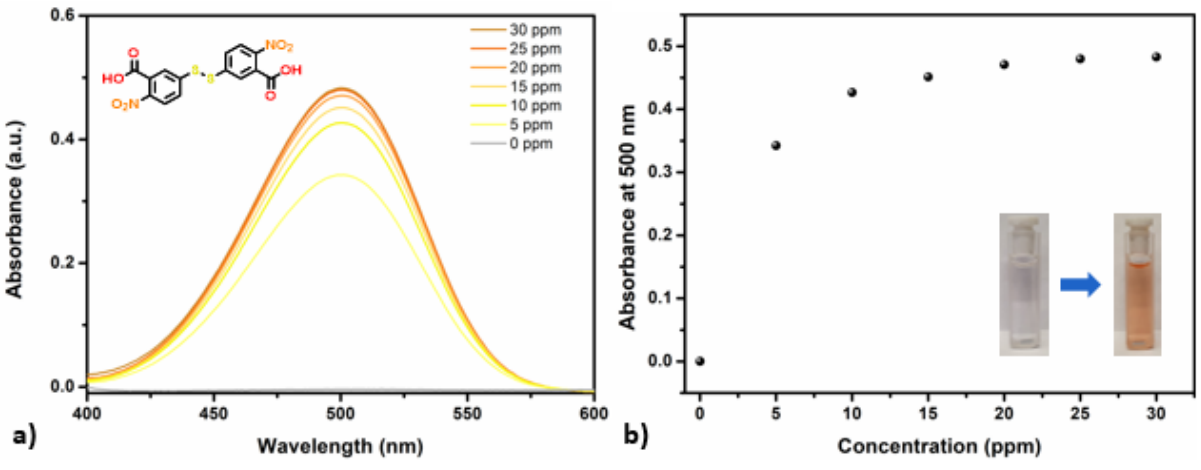

Figure 38 *a) Absorption spectrum of C_3 (2 x 10^{-5} M) upon stepwise addition of cysteine ethyl ester. b) Absorption at 500 nm of C_3 and pictures of corresponding solutions of C_3 in DMSO with 0 ppm (left) and 30 ppm cysteine ethyl ester (right).*

3.3 Colorimetric sensor carrier material

As mentioned in the introduction, colorimetric sensors have already been widely studied in literature and various applications have already been developed. The popularity of colour-based sensors can be understood due to their ease of use and self-explanatory, naked-eye detection signals. However, the subset of solid-state colorimetric sensors utilising a functional carrier material to immobilize their colourants, which is the scope of this research, often requires tedious chemical modifications or harsh reaction conditions. Leading to low valorisation potential and highly niche applications. Two different types of dye immobilization were observed in the literature, the use of ionic interactions between carrier platform and dye compounds, as is seen with the colour catcher©[58,64,112], and covalent linkage to a carrier material.[57,65,113] The first technique of using ionic interactions to link the dye to a charged carrier material is simple, efficient, and straightforward, but limits the applicability only to ionisable dye molecules, potentially inhibiting the sensing mechanism.[105,112,114,115] Furthermore, as discussed in section 2.2.1, the problem of possible dye leaching due to the non-covalent character of the materials holds a serious, undesirable risk within food applications.

The second group, which uses the covalent attachment method, forms the focus group within this research. It proves, however, to be challenging to find compatible dye-carrier combinations. Aigner et al. displayed the use of click chemistry to conjugate the sensing structure to a carrier matrix. This is made possible through a modification of the sensing structure with a pentafluorophenyl group capable of attaching itself to mercapto groups present on the carrier material through thiol-ene reactions.[113] Other studies include reactive groups, such as iodo-phenyl, cyanuric chloride, or other halogenated groups, in the sensing molecule which are capable of engaging in conjugation reactions.[116,117] Due to the necessity of very specific chemical structures required for the conjugation reactions, often tedious chemical reactions or harsh conditions are required to obtain immobilization of the responsive dye molecules. Thus, limiting the choice of available dyes and carrier matrices.

In this research, the proposed carrier material is poly(2-isopropenyl-2-oxazoline) (PiPOx) which is a promising candidate, as it complies with the two aspects mentioned above. The PiPOx polymer is a versatile material, capable of covalently binding a large number of different

molecules (e.g., dyes) in a single step due to its reactivity with a common set of chemical ‘handles’, i.e., carboxylic groups.

3.3.1 Poly(2-isopropenyl-2-oxazoline)

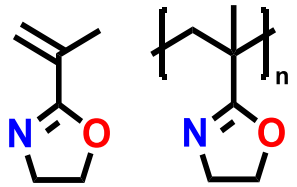

Figure 39 *Chemical structure of iPOx (left) and PiPOx (right).*

2-Isopropenyl-2-oxazoline (iPOx) is a monomer belonging to the 2-oxazolines class, which via its 2-vinyl substituent can be polymerized to PiPOx with the retention of the 2-oxazoline ring as reactive side-chain functionality. The polymerization of iPOx can be performed in several ways including free radical polymerization (FRP), Reversible addition−fragmentation chain transfer (RAFT) polymerization and single electron transfer living radical polymerization (SET-LRP).[118–121] During this project the FRP will be applied due to ease of use and since the material will be crosslinked for the application.

The polymer itself is easy to store as it shows high solubility in several organic solvents and water. In storage, it has chemical inertness to both moisture and oxygen, and good thermal stability resulting in a facile and safely storable polymer.[122–124] In terms of functionality, it offers a versatile chemical unit through the 2-oxazoline side chains. This 2-oxazoline ring has proven to be highly efficient for post-functionalisation of the polymer chains as it can engage in ring-opening addition reactions with several chemical groups, including carboxylic acids as depicted in Figure 40.[125] If the desired compound contains a carboxylic acid group, then rapid functionalization can be achieved at elevated temperatures without the need of catalysts or the formation of by-products.[121,122,125]

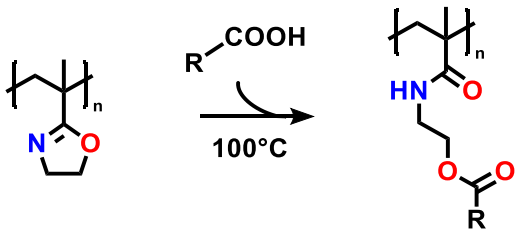

Figure 40 *Reaction mechanism for functionalisation of PiPOx with Carboxylic acids.*

Furthermore, to be applied within any food-related setting, the carrier material is required to be safe for human health. PiPOx fulfils this requirement as it is proven to be non-cytotoxic after direct administration to cells, even at concentrations of 10 mg/ml. Since the polymer has no noticeable negative effect on cell viability and shows such versatile usage for functionalisation, it has also been promoted in several fields in biomedicine.[121,125]

3.3.2 Polymerization

Within this project, the FRP procedure was optimised for PiPOx synthesis to obtain polymerization conditions that lead to high monomer conversion, which previously was reported to be challenging, as well as a polymer molecular weight useable in electrospinning. Solvent electrospinning requires polymer solutions with sufficient high viscosity of the polymer solution, which is related to the polymer chain entanglement. To obtain these chain entanglements a certain degree of polymerization (DP) should be present. This DP or chain length is characterised by three key molar mass values, Mn, Mw, and Mp, displayed in kg/mol. Based on the literature, an estimation was made that solvent electrospinning spinning would require polymers with an Mn of roughly 30 kg/mol to produce narrow nanofibrous materials[81], albeit this will strongly vary with polymer structure and the solvent.

The conditions that were optimised include the type of initiator, initiator concentration and monomer concentration as noted in Table 1. All polymers were characterised by size exclusion chromatography with a light scattering detector (SEC-LS) and ^{1}H-NMR spectroscopy. At the start, an estimation of the most efficient initiator was made by comparing different azo-initiators V-70, VA-044, and AIBN, each at the reported temperatures resulting in an initiator half-life time of 10 hours. According to the obtained results, AIBN proved to be the most promising candidate, as V-70 resulted in both low molecular weight polymers and low conversion. Although VA-044 illustrated similar results as AIBN, solubility issues in DMSO resulted in irreproducibility among different polymer batches. Therefore, further optimisation was performed using AIBN. The next step consisted of obtaining an optimal initiator to monomer ratio in terms of conversion. As expected, an increase of molecular weight was observed with increasing monomer concentration due to the higher abundance of monomer units compared to the number of growing chains. Furthermore, increasing the initiator concentration resulted in lower molecular weight polymers due to the increased concentration of radicals. Combining both trends resulted in an optimal monomer to initiator

ratio of 267, utilising both a monomer concentration of 4 mol/l and an initiator concentration of 0.015 mol/l. These parameters provided polymers with a conversion of 57 % and an Mn of 34 kg/mol.

Table 1 *Polymerization parameters for FRP of PiPOx.*

[Monomer] (mol/l)	Initiator	[Initiator] (mol/l)	T (°C)	Mn (kg/mol)[a]	Đ[a]	Conversion (%)[b]
2	V-70	0.009	30	13.6	1.44	39
2	VA-044	0.009	44	30.1	1.54	47
2	AIBN	0.009	65	27.5	1.48	45
4	AIBN	0.009	65	55.8	1.41	41
6	AIBN	0.009	65	88.2	1.33	37
2	AIBN	0.015	65	23.6	1.52	51
2	AIBN	0.02	65	14.1	1.57	46
4	AIBN	0.015	65	34.4	1.52	57

[a] Determined using DMA SEC-LS.
[b] Calculated using ^{1}H-NMR spectrum in $CHCl_3$.

Next to solution FRP, a second polymerization method was utilised, bulk FRP, hereby directly dissolving the initiator in the pure monomer. This technique was included as it often leads to higher monomer conversion, potentially resulting in a more profitable synthesis method. The conditions applied for bulk polymerization were based on the already optimised procedure for solution FRP and are shown in Table 2.

Table 2 *Polymerization parameters for Bulk FRP of PiPOx.*

[Monomer] (mol/l)	Initiator	[Initiator] (mol/l)	T (°C)
28.6	AIBN	0.015	65

The comparison of both polymers is shown in Table 3, with an Mn value of 36.2 kg/mol and dispersity of 1.48, and 69.9 kg/mol with a dispersity of 2.76 for FRP and bulk, respectively. The respective conversion of 53.7 % and 85.5 % illustrated the anticipated higher conversions during bulk polymerizations.

Table 3 polymerization results and characteristics.

Technique	Mn (kg/mol)[a]	Mw (kg/mol)[a]	Mp (kg/mol)[a]	Đ[a]	Conversion (%)[b]
FRP	36.2	53.4	53.7	1.48	53.7
Bulk	69.9	63.6	192.6	2.76	85.5

[a] Determined using DMA SEC-LS.
[b] Calculated using ^{1}H-NMR spectrum in $CHCl_3$.

Both SEC traces are depicted in Figure 41, indicating a monomodal distribution for the polymer obtained in solution and a bimodal distribution for the bulk polymerization. Although the peak maximum of both plots is situated at the same time value, a large shoulder is observed in the bulk polymer, presumably due to the gelation of the polymer mixture.[126,127]

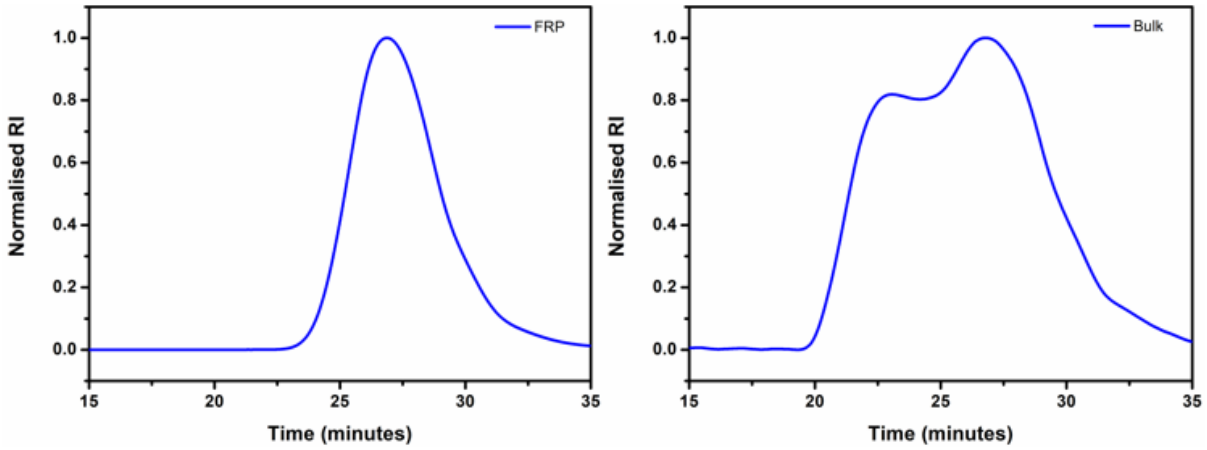

Figure 41 SEC traces of PiPOx synthesized by FRP in solution (left) and bulk (right).

3.3.3 WS-300

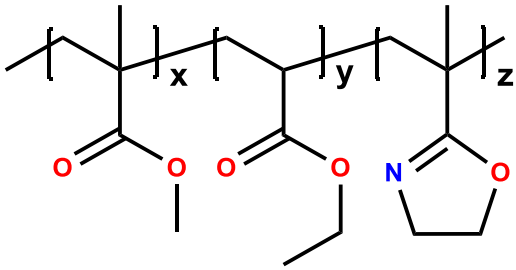

Figure 42 Chemical structure of WS-300.

In the scope of further valorisation of this work, a commercially available iPOx based copolymer is also included within this study, namely WS-300, which is a terpolymer composed of 70% iPOx and a 30% mixture of ethyl acrylate and methyl methacrylate. Electrospinning this

commercial material could pave the way towards an upscalable sensor production without the need for any polymerization chemistry and expertise.

SEC-analysis of the commercial polymer revealed a broad polymer peak, as shown in Figure 43, with an Mn value of ~70 kg/mol and a Đ of 4.26 according to PMMA standards, indicating a non-controlled polymerization system. Furthermore, ^{1}H-NMR spectroscopy confirmed the mainly iPOx-based terpolymer composition with the addition of the methyl and ethyl ester peaks, as displayed in Figure 44.

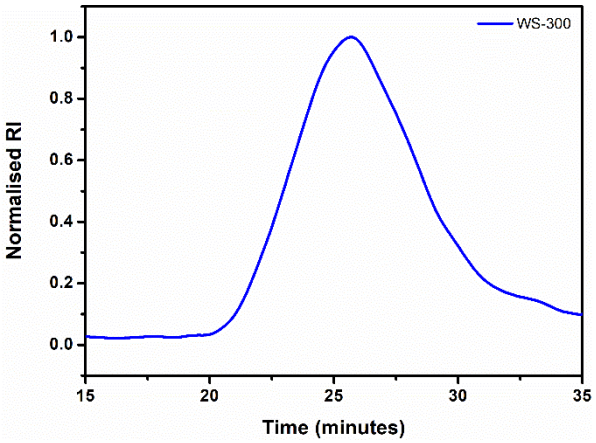

Figure 43 Sec trace of WS-300.

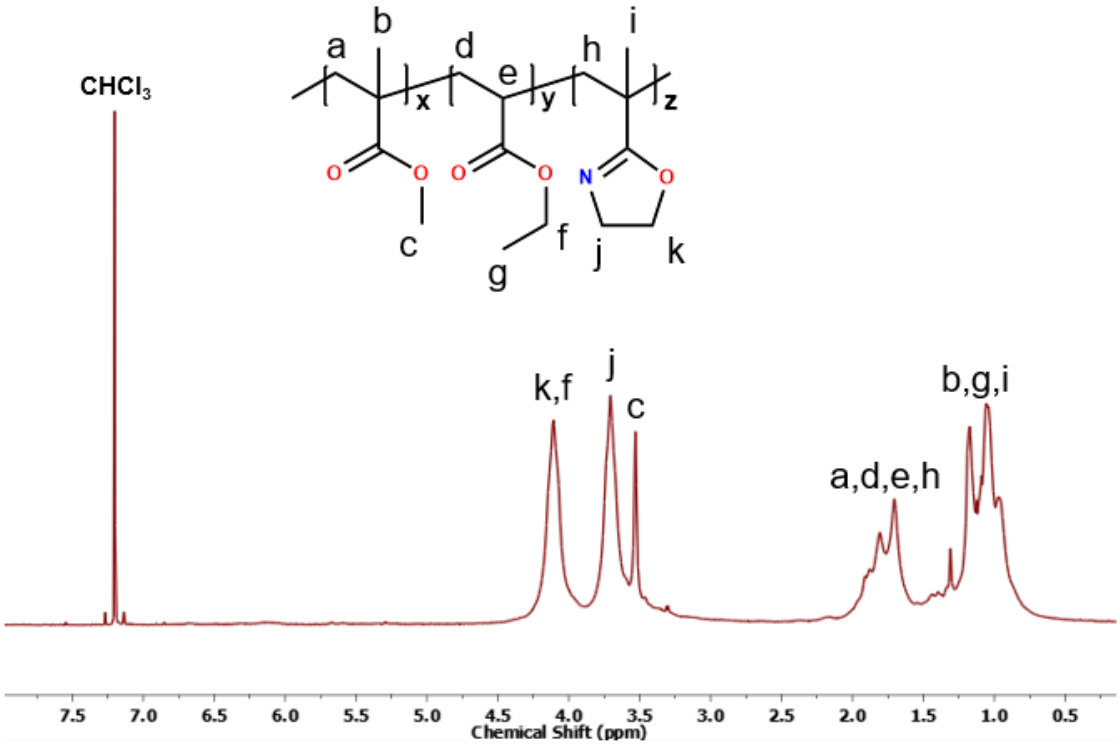

Figure 44 ^{1}H-NMR spectrum of WS-300.

3.4 Electrospinning

To design a sensor, the abovementioned dyes must be incorporated in the PiPOx support material. Nanofibrous membranes have already proven to behave well as ultra-sensitive sensor materials thanks to the large specific surface area created by the many pores between the fibres of sub-micron thickness.[77,78,128,129] To produce these thin fibres, which is commonly done by electrospinning, high molar mass polymers are typically required to form the necessary chain entanglements that keep the fibrous structure together. In line with the larger environmental scope of the application, ecologically friendly solvent electrospinning was chosen as the preferred processing method. In contrast to conventional solvent electrospinning where toxic solvents such as DMF were used. In this project, the PiPOx, for which electrospinning was never reported before, will be processed in green solvent mixtures consisting of ethanol and water. Furthermore, the experimental set-up contains a rotating collector drum to assure reproducibility processing and homogeneity in between membranes, as depicted in Figure 45.[130]

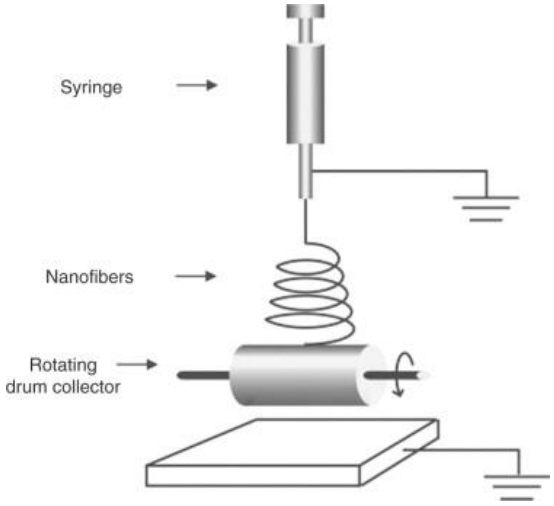

Figure 45 *Electrospinning setup with a rotating collector drum.*

3.4.1 Electrospinning procedure optimisation

To obtain well-defined nanofibers through electrospinning, several parameters must be considered as discussed in the introduction, including external parameters, such as temperature, ambient humidity, the weight percentage of the polymer solution, and the used solvents, as well as characteristics of the electrospinning setup itself, such as distance from needle to collector plane, applied voltage, and the solution feed rate. Within this research, an

optimisation study was performed on the abovementioned conditions to obtain high-quality membranes via a reproducible production process.

The temperature and ambient humidity were chosen to be kept constant at room temperature and 30% relative humidity. The optimisation was mainly focused on the solvent medium and the dissolved weight percentage of the polymer. Firstly, the solution itself is required to evaporate within the short travel distance between the needle tip and the collector plane. Therefore, the 50:50 water-ethanol ratio was chosen. Secondly, the polymer solution needs to be adequately viscous to allow efficient electrospinning without bead formation. To produce thin nanofibrous membranes, sufficient polymer concentrations are typically required to form the necessary chain entanglements that keep the fibrous structure together. Finally, the feed rate and source voltage were chosen according to the literature and previous experience of the research groups.[81] The final optimised set of conditions applied for electrospinning are noted in Table 4.

Table 4 *Optimised electrospinning parameters for PiPOx.*

Weight percentage polymer (%)	H_2O-ethanol ratio	Relative humidity (%)	Tip-Collector distance (cm)	Voltage (keV)	Feed rate (ml/h)	Diameter (nm)[a]	SD (nm)[a]
20	50/50	30	10	15	0.8	458	91

[a] Determined using SEM image analysis

Processing the PiPOx obtained by solution FRP resulted in well-defined, low diameter fibres with a high surface-to-volume ratio. The obtained nanofibrous membranes were analysed through scanning electron microscopy (SEM), displaying an average fibre diameter of 458 ± 91 nm, as depicted in Figure 46a.

Based on the previously optimised parameters for FRP polymers, a new set of parameters was optimised for solvent electrospinning of the commercial WS-300 polymer, as shown in Table 5. The polymer was effectively processed into nanofibers with a diameter of 168 ± 33 nm, as observed through SEM-imaging displayed in Figure 46b. The decrease in fibre diameter can be explained by the influence of the longer chain length resulting in more chain entanglements. Furthermore, the solvent ratio was altered due to the more hydrophobic character of WS-300, originating from the ester functionalities in the backbone.

Table 5 Optimised electrospinning parameters for WS-300.

Weight percentage polymer (%)	H_2O-ethanol ratio	Relative humidity (%)	Tip-Collector distance (cm)	Voltage (keV)	Feed rate (ml/h)	Diameter (nm)[a]	SD (nm)[a]
22	90/10	30	10	13	0.5	168	33

[a] Determined using SEM image analysis

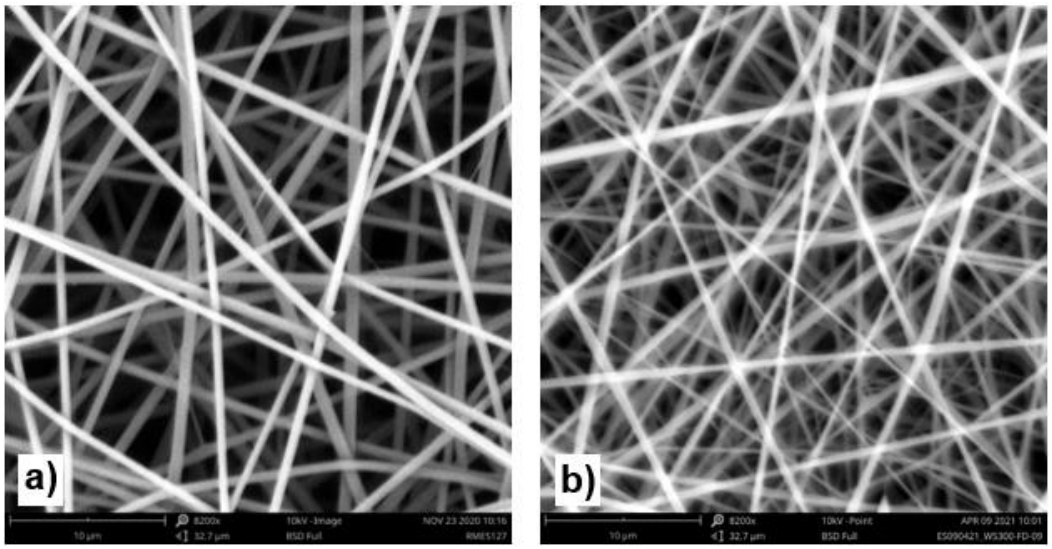

Figure 46 SEM images of the electrospun nanofibers of a) FRP and b) WS-300.

For the PiPOx synthesised in bulk, electrospinning was also attempted starting from the optimised conditions obtained for the polymer obtained by solution FRP. This, however, turned out to be very difficult, as throughout the experiments no fibres were obtained, likely due to a too high viscosity resulting from the higher molar mass of this polymer. Due to time constraints, the bulk polymers were chosen to be excluded from the scope of the thesis.

3.4.2 Mixture electrospinning

As the envisioned applications require stable nanofibers the hydrophilic PiPOx nanofibrous need to be crosslinked into a nanofibrous network, for which the inclusion of dicarboxylic acid in the fibre membrane will be required. In this study, one-pot electrospinning of PiPOx with added succinic acid was studied. Herein, succinic acid is included in the polymer solution during the electrospinning procedure, thus placing the succinic acid inside the obtained fibres. Having the succinic acid be electrospun together with the polymer may provide a valuable advantage over post electrospinning addition as it limits the number of processing steps, and

more importantly, results in more homogeneous incorporation of the dicarboxylic acid in the entire membrane.

The addition of another compound to the electrospinning solution may however introduce difficulties for electrospinning as it can influence the properties of the solution. Figure 47 displays the comparative study between fibres obtained through electrospinning of merely PiPOx and those from the one-pot method with succinic acid, the latter noted as FRP+X, revealing that little to no influence is observed from the addition of succinic acid to the electrospinning solution, thus proving the one-pot method to be very effective. For this study, all fibres were further electrospun using the one-pot procedure to obtain easily cross-linkable fibre membranes.

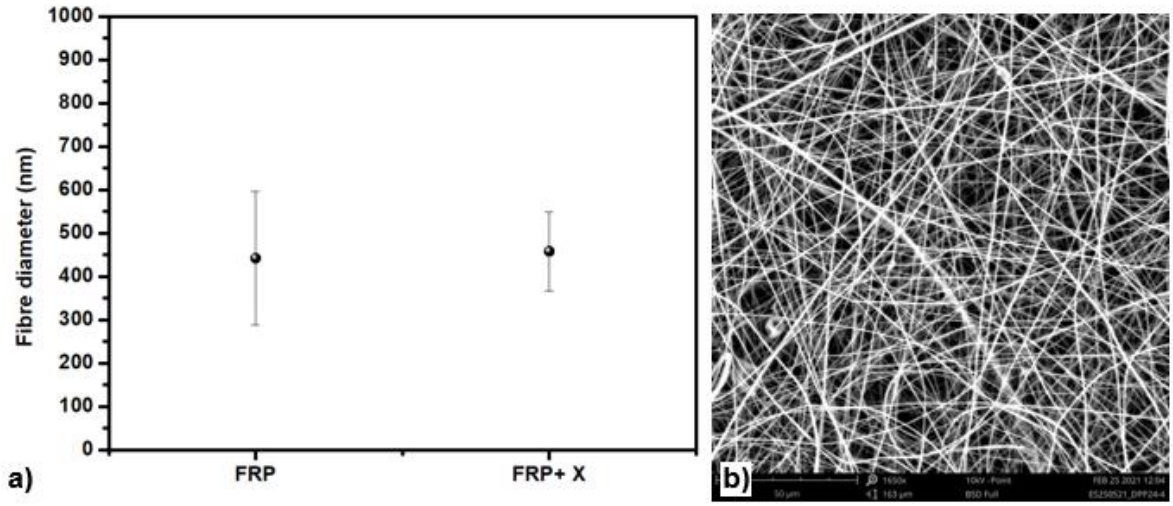

Figure 47 *a) Comparative study of the obtained fibre diameter for electrospinning of PiPOx with (FRP-X) and without (FRP) succinic acid as crosslinker. b) SEM image of fibres co-electrospun with succinic acid.*

3.4.3 Fibre crosslinking

As abovementioned, succinic acid is evenly distributed through the nanofibrous mats by co-electrospinning of PiPOx and succinic acid. By applying a thermal treatment of 140 °C for 5 hours, the fibres can be efficiently cross-linked, allowing succinic acid to engage in intermolecular ring-opening addition reactions linking two PiPOx units to construct the crosslinked nanofibrous network, as is shown in Figure 48.

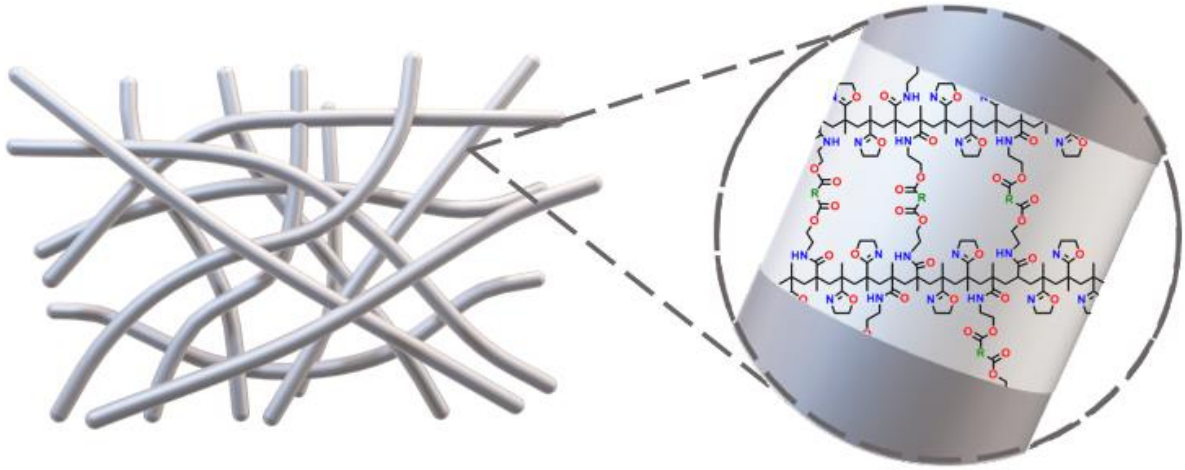

Figure 48 *Schematic representation of crosslinked PiPOx nanofiber networks.*

The primary crosslinking of the membranes is critical for further procedures. As mentioned before, PiPOx itself has a high solubility in a range of solvents. However, if the material is to function as a dye support material, the membrane must remain insoluble and stable in humid environments, as moisture is surely present within food packaging. The stability of the nanofibrous membranes after crosslinking was confirmed through water stability tests. The solubility test revealed the clear difference between fibres before and after heat treatment as the non-crosslinked fibres obtained after co-electrospinning dissolved instantaneously, while the crosslinked fibres obtained after heat treatment remained stable throughout the whole test. Snapshots of these tests are displayed in Figure 49.

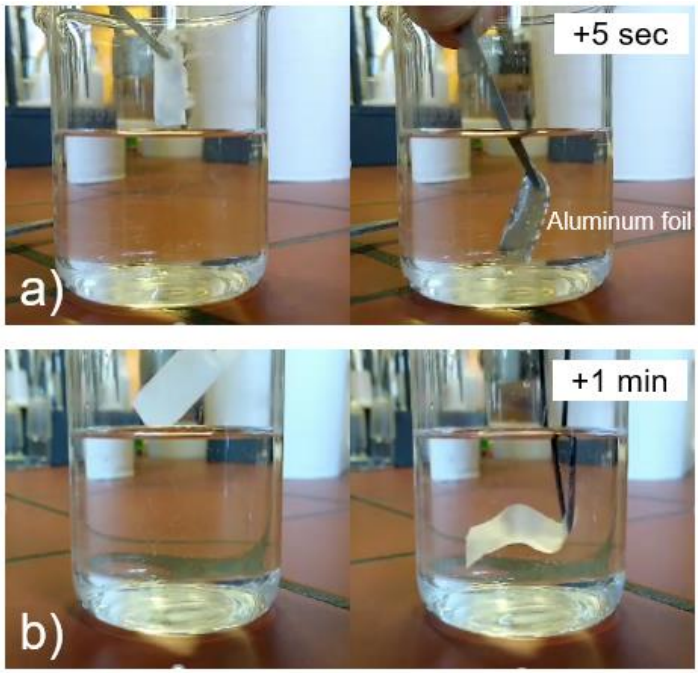

Figure 49 *Water stability test with a) non-crosslinked fibres, b) crosslinked fibres.*

To confirm the proposed crosslinking reaction between succinic acid and the PiPOx chains, IR spectroscopy was performed for both non-crosslinked and crosslinked membranes. These spectra, displayed in Figure 50, show the appearance of a peak at ca. 1727 cm^{-1} indicating the ester bond formation as a result of the ring-opening addition reaction, thus further confirming the effective crosslinking.

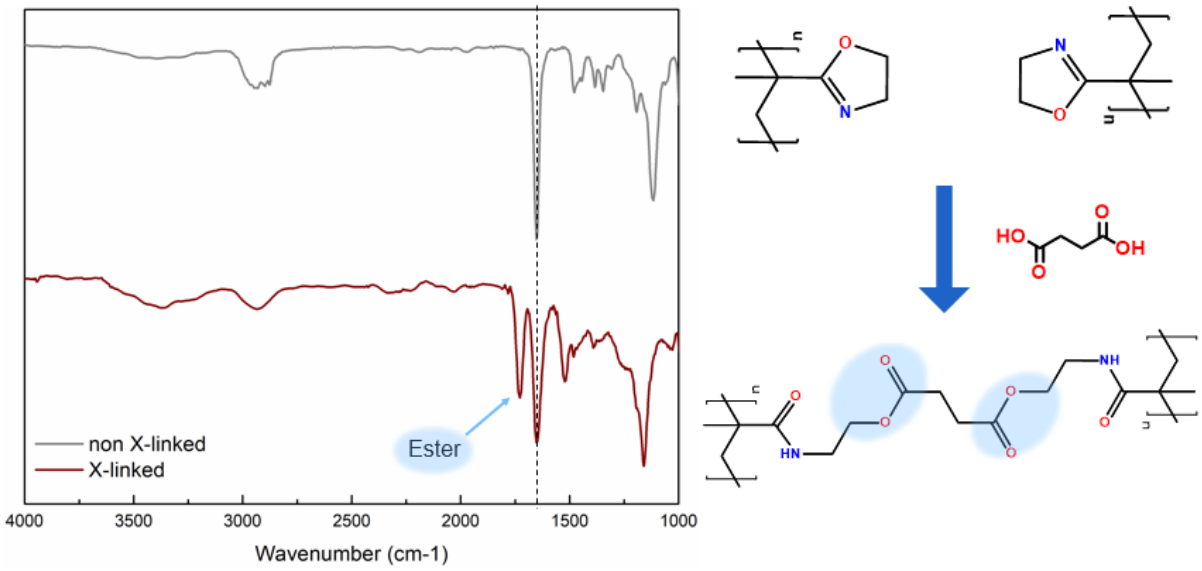

Figure 50 *IR spectra of non-crosslinked (top) and crosslinked membranes (bottom).*

3.5 Fibre functionalisation

Besides crosslinking the fibres into a network, functionalisation of the membranes with stimuli-responsive groups (e.g., dyes) is required to obtain stable, functional sensor membranes. Due to the nature of the PiPOx material, the possibility exists to conduct this either in a two-step or a one-pot fashion.

3.5.1 Two-step functionalisation

The first discussed technique is two-step functionalisation. The two steps imply the separate functionalisation with firstly, succinic acid, cross-linking the material to obtain the network, as was discussed in the previous section, and secondly, immobilizing the dye compounds upon the carrier network material. To functionalise the membranes with the respective dyes, the networks were simply soaked in a DMF solution containing a specified dye concentration at elevated temperatures of 140 °C for 24h to allow the conjugation to take place. Afterwards, the dye-modified membranes were washed to remove any remaining unbound dye and dried to obtain the final functionalised membranes. The different steps of the procedure are displayed below in Figure 51. As this technique is simple and accessible, it allows for quick optimisation. Due to the adaptable nature of the two-step procedure, minor alterations to the general methodology could be performed to obtain optimal outcomes, in terms of amounts of immobilised dye and observed response intensity, for each separate dye.

Figure 51 *Schematic procedure of the dye modification procedure for the crosslinked PiPOx fibrous mats.*

A quick visual test confirmed that the colour responsiveness was retained after immobilization of the dyes on the membranes. The testing was performed by administering propylamine (PA), hydrochloric acid (HCl), and butanethiol (BT) gasses to the $\mathbf{C_1}$, $\mathbf{C_4}$, and $\mathbf{C_3}$ functionalised membranes, respectively. The results, as displayed in Figure 52, demonstrate that all three

dyes have retained their responsiveness after immobilization on the nanofibrous material. The **C_1** membrane was revealed to be deprotonated after synthesis, revealing a yellow colour. After protonation with acid, the membrane obtained a clear orange colour, which returned to yellow after deprotonation by PA gas. The **C_4** membranes, on the other hand, showed to be responsive to administered HCl gas as the colour transitioned from red to purple after protonation. Finally, the **C_3** fibres revealed a colour change from white to a yellow-orange intermediate after several minutes of exposure to BT gas.

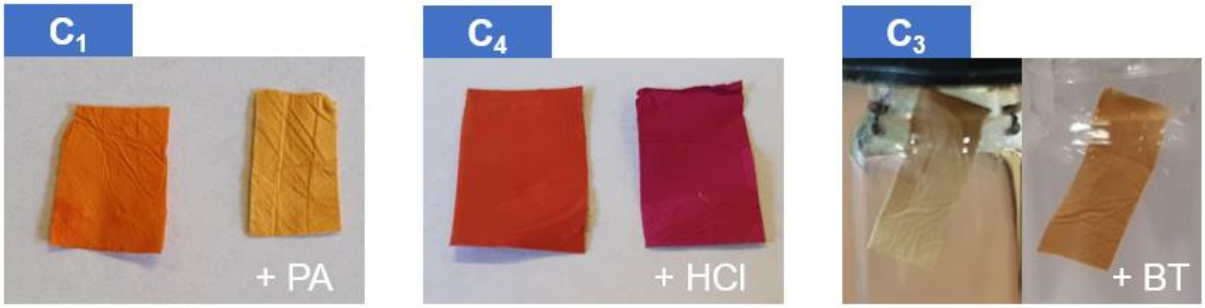

Figure 52 *Colour response test of functionalised PiPOx membranes with C_1 (left), C_4 (middle), and C_3 (right) towards PA, HCl, and BT respectively.*

3.5.2 One-step functionalisation

A one-step functionalisation procedure was also investigated in which both the crosslinking and dye immobilisation are combined into one step. To do so, both the dye and the succinic acid crosslinker are incorporated in the PiPOx fibrous membranes through the electrospinning procedure. Together with the succinic acid, the dye is added to the initial polymer solution and electrospun within the entire membrane. The electrospun membranes are then thermally treated, allowing both succinic acid and the dye compound to react with the pendant 2-oxazoline rings, achieving crosslinking and dye immobilisation at the same time. This technique requires less dye usage as electrospinning in presence of the dye results in a more efficient, near quantitative, inclusion of the dye within the membrane. Furthermore, it has no further need for any additional steps except for the thermal treatment step, thus allowing for a more efficient procedure for membrane functionalisation.

The one-pot electrospinning, including both succinic acid and compound **C_1**, was performed to evaluate its responsiveness to analytes. The obtained fibres were heat-treated at 140 °C, allowing the conjugation of the compounds, after which a response test was performed using PA. The outcome of the test, as displayed in Figure 53, proved the technique to be effective as a visual response was observed through deprotonation.

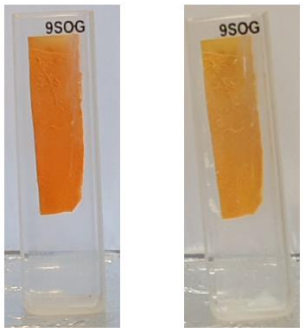

Figure 53 *Colour response of one-step functionalised C_1 membranes, protonated (left) and deprotonated state (right).*

Although this technique provides advantages compared to the two-step functionalisation method, it was found that a time-consuming optimisation was required for the electrospinning procedure in presence of the dye indicating that the polymer solution is significantly altered due to the presence of the dye. The changed properties influence the electrospinning outcome and therefore require a new optimisation procedure to maintain highly defined nanofibers. Secondly, compared to the more common DMF electrospinning solvent, in which most dyes are soluble and also used in the two-step functionalisation process, the water and ethanol mixture from the electrospinning procedure gives rise to solubility problems of the dye molecules. To optimise all these parameters more research is required for which no time was available in this master thesis project. Therefore, the two-step procedure was implemented for the membrane functionalisation for the membranes that were used for more in-depth evaluation of the sensing properties as well as the earlier mentioned additional WS-300 membranes.

3.6 Membrane response rate analysis

Quantitative analysis of the colorimetric response from the functionalised networks was performed through reflective UV-Vis spectroscopy. In this reflective UV-Vis setup, a second important aspect is determined, being the responsiveness of the fibres towards analytes in the gas phase. This is important as the final application requires the sensor to function within the headspace of food packaging. To mimic these conditions, small amounts of analytes are deposited on the bottom of the cuvette. Subsequently, a small piece of a functionalised sensor membrane was placed on the wall of the cuvette, preventing direct contact with the analyte. The cuvette was capped to allow the analyte to evaporate in the headspace and to reach its liquid-gas equilibrium. Upon equilibrium, the sample was measured.

Initially, the data of these experiments were measured as reflection intensities and were transformed to a value representing the absorption per wavelength. This is performed by using the Kubelka-Munk equation, which transforms the measured absolute reflectance $R\infty$ to K, the absorption coefficient, over S, the scattering coefficient. The K/S value can be used as a representative value for absorption thus allowing for better comparison between reflective UV-Vis and transmission UV-Vis spectra.

$$\frac{K}{S} = \frac{(1 - R\infty)^2}{2\,R\infty}$$

3.6.1 (E)-4-((4-hydroxyphenyl)diazenyl)benzoic acid

The response of compound **C_1** is targeted to detect a basic pH through acid-base interaction with amines. As mentioned earlier, preliminary tests revealed that the **C_1** functionalized membranes were deprotonated after synthesis, obstructing their use for the detection of basic compounds, i.e., amines. Therefore, the fibre was pre-treated through the addition of hydrochloride gas, resulting in orange colour. The halochromic behaviour, shown in Figure 54a, displays the initial bathochromic shift with a new absorption maximum at 440 nm from the protonation of the sensor after hydrochloride gas treatment. The addition of propylamine (PA) to this protonated network returned it towards the initial deprotonated state. A hypsochromic shift was observed as the absorption at 440 nm diminished, giving rise to the absorption maximum at 360 nm. The accompanying fibre pictures display the different colour states of the fibre membranes, as the initial deprotonated fibre has a yellow colour which

turns to a distinct orange colour upon protonation, to finally return to the deprotonated yellow state after in response to PA.

In the next step, the effectiveness of detection for secondary and tertiary amines was evaluated using diethylamine (DEA) and triethylamine (TEA). Furthermore, the sensitivity of the sensors was analysed through testing at equilibrium concentrations of 100 ppm of the analytes in the gas phase. The results, as displayed in Figure 54b, confirmed the capability of **C_1** networks to detect each of the three groups of primary, secondary and tertiary amines, as well as proving successful detection of analyte concentrations as low as 100 ppm within the gas phase. Visually, the tested sensors displayed a colorimetric change, ranging from orange to yellow.

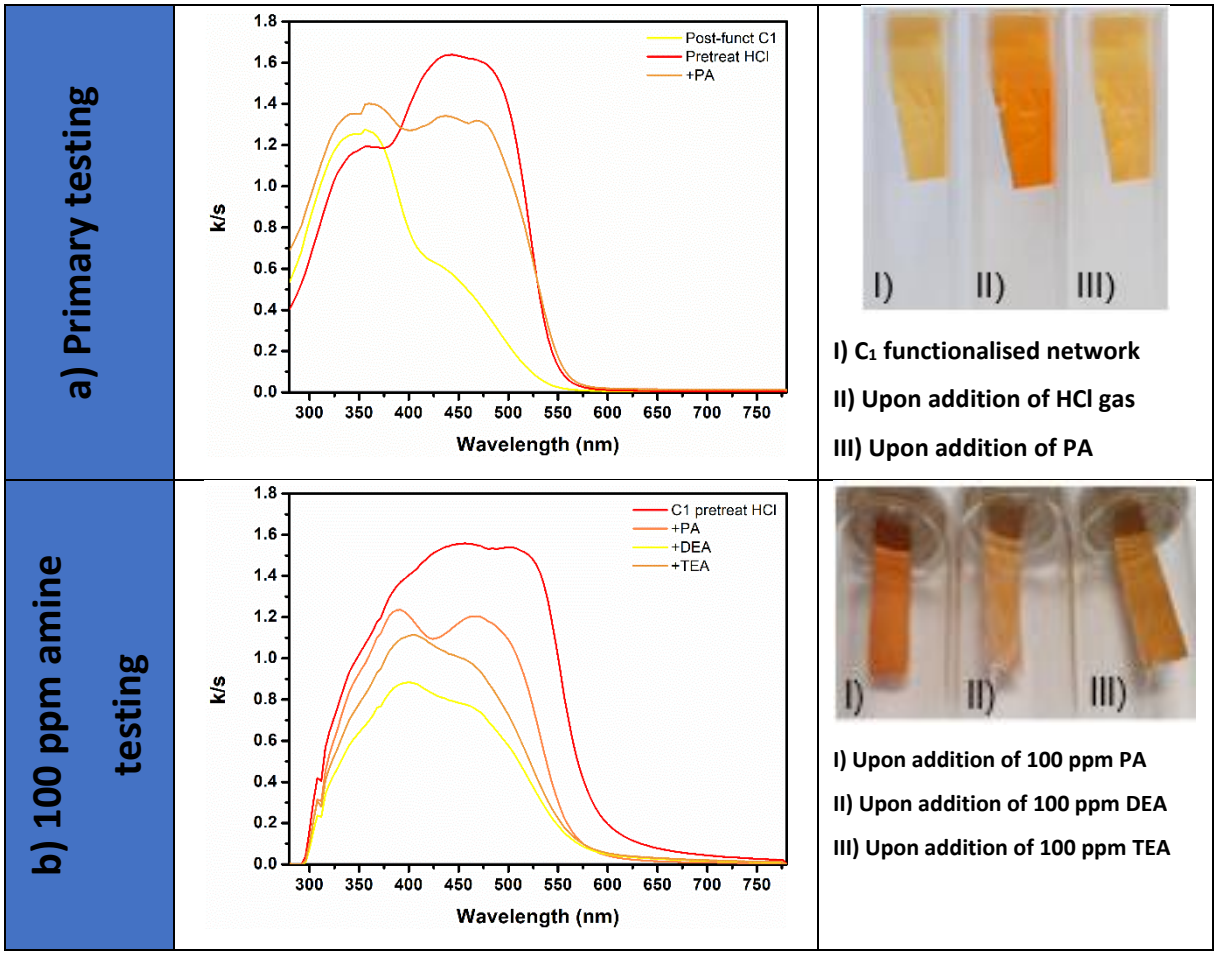

Figure 54 *Response rate analysis of C_1 functionalised membranes towards a) Propyl amine after HCl pre-treatment. b) 100 ppm concentrations of primary, secondary, and tertiary amines (PA, DEA, and TEA) after HCl pre-treatment.*

3.6.2 Linker-Disperse Red 1

The second pH-responsive dye, **C_4**, was tested through the administration of HCl gas to the cuvette containing the **C_4** functionalized PiPOx membranes. The obtained results are displayed

in Figure 55. The presence of the acid swiftly transitioned the sensor from the initial red colour to a deep purple colour, indicating the protonation of Disperse Red 1. The initial absorption maximum at 494 nm red-shifted towards 510 nm. Furthermore, the entire absorption spectrum revealed this bathochromic shift, which caused the clear shift to the purple colour.

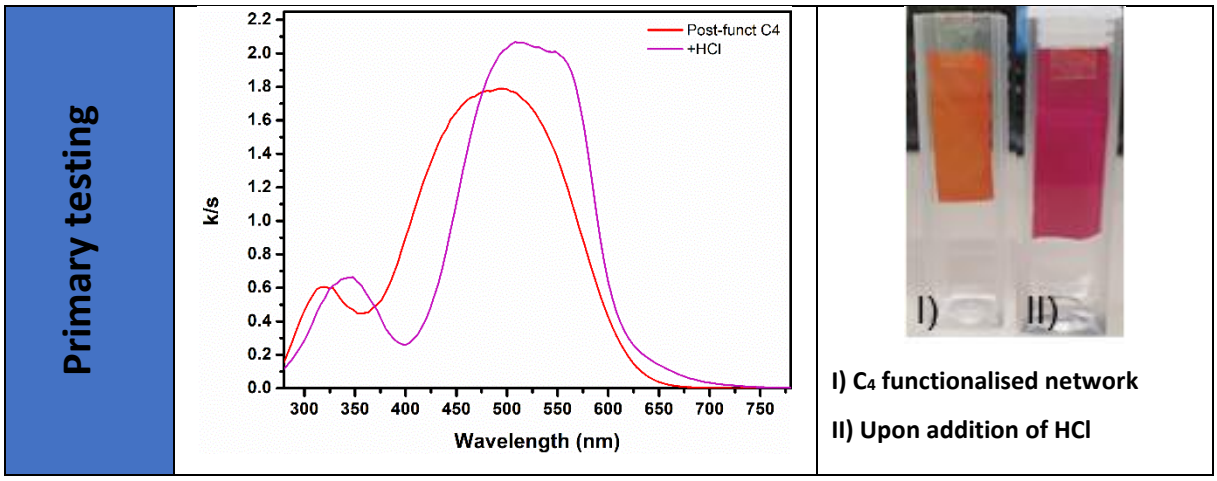

Figure 55 *Response rate analysis of C_4 functionalised membranes towards protonation with HCl.*

3.6.3 Ellman's reagent

The final PiPOx membrane, modified with **C_3**, was tested for thiol responsiveness through administration of butanethiol (BT) in the closed cuvette. The test, as shown in Figure 56a, revealed a response to the BT as the absorption pattern of the functionalised network itself lies mostly outside of the visible spectrum, thus resulting in a colourless membrane, where administration of the BT gave rise to the characteristic absorption peak of 2-nitro-5-thiobenzoate at 435 nm. As mentioned earlier, the colour response of Ellman's reagent is caused by cleavage of the central disulfide bridge, resulting in the formation of 2-nitro-5-thiobenzoate having a characteristic yellow colour. Since the sensor response was rather slow, it was expected to be accelerated in a basic environment due to the deprotonation of the thiol functional group. To investigate this hypothesis, PA was added to the cuvette together with BT, resulting in an instant orange colouration of the fibre network. A control experiment with merely the addition of PA gave the same colorimetric response, indicating that Ellman's reagent is also responsive to primary amines due to their basicity. In literature, it was reported that the reagent underwent hydrolytic cleavage in environments with a pH above 9 resulting in similar cleavage products.[131,132] Furthermore, when the **C_3** functionalised networks were exposed to tertiary amines, no instantaneous orange response was observed nor its respective absorption peak at 465 nm appeared. When left for longer reaction times, the same result as

with the PA was observed. However, if BT and TEA gas were both added to the fibres, an instantaneous response was also noted indicating the accelerating effect of the basic environment towards thiol detection. The results displayed respectively in Figure 56b and 56c indicate two important results. Firstly, it displays the responsiveness of **C_3** towards different analytes, such as BT, PA, and TEA. Secondly, it confirmed the dual effect of both BT and a base to further enhance the response of **C_3** functionalised networks. These results indicate that this is a valuable sensor for spoilage detection, however, the results cannot be simply interpreted as thiol detection.

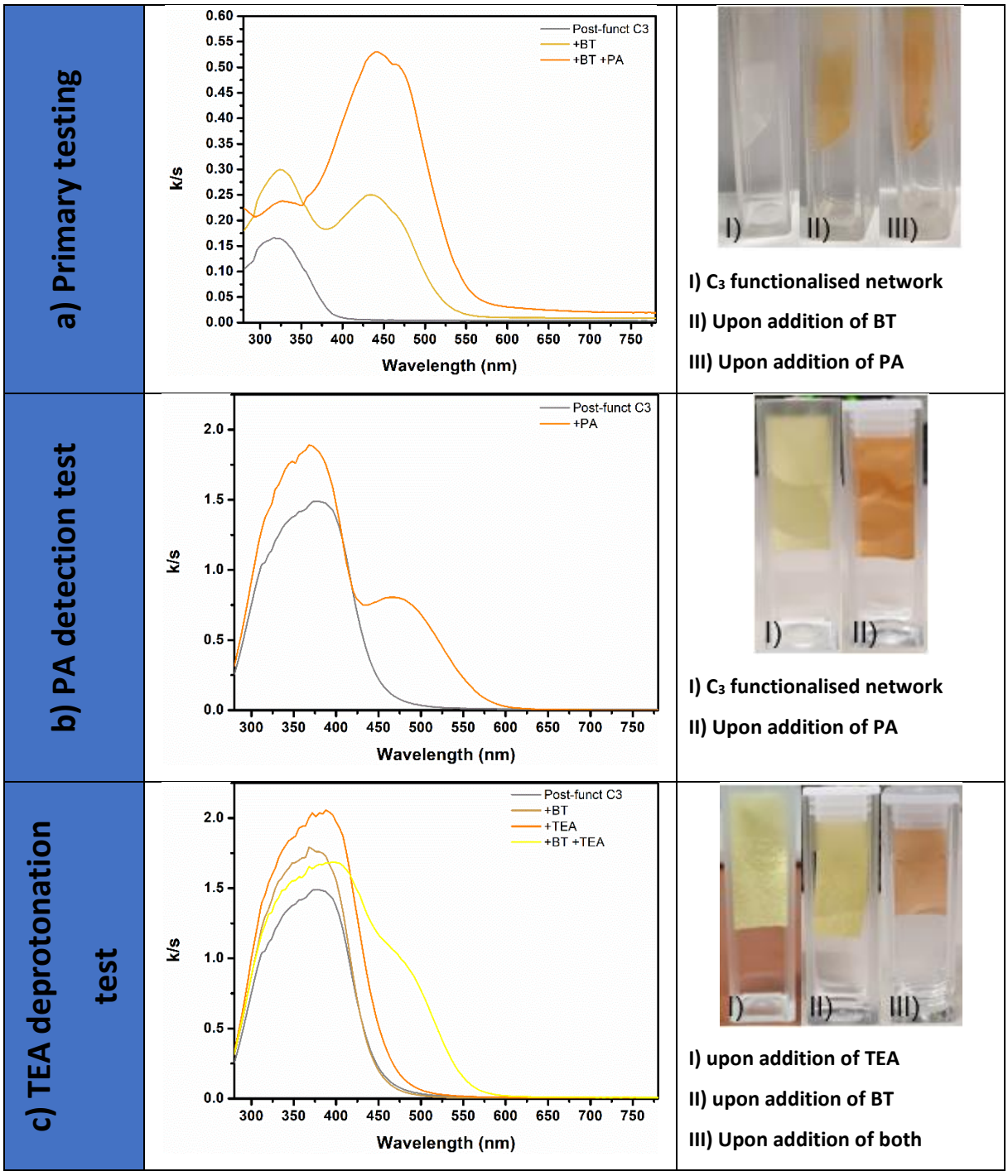

Figure 56 *Response rate analysis of C_1 functionalised membranes towards a) BT and the gas mixture of BT and PA. b) PA. c) TEA, BT, and the gas mixture of BT and TEA.*

3.7 Real-life samples

As a final proof-of-concept, the developed sensor materials were evaluated with real food samples to evaluate the effectiveness of the designed nanofiber sensor array. During this preliminary test, the spoilage of the food products could be detected in both ambient air and nitrogen atmosphere.

3.7.1 Ambient air atmosphere

The first set of tests were performed with chicken, cod, and beef samples that were placed in a container with ambient air at room temperature in presence of the sensor array. The obtained pictures from the sensor arrays throughout the test are displayed in Figure 57.

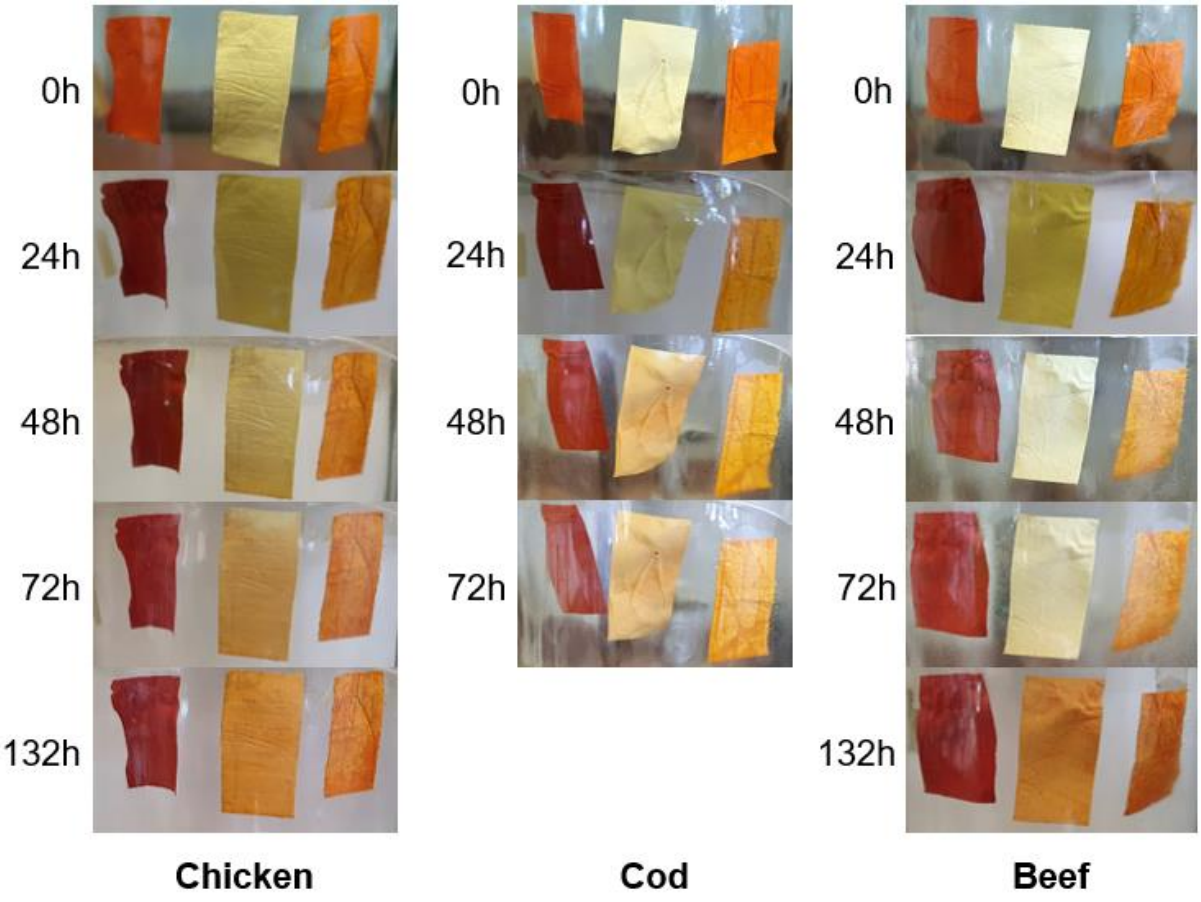

Figure 57 *All pictures contain from left to right three networks functionalised with C_4, C_3, and C_1. The columns contain the sensor array timeframe pictures monitoring responses towards chicken (left), cod (middle), and beef (right) samples in ambient air.*

The leftmost membrane, functionalised with **C_4**, was anticipated to show the hypsochromic shift upon protonation in the acidic environment. However, in all three tested samples, no clear visual colour shift was observed, thus indicating an insufficient concentration of acid for protonation. As the fibre was shown to be responsive in section 2.6.2, it indicates that the

effective acid detection range of the described sensor lies outside of the region of interest in the food spoilage environment.

The second sensor membrane, functionalised with **C_3**, showed a visual colour change in all three samples, albeit in different timeframes. In the cod sample, the colour change from yellow to orange was observed at the 48-hour mark. The chicken sample only revealed minor colour changes at 48 hours and a clear colour change at 74 hours. Lastly, the sensor in presence of the beef remained unchanged for the first 72 hours of the experiment. Only after 2 more days of further decay, a clear visual shift was observed as it fully transitioned into an orange colour. As the proof-of-concept was indicated for all three samples, these results are promising for further investigation.

The third membrane, carrying the **C_1** sensor dye, showed the halochromic shift after a couple of minutes of being inside the container with the food samples. It is suspected that the dye sensor is possibly too sensitive resulting in quick deprotonation due to low concentrations of base present in the headspace of the sample. Therefore, optimisation is required to optimise the sensor functioning for food packaging.

To further quantify the observed results in function of the colour change, this visual study was complemented by euclidean colour distance (ECD) calculations. Through the obtained ECD, this study attempts to provide the first step towards automatization of colour analysis, as the colour distance can allow objective classification of the analysed samples. The obtained results, as shown in Figure 58, display the calculated ECD throughout the different timeframes, always using the initial picture as the reference point. After 48 hours, a change in ECD value can be observed in all three samples for the **C_1** and **C_4** sensors, respectively sensing for a basic and acidic pH. However, as was indicated in Figure 57, **C_4** displayed no visible change in colour throughout this timeframe. This proves that an average of 70 to 100 ECD is required to obtain a visual response signal, as lower ECD values were no longer visible to the naked eye. Furthermore, after excluding the observation at the 24-hour mark due to using a very different exposure when making the photograph, a similar progression pattern is seen for **C_3**, the thiol-sensitive sensor, in both chicken and cod as visible changes were observed after 48 hours, which was confirmed by ECD analysis. The beef test, on the other hand, only displayed a rise in ECD after 72 hours, similarly to the first observed colour changes after this timeframe. However, our results demonstrate that the euclidean distance does not perform well under

changes in the exposure and illumination when taking the pictures. The obtained data point at 24 hours is therefore considered as an outlier for ECD evaluation, due to a different illumination, which influences the RGB values. Out of these preliminary results, it is possible to narrow down the timeframe in which food spoilage occurs under an ambient atmosphere at room temperature. This experiment thus further underlines the need for an optimised method of evaluation as continuity and exclusion of external factors is critical in obtaining significant and reliable outcomes. Further broadening of the sensor array, however, may improve the observed results of the ECD experiment due to the increase in vector dimension. Every addition to the sensor array will add an overall dimension increase of 3, leading to an enhanced categorical classification. Finally, the starting and the final colours were equal for all food product types, while a different time evolution was observed, depending on sample composition. This evidence is of paramount importance as it underlines the successful proof-of-concept for the here developed food spoilage sensor array.

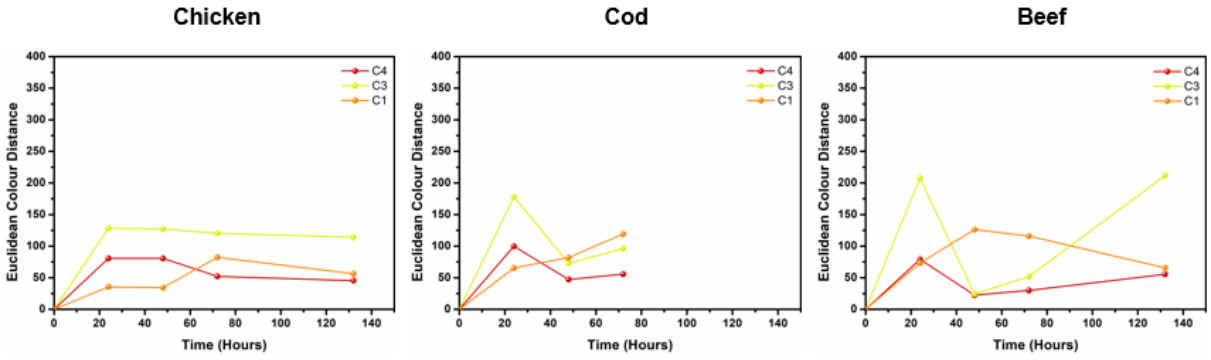

Figure 58 *Euclidean colour distance for sensors in ambient air, chicken (left), cod (middle), and beef (right).*

Within the scope of further valorisation, the use of the commercially available polymer WS-300 (Nippon Shokubai) was included in this research. The functionalised membranes were tested toward real-life samples within the same setup used for the PiPOx membranes based on the PiPOx synthesized by solution FRP. Response rate analysis was limited to only a cod sample in the air to determine its responsiveness to analytes produced during spoilage. The obtained timeframe pictures and ECD analysis are displayed in Figure 59a and 59b. As a similar colour evolution can be observed compared to the initial proof of concept, no indication was found that the WS-300 terpolymer's hydrophobic groups influence the sensor response in a negative way. Furthermore, in the ECD analysis, a gradual change can be noted over time resulting in the visible colour shift. Therefore, indicating the potential of WS-300 as a

replacement for home-made PiPOx homopolymers and its further valorisation as versatile nanofiber network material for sensor arrays.

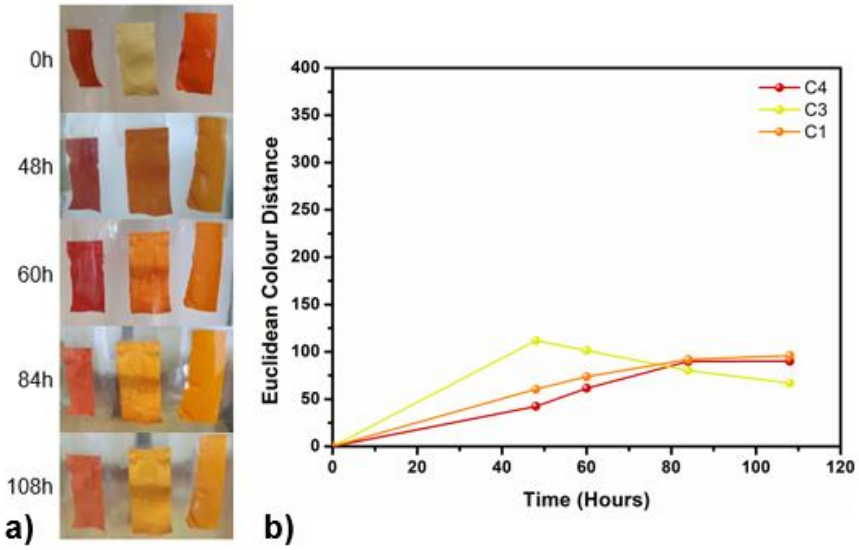

Figure 59 *a) All pictures contain from left to right three WS-300 based networks functionalised with C_4, C_3, and C_1. Sensor array timeframe pictures are depicted, monitoring responses towards cod samples in ambient air containing networks functionalised with C_4 (left), C_3 (middle), and C_1 (right). b) Euclidean colour distance for WS-300 sensors for cod sample in ambient air.*

3.7.2 Nitrogen atmosphere

The second set of tests was performed under a nitrogen gas atmosphere to mimic food packaging conditions in absence of oxygen. Now only including cod and chicken as these samples provided the fastest results during the initial proof-of-concept. The obtained results, displayed in Figure 60 illustrate a similar trend compared to those in air. Some colours appear to show stronger shifts compared to the previous test, however, this is more likely due to batch-to-batch differences in the membranes themselves, rather than due to influences from the environment.

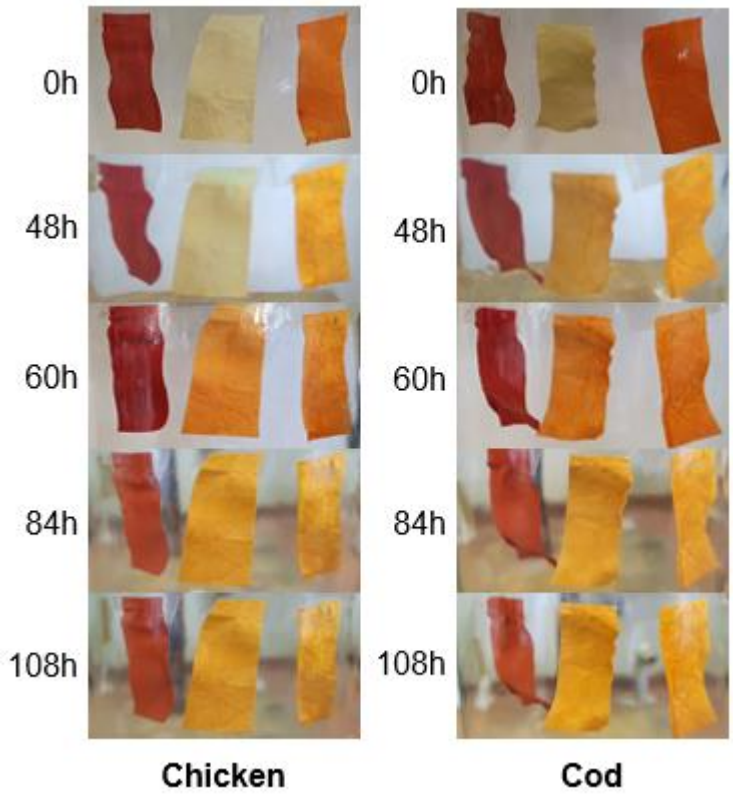

Figure 60 *All pictures contain from left to right three networks functionalised with C4, C3, and C1. The columns depict sensor array timeframe pictures monitoring responses towards chicken (left) and cod (middle) samples under nitrogen atmosphere.*

Similar results were observed within the nitrogen experiments. The **C_4** membranes revealed no clear colour response. The membranes modified with **C_3** again illustrated a clear colour response due to spoilage of the sample, thus effectively indicating the presence of spoilage metabolites. The **C_1** membrane also behaved similarly to the initial tests under ambient atmosphere, as it turned to its deprotonated state within minutes, resulting in the orange to yellow colour shift, before actual spoilage processes took place. Additionally, during the ECD analysis, displayed in Figure 61, a general increase in the colour distance throughout the experiment for each of the fibres was noted. However, the lack of consistent illumination while taking the photographs only allows a general interpretation of the results. Nonetheless, these results further support the proof-of-concept of this sensor array for detecting food spoilage. The inert environment within the container also promotes the growth of different bacterial species in comparison to those present in the ambient air environment, as was mentioned under section 1.5.1. The sensors, however, displayed no differential behaviour to the presence of the other species, further indicating that the concept of this type of sensor material is a promising candidate for detection in food packaging. However, the results again

demand further research and optimisation of the sensor dyes and their read-out to improve the value of the sensor array results.

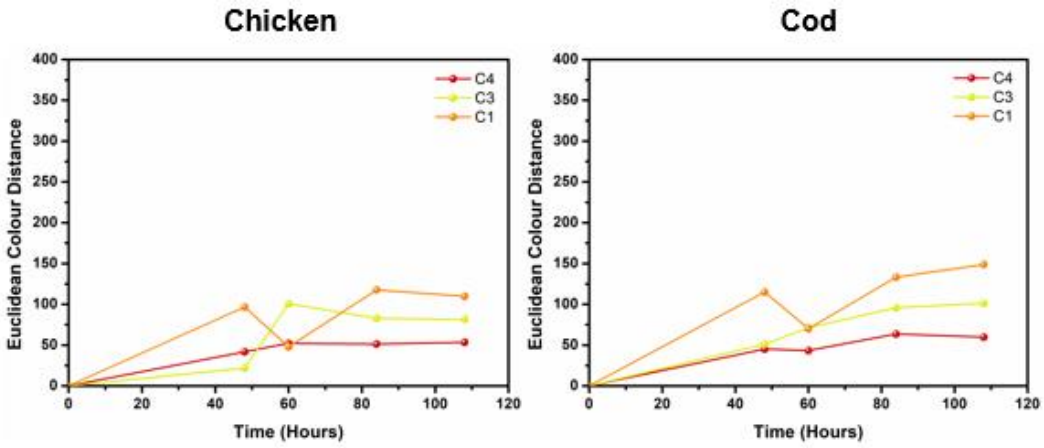

Figure 61 *Euclidean colour distance for sensors in a nitrogen environment, chicken (left) and cod (right).*

4. Conclusions and future work

Within this project, the synthesis, processing and photophysical properties of several modified nanofiber networks, based on poly(2-isopropenyl oxazoline), with analyte-responsive dyes were investigated. This project aimed at developing a colorimetric nanofibrous sensor array able to detect premature spoilage in food packaging applications. From this work, several conclusions can be drawn, regarding both the applied materials, their colour response, and the use of sensor arrays for detecting food spoilage.

Firstly, the choice of the base material, PiPOx, allowed via solvent electrospinning the facile production of narrow nanofibers with excellent tunability from green, sustainable solvents. Moreover, through the presence of pendant oxazoline groups in the sidechains, the PiPOx membranes could effortlessly be crosslinked into the respective nanofibrous networks by introducing a dicarboxylic acid functional molecule into the nanofibrous membranes during electrospinning. Within this study, this resulted in a versatile platform with potential for further functionalisation. Put into a broader context, PiPOx nanofiber networks can be implemented as a hydrophilic base material for various applications outside of the food spoilage scenario.

Secondly, from the applied analyte-responsive dyes, only Ellman's reagent provided an adequate colour response during the real-life sample spoilage tests. Although all dyes retained their specific response on the fibre matrix, it can be concluded that the sensor array should be expanded with halochromic dyes responsive within the region of interest.

Thirdly, the choice of optical sensors for food spoilage detection provides this sensor system with an output signal with no need for advanced analysis and/or skilled personnel as colour-based signals can be interpreted using only the naked eye. Furthermore, through image analysis, processing of photographs of the sensor array, taken by a smartphone, can be conducted in an automated manner via the herein described ECD analysis. The analysis, albeit limited at this point, was shown to have the potential for optimisation to eventually function as the basis for automated colour difference analysis. Through the application of smart devices, such as a common smartphone, automatic image analysis and pattern recognition can be effortlessly performed on the sensor array. This could allow the devices to make

categorical classifications on the edibility of food products based on a single image of the sensor array. This, however, first implicates optimisation of the procedure, since external factors such as illumination can greatly influence the obtained results, as seen within this project. To this extent, a calibration spot can be incorporated to prevent false positives.

As a general conclusion, we can say that the potential of PiPOx-based nanofibrous networks, capable of facile functionalisation, and its wide applicability cannot be underestimated. Although the designed nanofibrous sensor array provided proof-of-concept, it needs to be critically reviewed before further industrial-scale potential can be achieved. To industrialise the implementation of a sensor array onto food packaging, an on-line approach (e.g., inkjet printing) will be required rather than the two-step functionalisation method. Effective implementation of this procedure as well as the dye immobilization forms the new challenge for future research.

As the current aim for the application was focussed only on quality assessment of the food product through the detection of certain spoilage analytes, future work could include analysing the potential of colorimetric sensors as effective replacements for the currently used expiration dates. This would include measuring the membrane response rates in combination with continuous analysation of the packaging headspace for the presence and concentration of multiple food spoilage VOCs, for example through solid-phase microextraction linked to gas chromatography and mass spectrometry (SPME-GC-MS) as well as microbiological assessment of the growing microflora, to further fine-tune the sensitivity of the sensor.

In conclusion, both aspects of the master thesis, being the PiPOx nanofiber network and the designed sensor array, were proven to be effective as the final application displayed a colour change upon food spoilage without compromising the stability of the fibre network. By this, various ways could be explored to further optimize the colour response and design an accurate sensor network.

5. References

1. Xue, L. & Liu, G. Introduction to global food losses and food waste. in *Saving Food: Production, Supply Chain, Food Waste and Food Consumption* 1–31 (2019).
2. Stenmarck, Å. *et al. Estimates of European food waste levels*. *European Commission* (2016).
3. FAO. *Global food losses and food waste – Extent, causes and prevention*. (2011).
4. EPA. *Wasted food measurement methodology scoping memo*. (2020).
5. Ishangulyyev, R., Kim, S. & Lee, S. H. Understanding food loss and waste-why are we losing and wasting food? *Foods* **8**, 297–311 (2019).
6. Genter, M. B. & Doty, R. L. Toxic exposures and the senses of taste and smell. in *Handbook of Clinical Neurology* **164**, 389–408 (Elsevier B.V., 2019).
7. Lawless, H. The sense of smell in food quality and sensory evaluation. *J. Food Qual.* **14**, 33–60 (1991).
8. Takahashi, Y. K., Nagayama, S. & Mori, K. Detection and masking of spoiled food smells by odor maps in the olfactory bulb. *J. Neurosci.* **24**, 8690–8694 (2004).
9. Fao. *FAO/WHO guide for developing and improving national food recall systems*. (2012).
10. Samotyja, U. & Sielicka-Różyńska, M. How date type, freshness labelling and food category influence consumer rejection. *Int. J. Consum. Stud.* **45**, 441–455 (2021).
11. Newsome, R. *et al.* Applications and perceptions of date labeling of food. *Comprehensive Reviews in Food Science and Food Safety* **13**, 745–769 (2014).
12. Zielińska, D. *et al.* Consumer understanding of the date of minimum durability of food in association with quality evaluation of food products after expiration. *Int. J. Environ. Res. Public Health* **17**, 1632 (2020).
13. Skibsted, L. H., Risbo, J. & Andersen, M. L. *Chemical deterioration and physical instability of food and beverages*. (2010).
14. Masclaux-Daubresse, C., Chen, Q. & Havé, M. Regulation of nutrient recycling via autophagy. *Current Opinion in Plant Biology* **39**, 8–17 (2017).
15. Atkin, L. & Rippon, M. Autolysis: Mechanisms of action in the removal of devitalised tissue. *Br. J. Nurs.* **25**, S40–S47 (2016).
16. Cocariu, E. A. ndr. *et al.* Correlations Between the Autolytic Changes and Postmortem Interval in Refrigerated Cadavers. *Rom. J. Intern. Med.* **54**, 105–112 (2016).
17. Dave, D. & Ghaly, A. E. Meat spoilage mechanisms and preservation techniques: A critical review. *Am. J. Agric. Biol. Sci.* **6**, 486–510 (2011).
18. Hansen, L. T., Gill, T., Røntved, S. D. & Huss, H. H. Importance of autolysis and microbiological activity on quality of cold-smoked salmon. *Food Res. Int.* **29**, 181–188 (1996).

19. Lorenzo, J. M. *et al.* Main groups of microorganisms of relevance for food safety and stability: General aspects and overall description. in *Innovative technologies for food preservation: Inactivation of spoilage and pathogenic microorganisms* 53–107 (2018).

20. Zwietering, M. H., Jacxsens, L., Membré, J. M., Nauta, M. & Peterz, M. Relevance of microbial finished product testing in food safety management. *Food Control* **60**, 31–43 (2016).

21. Solomon, O., Kingsley, A. & Anosike, S. *Effects of salts on preservation and metabolic activities of fish and meat microflora*. (2018).

22. Cammack, R. *et al.* Nitrite and nitrosyl compounds in food preservation. *Biochimica et Biophysica Acta - Bioenergetics* **1411**, 475–488 (1999).

23. Lucera, A., Costa, C., Conte, A. & Del Nobile, M. A. Food applications of natural antimicrobial compounds. *Frontiers in Microbiology* **3**, 287 (2012).

24. Gonelimali, F. D. *et al.* Antimicrobial Properties and Mechanism of Action of Some Plant Extracts Against Food Pathogens and Spoilage Microorganisms. *Front. Microbiol.* **9**, 1639 (2018).

25. Quinto, E. J. *et al.* Food safety through natural antimicrobials. *Antibiotics* **8**, 208 (2019).

26. Irradiation in the production, processing and handling of food. Final rule. *Fed. Regist.* **73**, 49593–49603 (2008).

27. Gómez-López, V. M., Ragaert, P., Devliegher, F. & Debevere, J. Prolongation of the shelf-life of minimally processed vegetables by mild treatments. *Commun. Agric. Appl. Biol. Sci.* **71**, 155–158 (2006).

28. Gould, G. W. Preservation: past, present and future. *Br. Med. Bull.* **56**, 84–96 (2000).

29. McMillin, K. W. Where is MAP Going? A review and future potential of modified atmosphere packaging for meat. *Meat Science* **80**, 43–65 (2008).

30. Gill, C. O. Active packaging in practice: meat. in *Novel Food Packaging Techniques* 365–383 (2003).

31. Fraser, O. & Sumar, S. Compositional changes and spoilage in fish - an introduction. *Nutr. Food Sci.* **98**, 275–279 (1998).

32. Shahidi, F. The chemistry, processing technology and quality of seafoods — an overview. in *Seafoods: Chemistry, Processing Technology and Quality* 1–2 (Springer US, 1994).

33. Huis In't Veld, J. H. J. H. I. Microbial and biochemical spoilage of foods: An overview. *Int. J. Food Microbiol.* **33**, 1–18 (1996).

34. Gram, L. & Dalgaard, P. Fish spoilage bacteria - Problems and solutions. *Current Opinion in Biotechnology* **13**, 262–266 (2002).

35. Dalgaard, P., Madsen, H. L., Samieian, N. & Emborg, J. Biogenic amine formation and microbial spoilage in chilled garfish (Belone belone belone) - effect of modified atmosphere packaging and previous frozen storage. *J. Appl. Microbiol.* **101**, 80–95 (2006).

36. Emborg, J., Laursen, B. G. & Dalgaard, P. Significant histamine formation in tuna (Thunnus albacares) at 2°C - Effect of vacuum- and modified atmosphere-packaging on psychrotolerant bacteria. *Int. J. Food Microbiol.* **101**, 263–279 (2005).

37. Huss, H. Quality and quality changes in fresh fish. *Fish. Tech. Pap.* **348**, (1995).

38. Herbert, R. A. & Shewan, J. M. Precursors of the volatile sulphides in spoiling north sea cod (Gadus morhua). *J. Sci. Food Agric.* **26**, 1195–1202 (1975).

39. Herbert, R. A., Ellis, J. R. & Shewan, J. M. Isolation and identification of the volatile sulphides produced during chill-storage of north sea cod (gadus morhua). *J. Sci. Food Agric.* **26**, 1187–1194 (1975).

40. Whitfield, F. B. Microbiology of food taints. *Int. J. Food Sci. Technol.* **33**, 31–51 (1998).

41. Miller, A., Scanlan, R. A., Lee, J. S., Libbey, L. M. & Morgan, M. E. Volatile compounds produced in sterile fish muscle (Sebastes melanops) by Pseudomonas perolens. *Appl. Microbiol.* **25**, 257–261 (1973).

42. Nowsad, A. A. K. M. *et al.* Efficacy of electrolyzed water against bacteria on fresh fish for increasing the shelf-life during transportation and distribution. *J. fur Verbraucherschutz und Leb.* **15**, 351–362 (2020).

43. Borderías, A. J. & Sánchez-alonso, I. First Processing Steps and the Quality of Wild and Farmed Fish. *J. Food Sci.* **76**, R1–R5 (2011).

44. Segal, W. & Starkey, R. L. Microbial decomposition of methionine and identity of the resulting sulfur products. *J. Bacteriol.* **98**, 908–913 (1969).

45. Serio, A., Fusella, G. C., Chaves López, C., Sacchetti, G. & Paparella, A. A survey on bacteria isolated as hydrogen sulfide-producers from marine fish. *Food Control* **39**, 111–118 (2014).

46. Odeyemi, O. A., Alegbeleye, O. O., Strateva, M. & Stratev, D. Understanding spoilage microbial community and spoilage mechanisms in foods of animal origin. *Compr. Rev. Food Sci. Food Saf.* **19**, 311–331 (2020).

47. Nonaka, G. & Takumi, K. Cysteine degradation gene yhaM, encoding cysteine desulfidase, serves as a genetic engineering target to improve cysteine production in Escherichia coli. *AMB Express* **7**, 90 (2017).

48. Carbonero, F., Benefiel, A. C., Alizadeh-Ghamsari, A. H. & Gaskins, H. R. Microbial pathways in colonic sulfur metabolism and links with health and disease. *Front. Physiol.* **3**, 448 (2012).

49. Mustafa, F. & Andreescu, S. Chemical and biological sensors for food-quality monitoring and smart packaging. *Foods* **7**, 168 (2018).

50. Privett, B. J., Shin, J. H. & Schoenfisch, M. H. Electrochemical sensors. *Anal. Chem.* **82**, 4723–4741 (2010).

51. Assen, A. H., Yassine, O., Shekhah, O., Eddaoudi, M. & Salama, K. N. MOFs for the Sensitive Detection of Ammonia: Deployment of fcu-MOF Thin Films as Effective Chemical Capacitive Sensors. *ACS Sensors* **2**, 1294–1301 (2017).

52. Maeng, S. *et al.* SnO2 nanoslab as NO2 sensor: Identification of the NO2 sensing mechanism on a SnO2 surface. *ACS Appl. Mater. Interfaces* **6**, 357–363 (2014).

53. Zou, Y. *et al.* Highly efficient gas sensor using a hollow SnO2 microfiber for triethylamine detection. *ACS Sensors* **2**, 897–902 (2017).

54. Lobnik, A., Turel, M. & Korent, P. Optical Chemical Sensors:Design and Applications. in *Advances in Chemical Sensors* Ch. 1 (InTech, 2012).

55. Borisov, S. M. & Wolfbeis, O. S. Optical biosensors. *Chemical Reviews* **108**, 423–461 (2008).

56. Nassau, K. The fifteen causes of color: The physics and chemistry of color. *Color Res. Appl.* **12**, 4–26 (1987).

57. Mohr, G. J. *et al.* Design of acidochromic dyes for facile preparation of pH sensor layers. *Anal. Bioanal. Chem.* **392**, 1411–1418 (2008).

58. Alberti, G., Nurchi, V. M., Magnaghi, L. R. & Biesuz, R. A portable, disposable, and low-cost optode for sulphide and thiol detection. *Anal. Methods* **11**, 4464–4470 (2019).

59. Kim, M. O. *et al.* Development of VOCs gas sensor with high sensitivity using colorimetric polymer nanofiber: A unique sensing method. *Mater. Res. Express* **6**, 105372 (2019).

60. Zhong, X. *et al.* Rapid recognition of volatile organic compounds with colorimetric sensor arrays for lung cancer screening. *Anal. Bioanal. Chem.* **410**, 3671–3681 (2018).

61. Janzen, M. C., Ponder, J. B., Bailey, D. P., Ingison, C. K. & Suslick, K. S. Colorimetric sensor arrays for volatile organic compounds. *Anal. Chem.* **78**, 3591–3600 (2006).

62. He, W., Luo, L., Liu, Q. & Chen, Z. Colorimetric Sensor Array for Discrimination of Heavy Metal Ions in Aqueous Solution Based on Three Kinds of Thiols as Receptors. *Anal. Chem.* **90**, 4770–4775 (2018).

63. Fan, J., Qi, L., Han, H. & Ding, L. Array-Based Discriminative Optical Biosensors for Identifying Multiple Proteins in Aqueous Solution and Biofluids. *Frontiers in Chemistry* **8**, 572234 (2020).

64. Magnaghi, L. R. *et al.* Colorimetric sensor array for monitoring, modelling and comparing spoilage processes of different meat and fish foods. *Foods* **9**, 684 (2020).

65. De Smet, L. *et al.* Plasma dye coating as straightforward and widely applicable procedure for dye immobilization on polymeric materials. *Nat. Commun.* **9**, 1–11 (2018).

66. Van Der Schueren, L., Mollet, T., Ceylan, Ö. & De Clerck, K. The development of polyamide 6.6 nanofibres with a pH-sensitive function by electrospinning. *Eur. Polym. J.* **46**, 2229–2239 (2010).

67. He, X. & Hwang, H. M. Nanotechnology in food science: Functionality, applicability, and safety assessment. *Journal of Food and Drug Analysis* **24**, 671–681 (2016).

68. Zhang, X., Guo, Q. & Cui, D. Recent advances in nanotechnology applied to biosensors. *Sensors* **9**, 1033–1053 (2009).

69. Abdel-Karim, R., Reda, Y. & Abdel-Fattah, A. Review—Nanostructured Materials-Based Nanosensors. *J. Electrochem. Soc.* **167**, 037554 (2020).

70. Bülbül, G., Hayat, A. & Andreescu, S. Portable nanoparticle-based sensors for food safety assessment. *Sensors (Switzerland)* **15**, 30736–30758 (2015).

71. Mustafa, F. & Andreescu, S. Nanotechnology-based approaches for food sensing and packaging applications. *RSC Advances* **10**, 19309–19336 (2020).

72. Arduini, F., Cinti, S., Scognamiglio, V. & Moscone, D. Nanomaterial-based sensors. in *Handbook of Nanomaterials in Analytical Chemistry: Modern Trends in Analysis* 329–359 (2019).

73. Fong, J. K. *et al.* Fluorescent-Dye Doped Thin-Film Sensors for the Detection of Alcohol Vapors. *Am. J. Anal. Chem.* **05**, 566–580 (2014).

74. Briglin, S. M., Gao, T. & Lewis, N. S. Detection of Organic Mercaptan Vapors Using Thin Films of Alkylamine-Passivated Gold Nanocrystals. *Langmuir* **20**, 299–305 (2004).

75. A. Camposeo, M. Moffa, and L. P. *Electrospinning for High Performance Sensors*. *NanoScience and Technology* (Springer International Publishing, 2015).

76. Persano, L., Camposeo, A., Tekmen, C. & Pisignano, D. Industrial Upscaling of Electrospinning and Applications of Polymer Nanofibers: A Review. *Macromol. Mater. Eng.* **298**, 504–520 (2013).

77. Cha, J. H., Kim, D. H., Choi, S. J., Koo, W. T. & Kim, I. D. Sub-Parts-per-Million Hydrogen Sulfide Colorimetric Sensor: Lead Acetate Anchored Nanofibers toward Halitosis Diagnosis. *Anal. Chem.* **90**, 8769–8775 (2018).

78. Schoolaert, E., Hoogenboom, R. & De Clerck, K. Colorimetric Nanofibers as Optical Sensors. *Adv. Funct. Mater.* **27**, 1702646 (2017).

79. Agarwal, S., Burgard, M., Greiner, A. & Wendorff, J. *Electrospinning*. *Electrospinning* (De Gruyter, 2016).

80. Subbiah, T., Bhat, G. S., Tock, R. W., Parameswaran, S. & Ramkumar, S. S. Electrospinning of nanofibers. *J. Appl. Polym. Sci.* **96**, 557–569 (2005).

81. Stubbe, B. *et al.* Aqueous electrospinning of poly(2-ethyl-2-oxazoline): Mapping the parameter space. *Eur. Polym. J.* **88**, 724–732 (2017).

82. Li, D. & Xia, Y. Electrospinning of nanofibers: Reinventing the wheel? *Advanced Materials* **16**, 1151–1170 (2004).

83. Bhardwaj, N. & Kundu, S. C. Electrospinning: A fascinating fiber fabrication technique. *Biotechnology Advances* **28**, 325–347 (2010).

84. Ziabari, M., Mottaghitalab, V. & Haghi, A. K. Application of direct tracking method for measuring electrospun nanofiber diameter. *Brazilian J. Chem. Eng.* **26**, 53–62 (2009).

85. Steyaert, I., Vancoillie, G., Hoogenboom, R. & De Clerck, K. Dye immobilization in halochromic nanofibers through blend electrospinning of a dye-containing copolymer and polyamide-6. *Polym. Chem.* **6**, 2685–2694 (2015).

86. Liu, M., Duan, X. P., Li, Y. M., Yang, D. P. & Long, Y. Z. Electrospun nanofibers for wound healing. *Materials Science and Engineering C* **76**, 1413–1423 (2017).

87. Barani, H. Antibacterial continuous nanofibrous hybrid yarn through in situ synthesis of silver nanoparticles: Preparation and characterization. *Mater. Sci. Eng. C* **43**, 50–57 (2014).

88. Liu, Z., Ramakrishna, S. & Liu, X. Electrospinning and emerging healthcare and medicine possibilities. *APL Bioengineering* **4**, 30901 (2020).

89. Mercante, L. A., Scagion, V. P., Migliorini, F. L., Mattoso, L. H. C. & Correa, D. S. Electrospinning-based (bio)sensors for food and agricultural applications: A review. *TrAC - Trends in Analytical Chemistry* **91**, 91–103 (2017).

90. Panichpakdee, J. *et al.* Electrospinning of natural rubber latex-blended polyvinyl alcohol. *Mater. Today Proc.* **17**, 2020–2027 (2019).

91. Nikmaram, N. *et al.* Emulsion-based systems for fabrication of electrospun nanofibers: Food, pharmaceutical and biomedical applications. *RSC Adv.* **7**, 28951–28964 (2017).

92. Lannutti, J., Reneker, D., Ma, T., Tomasko, D. & Farson, D. Electrospinning for tissue engineering scaffolds. *Mater. Sci. Eng. C* **27**, 504–509 (2007).

93. Haider, S. *et al.* Highly aligned narrow diameter chitosan electrospun nanofibers. *J. Polym. Res.* **20**, 1–11 (2013).

94. Luzio, A., Canesi, E. V., Bertarelli, C. & Caironi, M. Electrospun polymer fibers for electronic applications. *Materials* **7**, 906–947 (2014).

95. Basson, N. Free volume of electrospun organic-inorganic, MSc thesis, University of Stellenbosch. (2014).

96. Megelski, S., Stephens, J. S., Bruce Chase, D. & Rabolt, J. F. Micro- and nanostructured surface morphology on electrospun polymer fibers. *Macromolecules* **35**, 8456–8466 (2002).

97. Jacobs, V., Anandjiwala, R. D. & Maaza, M. The influence of electrospinning parameters on the structural morphology and diameter of electrospun nanofibers. *J. Appl. Polym. Sci.* **115**, 3130–3136 (2010).

98. Teli, M. D. & Nadathur, G. T. Reversible colourimetric sensing of volatile phase by dye doped electrospun silica based nanofibers. *J. Environ. Chem. Eng.* **8**, 103920 (2020).

99. Yang, Y. *et al.* A simple fabrication of electrospun nanofiber sensing materials based on fluorophore-doped polymer. *J. Mater. Chem.* **19**, 7290–7295 (2009).

100. Wang, X. *et al.* Electrospun Nanofibrous Membranes for Highly Sensitive Optical Sensors. *Nano Lett.* **2**, 1273–1275 (2002).

101. Baert, J. J., De Clippeleer, J., De Cooman, L. & Aerts, G. Exploring the binding behavior of beer staling aldehydes in model systems. *J. Am. Soc. Brew. Chem.* **73**, 100–108 (2015).

102. Zhang, D. *et al.* Highly selective colorimetric sensor for cysteine and homocysteine based on azo derivatives. *Tetrahedron Lett.* **47**, 7093–7096 (2006).

103. Kangas, M. J. *et al.* Colorimetric Sensor Arrays for the Detection and Identification of Chemical Weapons and Explosives. *Critical Reviews in Analytical Chemistry* **47**, 138–153 (2017).

104. Huang, C. H. *et al.* A study of diagnostic accuracy using a chemical sensor array and a machine learning technique to detect lung cancer. *Sensors (Switzerland)* **18**, 2845 (2018).

105. Magnaghi, L. R. *et al.* Colorimetric sensor array for monitoring, modelling and comparing spoilage processes of different meat and fish foods. *Foods* **9**, 684 (2020).

106. Chen, Q., Hui, Z., Zhao, J. & Ouyang, Q. Evaluation of chicken freshness using a low-cost colorimetric sensor array with AdaBoost-OLDA classification algorithm. *LWT - Food Sci. Technol.* **57**, 502–507 (2014).

107. Arslan, Ö., Yalçin, E., Seferoğlu, N., Yaman, M. & Seferoğlu, Z. Molecular structure analysis and spectroscopic properties of Monoazo disperse dye from N,N-dimethylaniline. *Gazi Univ. J. Sci.* **30**, 175–189 (2017).

108. Güçlü, K., Özyürek, M., Güngör, N., Baki, S. & Apak, R. Selective optical sensing of biothiols with Ellman's reagent: 5,5'-Dithio-bis(2-nitrobenzoic acid)-modified gold nanoparticles. *Anal. Chim. Acta* **794**, 90–98 (2013).

109. Yang, Y. & Guan, X. Rapid and thiol-specific high-throughput assay for simultaneous relative quantification of total thiols, protein thiols, and nonprotein thiols in cells. *Anal. Chem.* **87**, 649–655 (2015).

110. Aitken, A. & Learmonth, M. Estimation of Disulfide Bonds Using EllmanÕs Reagent. in *Protein Protocols Handbook* 595–596 (Humana Press, Totowa, NJ, 2003).

111. Winther, J. R. & Thorpe, C. Quantification of thiols and disulfides. *Biochimica et Biophysica Acta - General Subjects* **1840**, 838–846 (2014).

112. Biesuz, R., Nurchi, V. M., Magnaghi, L. R. & Alberti, G. Inexpensive Alizarin Red S-based optical device for the simultaneous detection of Fe(III) and Al(III). *Microchem. J.* **149**, 104036 (2019).

113. Aigner, D. *et al.* New fluorescent pH sensors based on covalently linkable PET rhodamines. *Talanta* **99**, 194–201 (2012).

114. Magnaghi, L. R. *et al.* Development of a dye-based device to assess the poultry meat spoilage. Part II: Array on act. *J. Agric. Food Chem.* **68**, 12710–12718 (2020).

115. Alberti, G., Nurchi, V. M., Magnaghi, L. R. & Biesuz, R. A portable, disposable, and low-cost optode for sulphide and thiol detection. *Anal. Methods* **11**, 4464–4470 (2019).

116. Ziessel, R. *et al.* Solid-State Gas Sensors Developed from Functional Difluoroboradiazaindacene Dyes. *Chem. - A Eur. J.* **15**, 1359–1369 (2009).

117. Tan, S. Z., Hu, Y. J., Chen, J. W., Shen, G. L. & Yu, R. Q. An optical sensor based on covalent immobilization of 1-aminopyrene using Au nanoparticles as bridges and carriers. *Sensors Actuators, B Chem.* **124**, 68–73 (2007).

118. Weber, C. *et al.* 2-Isopropenyl-2-oxazoline: A versatile monomer for functionalization

of polymers obtained via RAFT. *Macromolecules* **45**, 20–27 (2012).

119. Altenbuchner, P. T. *et al.* Versatile 2-methoxyethylaminobis(phenolate)yttrium catalysts: Catalytic precision polymerization of polar monomers via rare earth metal-mediated group transfer polymerization. *Macromolecules* **47**, 7742–7749 (2014).

120. Zhang, N., Salzinger, S., Soller, B. S. & Rieger, B. Rare earth metal-mediated group-transfer polymerization: From defined polymer microstructures to high-precision nano-scaled objects. *J. Am. Chem. Soc.* **135**, 8810–8813 (2013).

121. Jerca, F. A., Jerca, V. V., Anghelache, A. M., Vuluga, D. M. & Hoogenboom, R. Poly(2-isopropenyl-2-oxazoline) as a versatile platform towards thermoresponsive copolymers. *Polym. Chem.* **9**, 3473–3478 (2018).

122. Jerca, F. A. *et al.* Poly(2-isopropenyl-2-oxazoline) Hydrogels for Biomedical Applications. *Chem. Mater.* **30**, 7938–7949 (2018).

123. Jerca, V. V. *et al.* Oxazoline-functional polymer particles graft with azo-dye. *React. Funct. Polym.* **71**, 373–379 (2011).

124. Spiridon, M. C., Jerca, F. A., Jerca, V. V., Vasilescu, D. S. & Vuluga, D. M. 2-Oxazoline based photo-responsive azo-polymers. Synthesis, characterization and isomerization kinetics. *Eur. Polym. J.* **49**, 452–463 (2013).

125. Kroneková, Z. *et al.* Ex Vivo and In Vitro Studies on the Cytotoxicity and Immunomodulative Properties of Poly(2-isopropenyl-2-oxazoline) as a New Type of Biomedical Polymer. *Macromol. Biosci.* **16**, 1200–1211 (2016).

126. Oliveira, J. T. & Reis, R. L. Hydrogels from polysaccharide-based materials: Fundamentals and applications in regenerative medicine. in *Natural-Based Polymers for Biomedical Applications* 485–514 (Elsevier Ltd., 2008).

127. Odian, G. *Principles of Polymerization*. *Principles of Polymerization* (John Wiley & Sons, Inc., 2004).

128. A. Macagnano, E. Zampetti, and E. K. *Electrospinning for High Performance Sensors*. *NanoScience and Technology* (Springer International Publishing, 2015).

129. Oh, H. J. *et al.* Washable colorimetric nanofiber nonwoven for ammonia gas detection. *Polymers (Basel).* **12**, 1–12 (2020).

130. Marti, M. E., Sharma, A. D., Sakaguchi, D. S. & Mallapragada, S. K. Nanomaterials for neural tissue engineering. in *Nanomaterials in Tissue Engineering: Fabrication and Applications* 275–301 (Elsevier Ltd, 2013).

131. Zhu, J., Dhimitruka, I. & Pei, D. 5-(2-Aminoethyl)dithio-2-nitrobenzoate as a more base-stable alternative to ellman's reagent. *Org. Lett.* **6**, 3809–3812 (2004).

132. Riddles, P. W., Blakeley, R. L. & Zerner, B. Reassessment of Ellman's Reagent. *Methods Enzymol.* **91**, 49–60 (1983).